NTNU
Norwegian University of
Science and Technology

Evaluation of a Medium-Voltage High-Power Bidirectional Dual Active Bridge DC/DC Converter for Marine Applications

Sindre Helland

Abstract

Due to an increased focus on the development of high-power marine microgrids, new vessels are being installed with large power systems including highly fluctuating loads operating at high efficiency and with low emissions. The introduction of a battery energy storage system in a shipboard DC grid allows for operating the diesel gensets at variable speeds, not being locked to a fixed frequency or speed. The transient performance of the system can also be improved and an optimal load leveling of the different prime movers can be achieved by the proper implementation of a battery. Thus, the system can operate efficiently with highly fluctuating loads while keeping the fuel consumption low.

In order to integrate the batteries into the shipboard DC grid, high-power bidirectional DC/DC converters are needed. Many converter configurations are available, yielding different advantages and disadvantages. Thus, each different system should be evaluated in order to see which converter topology is best suited for that specific system. The stress levels on the switching devices are also higher than before, which can be seen as a result of the utilization of higher voltages and currents in the shipboard grids. Isolated bidirectional DC/DC converters for high power applications can provide the proper connection, but along with the increased loads comes higher requirements to component ratings as well as a more complex control system.

A high-power medium-voltage DC/DC converter suitable for implementing such a battery is analyzed in this thesis after explaining the shipboard electrical system. The converter has a rated power of $4MW$ with an equal input and output voltage of $1100V$ and with a high-frequency transformer providing galvanic isolation between the shipboard power grid and the battery. Its performance is evaluated by means of modeling it in Matlab/Simulink where the focus has been on the switch resonance components in order to achieve a high-performance, soft-switched converter.

A PI controller is also implemented in order regulate the output voltage of the converter for different load levels. As some of the converter requirements are a robust design, high operating efficiency and a fast response, the PI controller is tuned in order achieve this and it is seen that the converter responds fast with small deviations in parameter values for load variations of several megawatts. A gate signal generator is also made, where the output of the PI controller is used as input, delaying the gate signals to switches in either the primary or secondary side, depending on the power flow direction.

The model is used to analyze the current waveforms through the switches and the transformer, and by doing measurements and calculations based on the simulation results, the efficiency of the converter is calculated at different load steps ranging from 0 to $4MW$. It is seen that the converter operates at an efficiency of 97.2% at an output power of $4MW$ with increasing efficiency for lower load levels due to the lower conduction losses. However, the high-frequency transformer is assumed ideal in this thesis and thus the efficiency will be somewhat lower with the transformer losses included.

Sammendrag

Grunnet et økt fokus rundt utviklingen av store marine mikrogrid blir flere og flere nye skip installert med store kraftsystemer som inneholder svært varierende laster og samtidig opererer med høy virkningsgrad og lave utslipp. Ved å innføre et energilagringssystem i form av et batteri i et DC nett har man muligheten til å kjøre dieselgeneratorene med variable hastigheter uten å være låst til én frekvens og dermed én hastighet. Den transiente ytelsen til systemet kan også forbedres i et slikt system og en optimal lastutjevning av de forskjellige hovedmotorene kan oppnås ved riktig implementering av et batteri. Dermed kan systemet operere effektivt med høyt svingende laster samtidig som det holder et lavt drivstofforbruk.

For å kunne integrere batteriene i DC-nettet ombord er det nødvendig med DC/DC-omformere som kan operere med effektflyt i begge retninger. Mange omformerkonfigurasjoner er tilgjengelige og gir ulike fordeler og ulemper. Dermed burde hvert system evalueres separat for å kunne se hvilken omformertopologi som egner seg best for det gitte systemet. Stressnivåene som bryterne må tåle er også høyere enn tidligere, noe som kan ses som et resultat av større laster og dermed bruken av høyere spenninger og strømmer ombord på skipene. Ved å bruke isolerte toveis omformere for høye effektnivåer kan en oppnå en kobling mellom batteriene og skipsnettet, men sammen med de økte belastningene følger også høyere krav til enkeltkomponenter samt et mer komplekst styresystem.

Denne masteroppgaven evaluerer en DC/DC omformer ment for implementering av et batteri i et skip med mellomspent spenningnivå og høye effektflyter. Med tanke på at et slikt skipsnett inneholder mange komponenter som alle trenger å kommunisere sammen for å operere optimalt er hele skipssystemet først beskrevet slik at en omformertopologi kan velges. Omformeren har en nominell effekt på $4MW$ med en lik inngangs- og utgangsspenning på $1100V$ og med en høyfrekvent transformator som gir galvanisk skille mellom skipsnettet og batteriet. Ytelsen vurderes ved å modellere den i Matlab/Simulink hvor fokuset har vært på bryternes resonanskomponenter slik at en omformer med høy ytelse og lave brytertap kan lages.

En PI-regulator er også implementert for å regulere utgangsspenningen til omformeren for forskjellige belastningsnivåer. Siden noen av kravene til omformeren er å ha et robust design, en høy driftseffektivitet og en rask respons er PI-regulatoren innstilt for å oppnå dette. Simuleringsresultatene viser at omformeren reagerer raskt med små avvik i parameterverdier for lastvariasjoner på flere megawatt. En signalgenerator som styrer når de ulike bryterne skal slås av og på er også laget, hvor utgangen av PI-kontrolleren brukes som inngang til signalgeneratoren. Dette vil forsinke signalene til bryterne i primær- eller sekundærsiden av omformeren avhengig av hvilken retning effekten flyter.

Modellen brukes videre til å analysere stømmene gjennom bryterne og transformatoren, og ved å gjøre målinger og beregninger basert på simuleringsresultatene beregnes effektiviteten til omformeren ved forskjellige belastningstrinn. Disse trinnene varierer fra 0 til $4MW$ og en kan se at omformeren opererer med en effektivitet på 97.2% ved en utgangseffekt på $4MW$, med økende effektivitet for lavere belastningsnivåer grunnet de lavere ledningstapene. Siden transformatoren antas ideell i denne oppgaven vil effektiviteten dermed være noe lavere når tapene i denne er inkludert.

Preface

This thesis work has been carried out at the Department of Electric Power Engineering at the Norwegian University of Science and Technology in Trondheim, Norway. The work has been performed in cooperation with Rolls-Royce Marine Trondheim.

The work in this thesis is a continuation of the specialization project done in the fall of 2016, which investigates different hybrid diesel-electric shipboard topologies for offshore supply vessel with active heave compensated cranes operating with dynamic positioning. The master thesis project has been narrowed down in order to analyze the performance of a bidirectional converter for battery storage in offshore supply vessels. A lot of time has been spent on making a Simulink model of the DC/DC converter and making figures that presents how the model performs.

I would like to thank my supervisor at NTNU, Dimosthenis Peftitsis for his help and educational discussions during this thesis work. Also a very special thank to my co-supervisor at Rolls-Royce Marine Trondheim, Eirik Elvestad for his valuable input and experience from the industry.

Sindre Helland
Trondheim, Norway
June 2017

Contents

List of Figures

List of Tables

Nomenclature

The following list describes several abbreviations that will be used later within the body of the document.

AC   Alternating Current

AES   All-Electric Ship

AFE   Active Front End

AHC   Active Heave Compensation

AVR   Automatic Voltage Regulator

BJT   Bipolar Junction Transistor

BMS   Battery Management System

CB   Circuit Breaker

CPL   Constant Power Load

DAB   Dual Active Bridge

DC   Direct Current

DHB   Dual active Half Bridge

DOD   Depth Of Discharge

DP   Dynamic Positioning

DPS   Dual Phase-Shift

EMI   Electromagnetic Interference

EPS   Extended Phase-Shift

ESS   Energy Storage System

FB   Full-Bridge

FCL   Fault Current Limiter

G   Generator

GTO   Gate Turn-Off thyristor

HB   Half-Bridge

HF   High-Frequency

HVSC High Voltage Shore Connection

IBDC Isolated Bidirectional DC/DC

IGBT Insulated Gate Bipolar Transistor

IPS   Integrated Power System

LFP   Lithium-Iron-Phosphate

Li-ion Lithium-ion

LMO Lithium-Manganese-Spinel

LTO   Lithium Titanate

M   Motor

MOSFET Metal-Oxide Semiconductor Field-Effect Transistor

NCA   Nickel-Cobalt-Aluminum

NMC   Nickel-Manganese-Cobalt

OSV   Offshore Supply Vessel

p.u.   Per Unit

PI   Proportional-Integral

PMS   Power Management System

PWM   Pulse-Width Modulation

RMS   Root Mean Square

SLD   Single Line Diagram

SOC   State Of Charge

SPS   Single Phase-Shift

THD   Total Harmonic Distortion

VSD   Variable Speed Drive

VSI   Voltage Source Inverter

ZCS   Zero-Current Switching

ZVS   Zero-Voltage Switching

1 Introduction

Offshore supply vessels face ever increasing loads and due to the fluctuating characteristics of the loads the efficient operation of combustion engines become a challenge. Therefore, the development has gone towards the utilization of hybrid diesel-electric power systems in ships[1]. The type of operations performed by these ships require reliable systems as a fault in the propulsion system during for example off-loading to an oil platform can have devastating consequences. Research and development in the 1970's and 1980's in Variable Speed Drives (VSD) lead to a transition, moving away from the traditional mechanical propulsion with a direct connection between the diesel engines and the propellers and towards having electrically propelled ships[2]. This has introduced large shipboard power systems, being able to have a common electrical system for both the propulsion loads but also for other auxiliary and service loads. These Integrated Power Systems (IPS) have lead to several advantages with regards to robustness, efficiency and emissions and thus intelligent control systems can be used in order to match the generation and consumption in an optimal way. As a result of this, the number of generators needed onboard the All-Electric Ship (AES) is minimized and the different machines can be placed around the vessel in a flexible way, allowing for more space for payload as seen in figure 1.
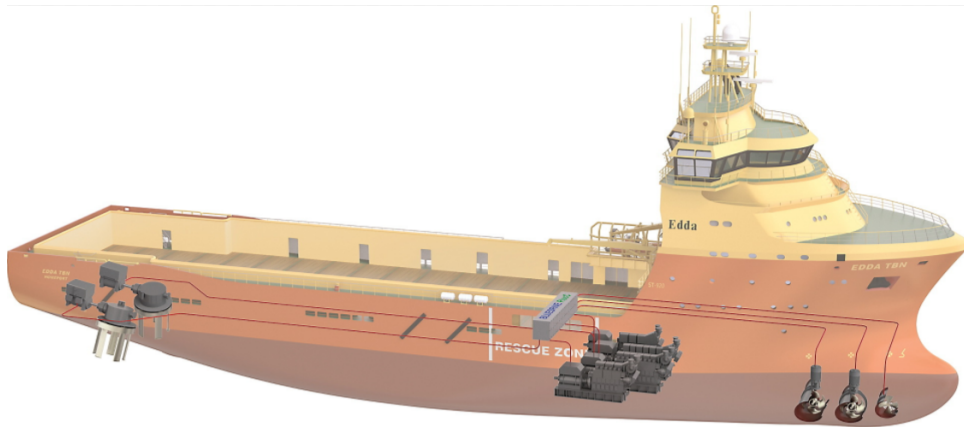
Figure 1: All-electric ship illustrating how components such as prime movers, propulsion system and energy storage can be placed in different parts of the ship[3].

Even though the majority of present AES utilize AC grids, the development and increased use of power electronic devices has lead to a growing attention around DC grids in ships[4]. Among the advantages with a DC electrical grid is that the inclusion of an Energy Storage System (ESS) is simplified as a result of DC-operated systems on both sides of the connection. The ESS can be for example a battery, providing services like peak shaving, grid support functions and back-up power. This battery can also contribute to the power supply when the ship is at berth, being an alternative to the High Voltage Shore Connection (HVSC), which introduce large challenges in supplying all the large shipboard power systems at harbor[5]. The connection of such an ESS to the DC grid is made by using high power bidirectional DC/DC converters utilizing power electronic components to control the power flows in order to charge and discharge the battery. Thus, having a properly sized energy storage and a controlled power flow are crucial in order to achieve an increased fuel efficiency and a reduced need for maintenance. As the shipboard loads are getting ever larger, the requirements to these bidirectional converters are also getting more strict[2]. Large winches in Active Heave Compensated (AHC) cranes in combination with Dynamic Positioning (DP) are examples of operations where the loads are high and fluctuating and having an efficient operation of the diesel engines in the traditional ships can be difficult. The difference in time constants in the mechanical diesel engines and the electrical drives supplying the loads are also big, leading to possibilities of unequal generation and consumption. The proper implementation of a battery system working in coherence with the rest of the electrical grid can thus contribute to a more efficient operation. However, it also introduce challenges due to the increased complexity and need for communication systems between the different devices in the power system.

1.1 Objectives and Problem Definition

The work in this thesis is based on a shipboard DC grid, operating partly with power supplied only from its diesel generators and partly in a hybrid mode, combining diesel generators and batteries. The focus is on the integration of the batteries to the main electrical grid through high-power bidirectional DC/DC converters and their operation. The example vessel contains large loads, represented by a large propulsion unit. Other large loads on the vessel can be winches and cranes. Due to the use of DP systems, the propulsion units will also have to counteract external forces such as waves, wind and ocean currents. This leads to large, fluctuating loads, introducing challenges to the efficient use of the diesel generators.

An overview of the whole system will be given in chapter 2 in order to better understand the different sub-systems and their operational principles. Then, the integration of a battery bank to the electrical grid will be discussed by looking at high-power bidirectional DC/DC converters suitable for marine applications in chapter 3. These have constraints with regards to size, weight and reliability and the proper analysis of the system is therefore necessary before choosing a topology. The steady-state operation of the chosen converter type is discussed in chapter 4 before the component values are found in chapter 5. Also, due to the industry focus on protection schemes and control systems in marine DC grids, these are briefly discussed as well in order to address the present technology in addition to the challenges these systems introduce. It should be noticed that previous work has been performed on simulating the unidirectional Dual Active Bridge (DAB) converter[6] and the bidirectional DAB converter [7] with a locked output voltage. However, in this thesis, a bidirectional DAB converter with an output voltage regulated by a control system is investigated and its operation and performance will be evaluated. In order to evaluate the performance of the chosen converter, a model is built in Matlab/Simulink in order to analyze the dynamic behavior of the system when all of the components work together and the results are presented in chapter 6. The model is based on a ship profile given from Rolls-Royce Marine Trondheim, and this will be used for dimensioning the system components in an optimal way. Chapter 7 give the main conclusions from the study and present suggestions for further work.

2 System Configuration

2.1 Motivation

The increasing shipboard loads have lead to a development in high-power DC grids in recent years[8]. Among the main advantages with a DC grid is the independence from a fixed frequency and speed of the gensets. This eases the design of the system as the alternator does not directly connect to a fixed frequency grid. By having an AC/DC interface converter between the generating units and the DC-grid, the prime movers can be operated at different speeds and frequencies, independently of the loads. This allows for large power systems to operate each genset at different speeds in order to maximize the efficiency of each genset as the system loads are changing. Also, in DC grids there are no reactive power flows in the cables and neither phase angle synchronization needs nor imbalance between different phases are present[9]. This, in addition to the more compact structure and lower losses of DC cables compared to AC cables has lead to clear advantages of utilizing a direct current grid instead of an alternating current grid for certain systems.

As mentioned briefly in the introduction, the inclusion of a battery storage system can enhance the performance of the electrical grid by performing services like peak shaving, grid support functions and back-up power. According to [10] a shipboard DC grid can increase the energy efficiency of an Offshore Supply Vessel (OSV) by up to 20%. In addition it can reduce the number of electrical equipment by up to 30% and with a return-on-investment time as low as 1 year the industry has gained an increasing attention for this solution. However, it also introduce challenges related to the implementation of several fault-current sources in the power system, and the complexity of the system as well as requirements to control systems increase as the electrical grid grows. As seen in figure 2, the number of controllable converters in a propulsion system can be significant, and thus some of the challenges related to fault current sources can be reduced.
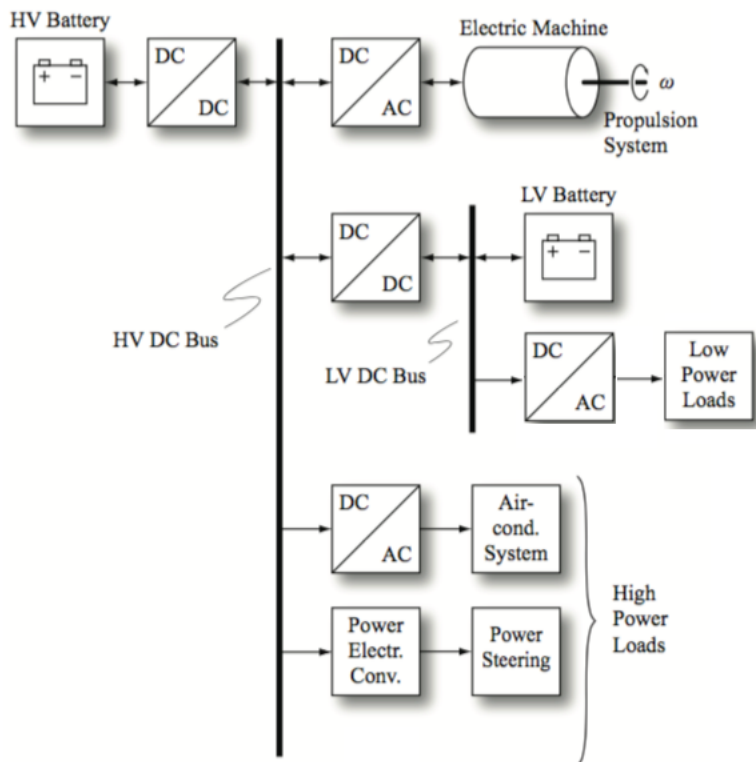
Figure 2: Hybrid power system architecture[11].

Other challenges are related to the low short-circuit impedance of the components, leading to large rates of change in the current with respect to time and the lack of a natural zero-crossing of the currents in a DC grid[12]. Therefore, the use of mechanical breakers are non-efficient in the sense that they will

cause large arcs and long interruption times, possibly threatening system components. This introduce the need for reliable, controllable and efficient converters between the battery and the shipboard grid.

However, due to an industry focus on the development of DC breakers and switches, recent research in both protection schemes and power electronic technology has lead to attractive solutions for DC grids[13]. Among these advantages are the development in and ability of converters utilizing controllable switches to limit fault currents and identifying them in a controlled way in matter of microseconds. In addition to improving the fault handling capabilities of the system, the utilization of converters allow for controlling the power flows in the electrical grid. This chapter will describe the different sub-systems of the shipboard electrical grid before some converter topologies suitable for battery implementation in DC grids are analyzed in chapter 3.

2.2 Electric Power Distribution

Due to the high load levels in the range of several megawatts a high-voltage distribution system can provide advantages related to its associated lower current flows[14]. On the other hand, a too high voltage will introduce challenges related to the semiconductor devices breakdown voltage and thus several modules will have to be series-connected. This introduce challenges related to the failure of one module. There is thus a trade-off between reliability and complexity that has to be considered and thus a medium voltage level of $1100V$ is found to be beneficial for the given system.

Figure 3 shows an example configuration of a DC distribution grid. Both the gensets, named G, and the motors supplying the loads, M, are connected to the grid through converters in order to make the conversion between AC and DC, make steps in the voltage and to control the power flows. The system is also divided into two parts, separated by a DC bus-tie breaker. This allows for half of the battery capacity to be available in each of the two sub-grids, increasing the redundancy of the network. This division into electrical zones allow for a split-mode operation where the two grids are independent from each other, increasing the redundancy of the grid with regards to faults like for example a short-circuit in one part of the system. This could be for operations where the loss of any loads are important to avoid. During normal operation the bus-tie breaker can be closed in order to achieve better flexibility in the configuration of operating gensets. Then all of the gensets can operate according to which ones are the most appropriate for that operation mode. In order to separate different parts, the control system determines which circuit breakers should be opened. Also, by dividing the power system into two equal parts with a bus-tie breaker, the maximum loss of power will be at most half of the total installed capacity. The disadvantage of running the system in split-mode operation is that it can be more difficult to run the gensets efficiently due to a lower average load per genset.
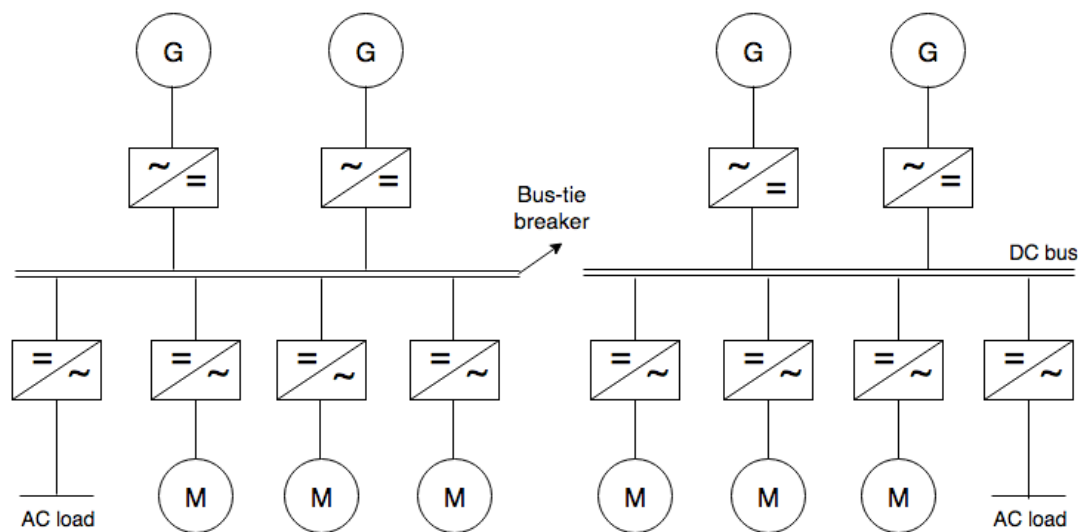
Figure 3: Shipboard electrical distribution system.

Some of the reasons for choosing a DC grid have already been explained, but the main advantages compared to an AC system are given[14]:

- Replacement of the big and bulky low-frequency transformers with compact power electronic converters;

- Different DC-sources are easier connected to the system;

- The size of the switchboards is reduced;

- Harmonic currents and imbalance problems are eliminated;

- The need for synchronization between different sources is eliminated;

- Reactive power flows are eliminated.

As a direct consequence of removing the low-frequency transformers, inrush current problems of the transformers are also eliminated. The fact that the DC-grid is no longer a fixed-frequency grid also leads to the possibility of running each genset at its optimal speed, yielding significant fuel savings[15]. With regards to the connection between components by cables instead of metal shafts, a flexible placement of components in addition to savings in weight and space are also achieved. However, DC grids also introduce challenges related to the lack of a natural zero-crossing of the currents, high current rate of change and the lack of suitable DC breakers[12]. These challenges related to fault handling in DC grids will be further discussed in section 3.7.

2.3   Diesel Generators

Diesel generator sets (gensets) are often used as the main source of power in the shipboard power system[16]. These consist of a prime mover where the most frequently used is a two-stroke diesel engine, driving a generator that produce AC power. For diesel-electric systems the engines are normally medium- to high-speed engines due to a lower weight and cost compared to low-speed engines with the same rated power. Figure 3 also show that there are several gensets in the system. This allows for a more redundant system with regards to the failure of one genset, and by starting and stopping different gensets depending on the load levels, the efficiency can be kept high by operating each genset as close as possible to their optimum operating point. Having loads of less than 50% of the maximum continuous rating of the genset lowers the efficiency dramatically and therefore the proper running of diesel engines at their high-efficiency operating points can lead to significant fuel reductions[2]. However, even though diesel engines have become more efficient the last decades, only around 40% of the energy in the fuel is left for the loads.

The generators that are run by the diesel engines are synchronous machines operating at an output voltage of 690V, producing three-phase AC power with a frequency proportional to the number of poles p and the rotational speed n[17]:

$$f = \frac{p}{2} * \frac{n}{60} \tag{2.1}$$

As explained in the beginning of this chapter, and as can be seen from equation 2.1, when the system is frequency-independent, the gensets can run at different speeds, independently of the loads. This degree of freedom opens up for a more efficient, variable speed operation compared to an AC system. Also, the DC currents in the magnetizing windings on the rotor were earlier transferred by brushes and slip rings. However, in new generators, brushless excitation systems are being used in order to reduce the need for maintenance and thus non-operating time. The excitation system is controlled by an Automatic Voltage Regulator (AVR) and by comparing the actual voltage of the generator with a reference value, the AVR can give a voltage drop that can be used to ensure an equal distribution of the reactive power in different generators. Also, the terminal voltage of the generators should not exceed -15% or +20% of the nominal voltage[2]. In order to keep the generator voltages within its limits it is important not to overload the generators and a feed-forward control is often included in the AVR.

2.4 AC/DC Converters

A central component during the development of electric propulsion systems in the 1980's was the variable speed motor drive[2]. After the AC motor drives became commercially competitive the majority of new electric propulsion ships were based on the AC motor drive topologies. These converters are used to make a connection between systems operating at DC on one side and AC on the other side as shown previously in figure 3.

AC/DC converters are an important component in the shipboard DC grid as the majority of the power that is delivered to the system comes from three-phase alternating current machines and will thus have to be rectified. A similar interface is needed for the connection between the grid and the loads. If a diode rectifier is used, the current through them is non-controllable and unidirectional. It also require the generators to be of a wound rotor type, having an excitation system that regulates the generator voltage. For controllable currents, thyristor rectifiers are used. These will however be operated similar as a diode rectifier in normal operating mode. It is first when a fault happens the firing angle of the thyristor valves are adjusted in order to reduce or eliminate the fault current from the generating AC source side to the DC side[18]. The thyristor rectifier can either perform voltage or current control depending on what requirements the system have. For a permanent-magnet synchronous generator the rectifier would be controllable, being structured as a three-phase bridge converter.

The most common type is the Voltage Source Inverter (VSI) as shown in figure 4[2, 19]. Due to its good performance with synchronous, asynchronous and permanent magnet machines, in addition to having a high flexibility, it is the most used frequency converter in the industry. Also, due to the development in semiconductor components, drives exceeding $30MW$ are commercially available[20]. Among the advantages of having a DC grid is that instead of having a conversion from AC/DC/AC, one inversion stage can be skipped and therefore the converter is simplified compared to for an AC system. The diode rectifier part shown in the left part of figure 4 can not supply power in both directions and can thus be removed from the VSI used in shipboard AC systems. The inverter part can transfer power in both directions, allowing for regenerative operation of for example the propulsion units. This bidirectional power flow of the inverter is seen in the right part of figure 4.
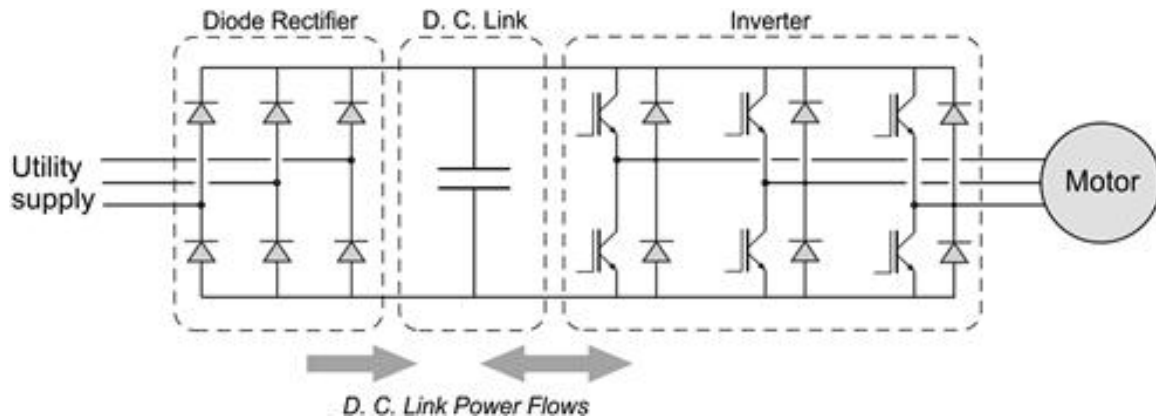
Figure 4: Topology of a voltage source inverter[19].

As mentioned in section 2.3, the input to the AC/DC rectifiers supplying power to the DC grid will be a constant voltage[21]. The converter control that is adopted should therefore be suitable for current control, as the rectifier output will be current-controlled, given a constant input voltage from the prime mover gensets. Having an LCL filter on the input of the converter leads to a high performance Active Frond End (AFE) rectifier and these are commonly used in order to connect the alternating gensets to the DC grid[22]. Figure 5 shows an AFE rectifier with its front-end filters, which is basically the VSI in figure 4 without the rectifier and with additional filters. The non-controllable diode rectifier is replaced by a self-commutated rectifier, showing regenerative capabilities by the use of IGBT switches and power filters[23]. These filters are designed in order to provide a line current supply that is sinusoidal with very low Total Harmonic Distortion (THD). In addition, the AFEs ability to boost the voltage is also desired

as the output voltage of the gensets is $690V$ while the DC-grid operates at $1100V$.
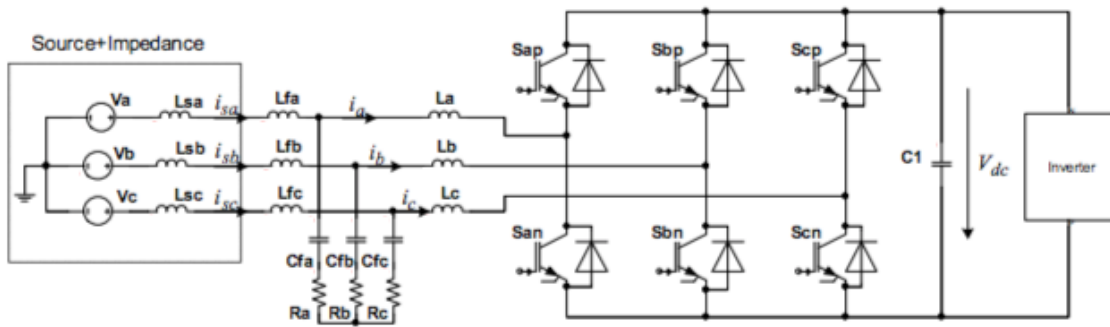
Figure 5: Three-phase AFE rectifier[22].

Among the advantages of having an AFE converter in vessels with electric propulsion are the following:

- It has a regenerative capability;

- It has low harmonics with THD of input current meeting industrial standards;

- The AFE boosts the input voltage to the given DC-grid voltage level;

- It is a cost-competitive converter (it has a high capital investment, but this should be offset by lower costs on cables, transformers, filters and other compensation equipment);

- It is a compact topology compared to other topologies with the same qualities.

The AFE converter is also suitable for systems where the input voltage is varying, making it appropriate for integration of energy storage systems as well. Among the disadvantages with the AFE converter are a relatively complex control system, a costly and bulky LCL filter and for soft line conditions, resonance may occur.

2.5   Loads

In order to convert electrical power into mechanical power, electrical motors are commonly used[2]. For OSVs, the largest loads are related to the propulsion units as well as large winches or cranes and these motors will therefore be used as examples in order to model the loads. These loads can perform operations varying from DP for standby operations with AHC cranes and harbor operations that require pumps, cranes, heat, light and other electric equipment to run. Transit operations require both propulsion units and auxiliary system to run at the same time and will thus introduce large and fluctuating power demands[24].

Since DP is an operating mode with a high operation time in an OSV, some different DP operation modes are shown in the following in order to better understand the characteristics of a large shipboard load. The principle of DP is based on the counteraction of external forces such as wind, waves and sea currents in order to keep the ship stationary when performing work that require a steady position. Therefore, depending on the weather conditions, the DP loads can be classified as low DP, high DP or emergency evacuation[25]. Figure 6 shows the load profile during low DP operation, where it is seen that the load can vary as much as 30% within a time frame of only 15 seconds. According to a study made by ABB for an OSV, the propulsion loads can be in the range between $700-3500kW$ for calm weather operations, showing a large variation in power demand[25].

When the weather conditions are more harsh the loads can vary even more, ranging from $500-5000kW$ as seen in figure 7. Also, transients can occur due to free-spinning propellers as a result of large waves, and with the slow response of diesel gensets these transients can lead to large current peaks in the electrical grid and should therefore be avoided.
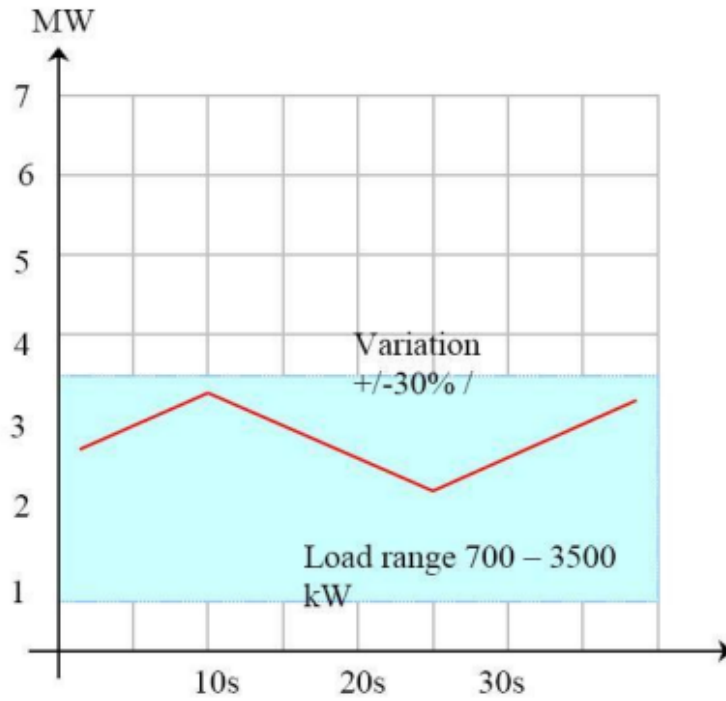
Figure 6: Ship load during low DP[25].
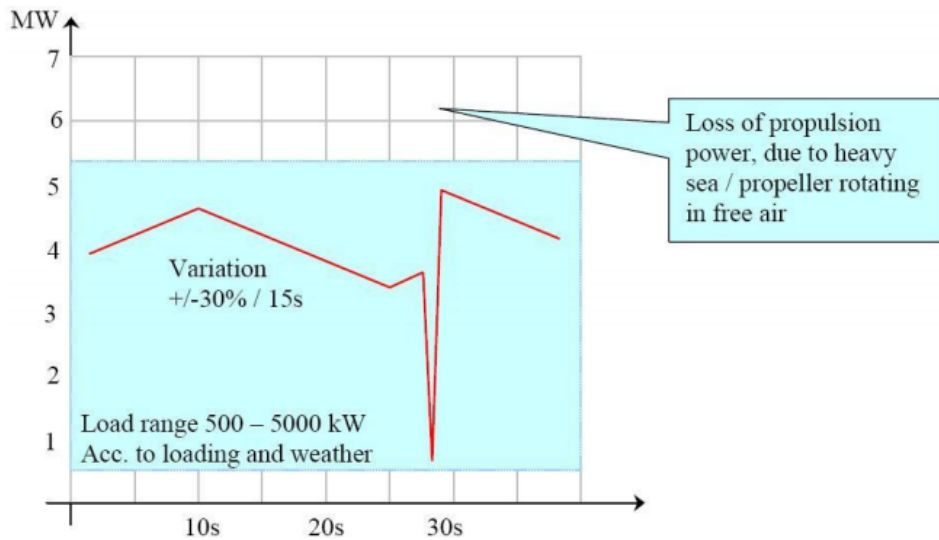
Figure 7: Ship load during high DP[25].

For emergency operations the load will increase rapidly in order to subtract as much power as possible from the thrusters. Figure 8 shows the linear relation between power and time, where the power drawn keeps on rising until the vessel is in its desired position. For active heave compensated cranes, the crane load of up to $2MW$ will come on top of these high propulsion loads during rough weather operation. It is therefore seen that the loads can be very high in addition to highly fluctuating within a short amount of time.
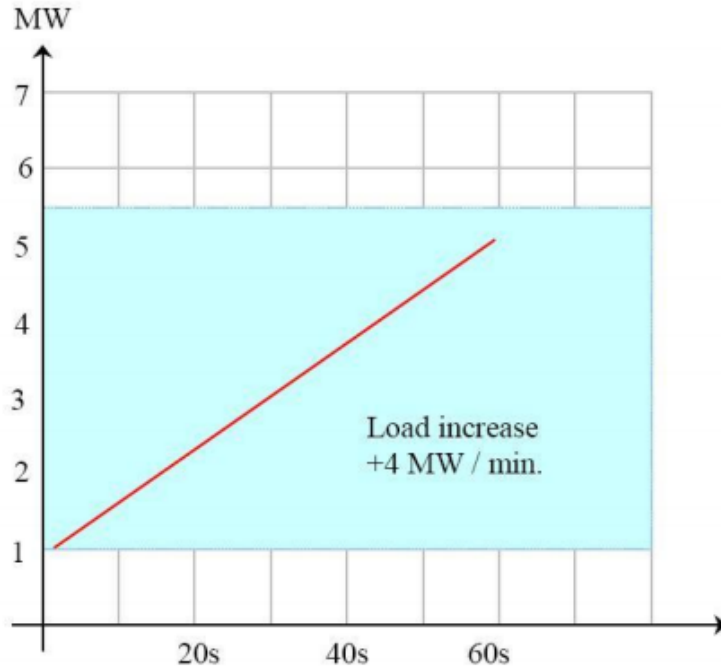
Figure 8: Ship load during emergency DP[25].

An example load profile is therefore created in order to see how the demand changes over time during a specific operation such as for example a crane operation with DP. Table 1 shows the load values at different times, and figure 9 also show the load changes illustrated in a diagram. With an average power of $6MW$, which is delivered from the diesel gensets, the battery should be able to deliver a peak power of $4MW$ in order to meet the maximum load demand of $10MW$. Also, in reality the diesel gensets would have to deliver a little bit more than $6MW$ in order to account for the losses in the system. For an example total operation time of 50 seconds, a load change will happen every 10 seconds for the given load profile.

Time[% of total operation time]	0	20	40	60	80	100
Power[MW]	4	5	10	7	4	4

Table 1: Operating modes and load profile for the OSV.

It is thus seen that the battery and DC/DC converter should be able to supply a power of $4MW$ in order to operate the diesel gensets at a steady output power of $6MW$. The design of this converter will be further discussed in chapter 6 where a model is built in order to investigate the operation of the converter with a variable load. The model will also run the converter with power transfer in one direction in order to have a simplified control system. This means that a total power demand of $4MW$, which is a negative power demand of $2MW$ of the converter, will be modelled as a positive power of $2MW$.
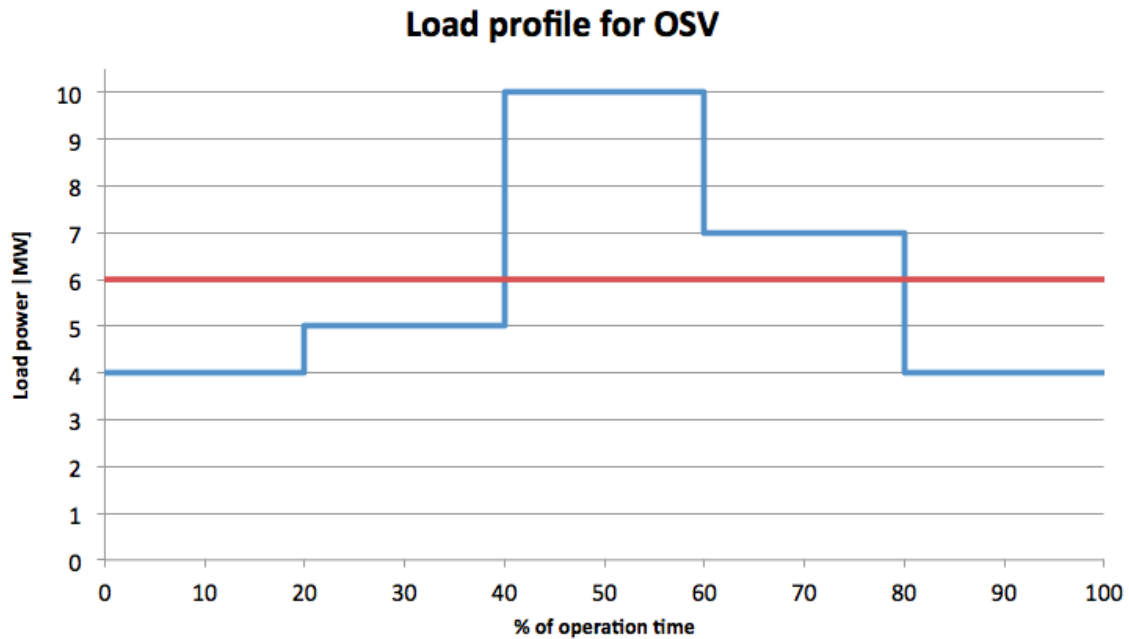
Figure 9: Load variation of offshore supply vessel. The average power of $6MW$ is delivered by the diesel gensets and the deviation is absorbed or delivered by the ESS.

2.6 Energy Storage System

The attention around energy storage systems in combination with combustion engines has increased the last years due to efficiency, performance and safety reasons[1]. The development in battery technology has also lead to both technically and economically viable storage systems to be used in shipboard power systems. Among the main goals of implementing an ESS is to make sure the energy from the batteries is available to the loads when needed and that they can be charged when appropriate in order to increase the efficiency and robustness of the electrical grid. This section will explain the battery system in order to better understand the coherence between the battery and the DC/DC converter.

For systems that run with energy entirely from a battery the control system and integration is relatively straightforward. However, when batteries are used in addition to combustion engines and generators, the performance of the system is more dependent on a properly designed Power Management System (PMS). As the diesel gensets deliver the average power, operating at a steady and efficient level, the batteries will be used for peak shaving. Fast responding batteries with the capability of discharging high power is then necessary. For these kind of functions, high-power batteries can be used. The dimensioning of the batteries will then depend on both the size and duration of the load variations[26]. Figure 10 shows the strategy of having a peak shaving storage system where the diesel generators supply a constant power equal to the average load demand and the storage device cover the load fluctuations.
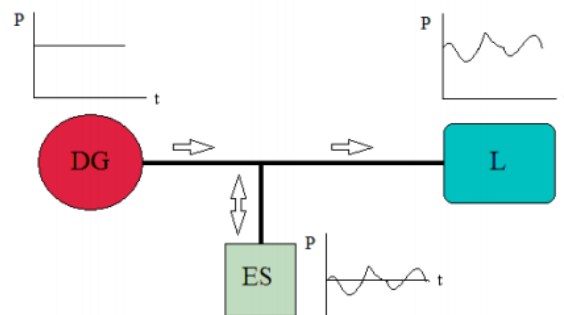
Figure 10: Illustration of peak shaving in order to compensate for load variations[24].

Another way to use the ESS is to utilize a PMS that makes the storage device partially cover the load for a limited amount of time. The diesel gensets will then cover the rest of the load. This requires a storage device with both high power and high energy since it will have to deliver power without being charged for a longer amount of time. A combination of a high-energy battery and a supercapacitor can therefore be suitable. This method is referred to as load sharing[27]. As in the peak shaving method, the storage device should be dimensioned based on the size of the load that it must cover and the duration it must be operational. After the period of power supply to the loads, the ESS can be charged by the diesel gensets. The strategy is illustrated in figure 11.
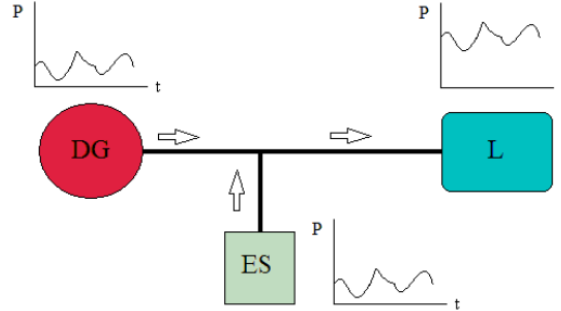
Figure 11: Illustration of load sharing[24].

For both the mentioned strategies, the energy balance between the load demand, P_{load}, energy storage power, P_{ES}, and generated power, P_G will be

$$P_{load} = P_{ES} + P_G \qquad [W] \tag{2.2}$$

As discussed, the diesel engines operates more efficient at constant output levels and it is therefore desired to avoid an intermittent and fluctuating operation. Due to the fluctuating, high-power loads and the high power-density of new batteries, the ESS that is included in the system will therefore be a battery system operating according to the peak shaving method. In addition to the advantages mentioned regarding peak shaving, the battery can take several functions in the shipboard electrical system such as[1]:

- The ESS can function as spinning reserve in order to reduce the need for combustion engines running. In case of sudden increase in loads or loss of generation, the battery supplies the necessary power for a predefined amount of time. This can also improve the performance of the system during split-mode operation.

- It provides an improved fault ride-through capability. This means that it maintains the system voltage during faults in a sub-system of the grid like for example in a crane or a thruster.

- As the batteries can cover peak demands and be charged when the load demand is lower, the dynamic performance of the electrical grid can be enhanced. Thus, peak shaving automatically leads to increased dynamic performance.

- If the Battery Management System (BMS) is properly designed, the battery loading can be controlled in order to optimize the running of the diesel engines.

- The inclusion of batteries also introduce the opportunity to have an all-electric propulsion and therefore a zero-emission operation for a predetermined amount of time. This will of course depend on the size of the storage system.

Since batteries are expensive units they should therefore be implemented properly into the system in order to yield the best possible features. Avoiding operation at high C-rates will be beneficial for the battery performance and this should be taken into consideration during the design process[28]. The temperature control is also important, and power flows will be limited as the reaction rate is reduced

if the ambient temperature is too low. On the other hand, the reaction rate will be increased in high-temperature operation but this can lead to a parasitic side reaction, leading to a faster degradation of the battery[29]. A proper temperature control is therefore important in order to operate the battery as efficient as possible and to avoid degradation.

Due to the good characteristics of Lithium-ion (Li-ion) batteries such as a high power and energy density, these are often used in systems where weight and space are limiting constraints[30]. For a battery supplying a load over a longer period of time, a high-energy battery can be used. The limiting factor of such a battery is related to its high internal resistance, reducing its power rating. High operating temperatures and a reduced lifetime would be the result of a high drawn power, and this should therefore be avoided. The rating of the battery energy is given as

$$E_{battery} = C_b * V_{nom,bat} \tag{2.3}$$

where $V_{nom,bat}$ is the nominal battery voltage and C_b is the battery capacity. For applications where higher power is needed from the batteries, high-power batteries can be used. The main difference between high-energy and high-power batteries is related to their internal resistance. For high-power batteries the internal resistance is lower than for a high-energy battery during discharge, making it more suitable for high-current operations. However, this comes with a trade-off that the energy rating is lower. The actual battery rating that is installed will thus depend on the required dynamic performance of the system. Also, within the Lithium-ion battery technology there are different cell chemistry's that are used, where functions like high energy-density, long lifetime and low maintenance need are important for marine applications.
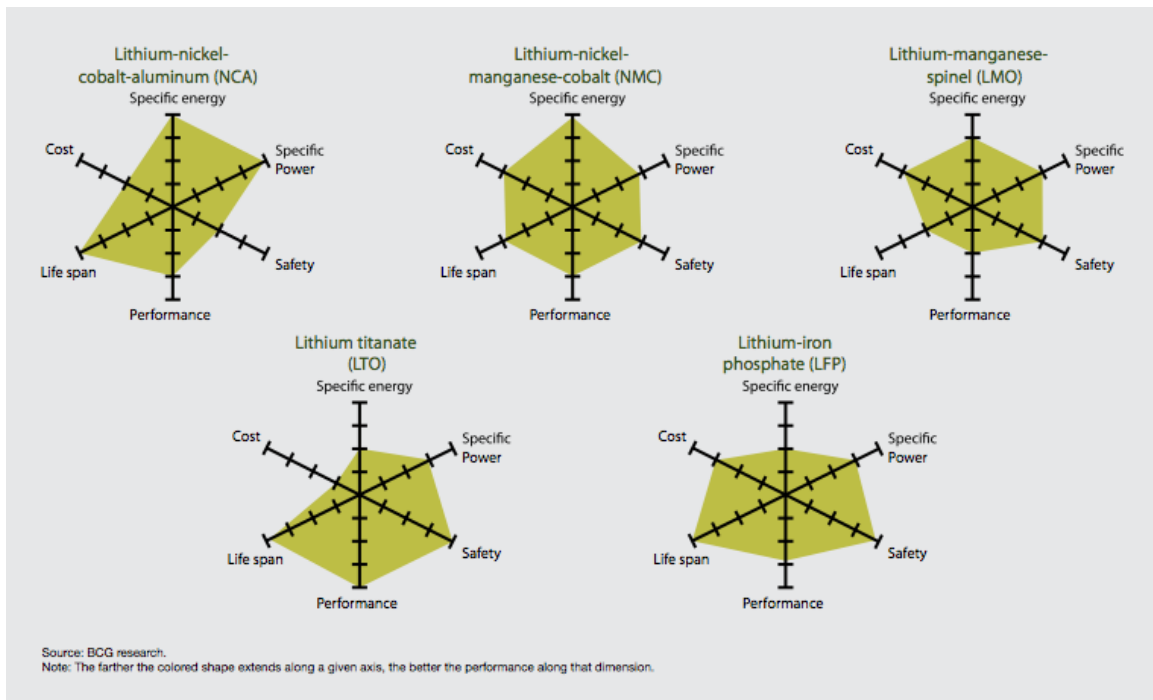
Figure 12: Comparison and trade-offs between the different Li-ion cell chemistry's. The NMC chemistry proves to meet the requirements for large-scale marine applications[31].

The principal types of chemistries that are present within the Li-ion technology are shown in figure 12[31]. It compares specific energy, specific power, safety, performance, life span and cost for different Li-ion technologies. As seen, the figure compares NCA, NMC, LMO, LTO and LFP (see figure 12 or nomenclature for full names). However, NCA proves to be unstable and is therefore not meeting the safety requirements of a shipboard electrical system. The LMO technology has a too short life span, the LTO batteries have a too low energy and power density for the given large-scale application, and LFP has challenges related to the manufacturing process, yielding scalable risks. The NMC chemistry does however meet the requirements regarding high power and energy density, safety and manufacturing.

Due to tough load profiles and high stress on the batteries in a shipboard power system, a reliable and safe battery pack are of great importance. The Lithium-NMC chemistry is therefore chosen due to its reliability, superior lifetime and performance in a shipboard environment. Table 2 shows a comparison of some variables for the different cell chemistries[32].

	LTO	LFP	LMO	NMC	NCA
Cell voltage [V]	2.4	3.2-3.3	3.7-3.8	3.6-3.7	3.6
Energy density [Wh/kg]	70-80	90-120	100-150	150-220	200-260
Charge [C-rate]	1-5	1-3.65	0.7-3	0.7-1	0.7
Discharge [C-rate]	10	1-25	1-10	1.2	1
Cycle life	3000-7000	1000-2000	300-700	1000-2000	500
Thermal runaway [°C]	Very safe	270	250	210	150
Price	Very high	Moderate	Moderate	Moderate	High

Table 2: Comparison of cell chemistry of Lithium-ion batteries[32].

Within the NMC chemistry, the cell can also be of different types with regards to cell connections[31]. Wound (rolled) types and prismatic types are familiar as the typical "AA" battery, but due to a high internal impedance of these batteries, they are more suitable for low-power applications. For high-power and large-scale applications like a shipboard electrical grid, the Z-fold type will be used as shown in the right part of figure 13. It has a low impedance and is therefore capable of charging and discharging with a high efficiency without having a high temperature rise related to it. Among the important features of a marine battery like energy density, power density, cycle life, internal impedance, safety and cost, the Li-ion NMC battery provides superior features compared to the other technologies mentioned earlier. It is also capable of achieving the same voltage level as the other technologies by using less series-connected cells, resulting in a lower interconnection between the cells and therefore a lower chance of failure.
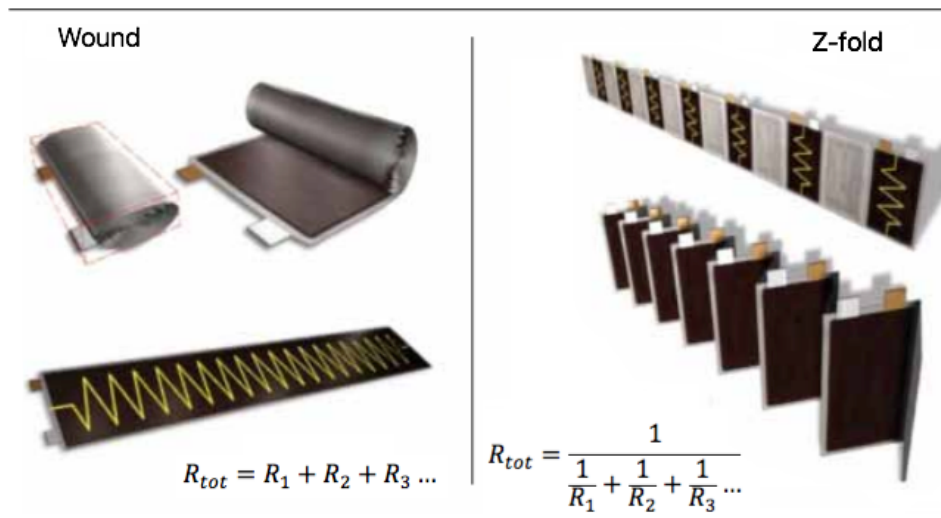
Figure 13: Wound and Z-fold battery cells[31].

To summarize the chemistry, the Z-fold type Lithium-ion NMC batteries have few series-connections, high charge/discharge efficiency, high energy-density, utilize a safe chemistry and a high-quality manufacture[31]. The Li-ion technology from one of the industry leaders Corvus is suggested, where the choice of battery pack falls on the Corvus AT6700-100 module[33]. It comes in modules operating at $100V$ with an energy level of $6.7kWh$, having a high power- and energy-density at a weight of only $72kg$. The data sheet of the AT6700 module is given in appendix 8.1.

When it comes to the dimensioning of the Li-ion battery system, there are three constraints that must be met:

1. Maximum power discharging capability of the battery.

2. Maximum power charging capability of the battery.

3. Maximum energy delivery capability of the battery.

For the first power constraint, the number of batteries connected in parallel must be found according to equation 2.4 after determining the battery voltage level:

$$N_{pow,parallel,dis} = \frac{P_{load,max,req}}{N_{series} * P_{bat,dis} * \eta_{eff,sys}} \tag{2.4}$$

Here, N_{series} is the number of battery cells connected in series, $P_{load,max,req}$ is the maximum power requested by the load, $P_{bat,dis}$ is the nominal power one Li-ion cell can deliver and $\eta_{eff,sys}$ is the efficiency of the energy storage system, including converter losses, battery losses, etc. As the number of battery cells connected in series, N_{series}, will determine the voltage of the battery storage system, this can be determined depending on the system voltage. However, having a large number of series connected battery cells is not desired as this reduce the reliability of the storage system. Further on, for the second constraint, the number of parallel connected strings is found as shown in equation 2.5:

$$N_{pow,parallel,cha} = \frac{P_{load,max,del}}{N_{series} * P_{bat,cha} * \eta_{eff,sys}} \tag{2.5}$$

where $P_{load,max,del}$ is the maximum power delivered to the battery and $P_{bat,cha}$ is the nominal charging power that a Li-ion cell can take. The third constraint is shown in equation 2.6 as:

$$N_{en,parallel,dis} = \frac{E_{load,max,req}}{N_{series} * E_{bat,dis} * \Delta DOD_B * \eta_{eff,sys}} \tag{2.6}$$

where $E_{load,max,req}$ is the maximum amount of energy the load will request, $E_{bat,dis}$ is the nominal energy in a battery cell and ΔDOD_B is the change in Depth Of Discharge (DOD). The change in DOD is given as

$$\Delta DOD_B = \frac{\int_{t_1}^{t_2} i(t)dt}{C_b} * 100\% \tag{2.7}$$

where $i(t)$ is the current flowing to/from the battery. This ΔDOD_B factor is added into the equation due to the fact that the State of Charge (SOC) of the battery cell will affect the amount of energy that is available in the cells. The relation between SOC and DOD of a battery is given as

$$SOC_B = 100\% - DOD_B \tag{2.8}$$

The highest number of the calculated values of $N_{pow,parallel,dis}$ and $N_{pow,parallel,cha}$ should be used in the design process of the battery bank in order to have sufficient power both during charge and discharge. Due to the high power levels, the SOC of the battery is changed during operation and therefore the amount of parallel connections in the battery should also be high enough in order to avoid operation at very high C-rates. Also, for low battery voltage levels, the currents would be very high at higher power levels, and therefore the power drawn should be limited at low battery voltage levels[34]. Since the filter size will be proportional to the currents, a high voltage energy storage is also beneficial from the DC/DC converter perspective.

Due to the fact that an unequal voltage and capacity of series connected batteries would cause an imbalance in the battery bank, the number of series connected batteries should not be too high since the one cell with a depressed voltage will lead to an end-of-discharge voltage sooner than normal, reducing the redundancy of the system[35]. Difference in internal resistance will also limit the performance of the string since the load voltage variation will be applied to the bad cell, leading to danger of heat-up or in worst case a shut-down[36]. However, in order to meet the voltage level of the $1.1kV$ shipboard DC grid, the turns ratio of the high-frequency transformer would be undesirably high if the battery voltage is too

low. As the AT6700-100 battery packs from Corvus operate at voltage levels between 76.8 and 100.8V, a series connection of 12 batteries operating at a nominal voltage of 92V leads to an operating voltage of 1104V. The turns ratio of the transformer is then 1:1 and the transformer only provides galvanic isolation and not a voltage step. This will yield advantages with regards to the soft-switching performance of the converter as will be discussed in chapter 4.

The parameters of the battery module is found from the Corvus AT6700-100 data sheet as shown in appendix 8.1. As the battery must be able to supply a power of 4MW at an operating voltage of 1100V, several battery modules will also have to be parallel connected in order to meet the current requirements. A summary of the specifications for the battery is given in table 3. The table shows specifications for one module as well as for 12 modules connected in series with 8 modules in parallel in order to be able to supply a maximum discharge power of 4MW. The battery will then have an energy level of 660kWh at an operating voltage of 1104V with a total weight of 6900kg. As a comparison, the OSV "Viking Lady" has a battery pack with a capacity of 442kWh and a weight of 4900kg. This is installed in a standard 20 foot container[37]. It is to be noted that the battery is dimensioned so that it can discharge up to 4MW while the continuous charge power is limited to approximately 2MW.

				Discharge		Charge	
Modules in series	Modules in parallel	Capacity [Ah]	Voltage min-max [V]	Peak current [A]	Continuous current [A]	Peak current [A]	Continuous current [A]
1	1	75	76.8-100.8	750	450	375	225
12	8	600	921.6-1209.6	6000	3600	3000	1800

Table 3: Summary of the battery bank specifications from the Corvus AT6700 data sheet[33].

As a summary, the battery can contribute to the efficient operation of the system by performing

- time shift for production;

- peak shaving;

- load smoothing;

- back-up power;

- grid support functions.

The implementation of a battery energy storage will therefore contribute to the efficient operation of the shipboard electrical system by delivering or achieving power from the point of common coupling[34].

2.7 DC/DC Converters

DC/DC converters are included in the system in order to make a connection between the DC storage device and the DC grid. They can be used both to control the power flow but also to make steps in the voltage where necessary. Most DC/DC converters will also have to be bidirectional in order to implement an energy storage device that can both receive and deliver power in order to charge and discharge, respectively. Due to the fact that it is desired to have a low amount of series connected batteries together for reliability reasons, there is often a need for boost converters in order to meet the battery voltage on one side of the converter and the system voltage on the other side[38]. In addition to this it can also improve the fault handling capabilities of the converter and it provides a galvanic isolation, removing the direct connection between the two sides of the converter. Chapter 3 will continue the discussion of DC/DC converters in detail. For more information about the different components in the shipboard system the reader is referred to the literature[2].

2.8 Complete System Configuration

Now that the different sub-systems are discussed they should all be connected together in order to make a shipboard DC grid. Figure 14 shows a Single Line Diagram (SLD) of the shipboard electrical system. It consists of a main DC-bus with a bus-tie breaker with two gensets on each side of the bus-tie. Other components are propulsion units, thrusters, cranes, hotel loads, batteries and converters as previously described. The combination of power from both the diesel gensets and the batteries makes the system redundant and reliable as the failure of one source can be compensated by another or at least run the system at a lower level instead of having a total blackout during a fault. The bus-tie also allows for a split-mode operation until the fault in one section is cleared and will thus disconnect the faulty part of the system. However, running the system with the bus-tie breaker closed leads to certain advantages such as more available gensets that can share the load in an efficient way. Among the main challenges is the fact that several sources are supplying power to the DC-grid, introducing high fault currents if not controlled properly. This puts high requirements to the protection system, where a fast and precise communication is needed between the components.

A flexible placement of the converter and battery is also allowed for by having an AES with cable connections instead of metal shafts. Thus more space is available for payload and the more heavy components can be placed at lower decks. The battery system is also shown as two different batteries in the SLD below. This is done to illustrate that the battery power is equally distributed between the two sections. Having the battery energy distributed and placed near loads can also lead to advantages related to dimensioning of cables and power flow. However, in the model built in this thesis, the ESS is modelled as one battery with one DC/DC converter connecting it to the grid.
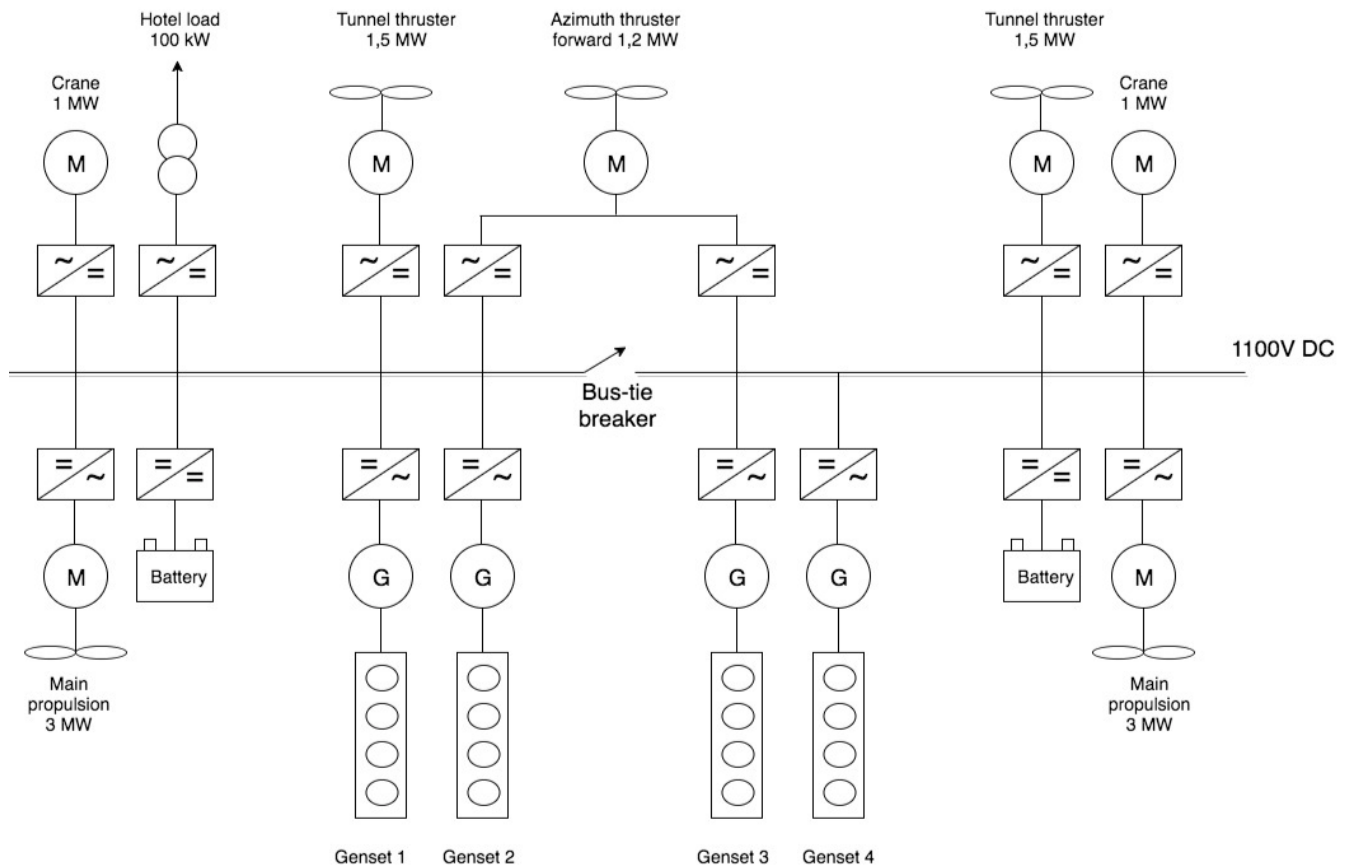
Figure 14: Single line diagram of the shipboard electrical system. The gensets are equally rated at $690V$, $60Hz$, 3200kVA and 2900kW.

2.9 Limitations and Simplifications

A challenge with the analysis of a bidirectional high-power DC/DC converter for a shipboard power system like this is related to the fact that the converter operates in cooperation with many other devices. As seen, the shipboard power system is large and complicated and requires a detailed analysis in order to understand how all the different sub-systems interact and depend on each other. Since this thesis will focus on integrating the battery storage system to the grid through a DC/DC converter, only a small part of the system is investigated in detail.

The system shown in figure 14 consist in general of energy supplies (diesel gensets and batteries), energy absorbers (loads) and energy transfer elements (converters and the grid). Therefore, the analyzed system is narrowed down to a small system containing a battery, a DC/DC converter and a single load, which proves to be a simple, but good, representation of the system for analysis purposes. For this system, the single load is representing all the different consumers on the vessel and the diesel gensets are assumed to deliver a constant power to the grid equal to the average power with a constant voltage of $1100V$ by means of AFE rectifiers. Thus, the battery and DC/DC converter will have to meet the fluctuating load demand with a maximum power transfer of $4MW$. Figure 15 shows the simplified system that will be analyzed where the focus will be on the DC/DC interface converter with a battery connected to one side and a load on the other side. The following chapter will explain some suitable converter topologies for the given system, where the goal is to find a topology that meet the requirements of the shipboard electrical system.
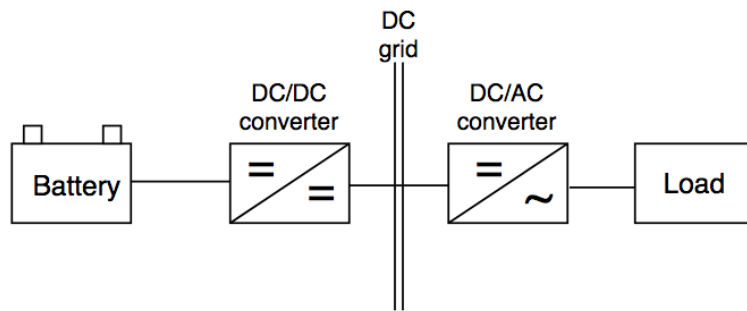
Figure 15: Single line diagram of the simplified shipboard electrical system.

3 DC/DC Converters for Integration of Batteries in Shipboard DC Grids

3.1 Introduction

The implementation of a high-power battery in a power system can occur in different ways depending on the topology of the grid, the application area of the system and the characteristics of the battery pack. As the storage system often operate at a lower voltage level than the grid, these converters allow for both charge and discharge of the storage device by operating in buck mode and boost mode, respectively. Different features of the converters are also desired for different systems. In some weight- and space constrained systems non-isolated converters are used as they can achieve a high efficiency and also avoid the isolating transformer[39]. However, a galvanic isolation is required between marine systems that may have grounds at different potentials and thus isolated converter topologies are highly relevant for the shipboard grid. Other features required in a shipboard converter for energy storage integration are a simple, reliable and robust design, low weight and volume, bidirectional power flow and high-power operation. Based on the discussion of the system as made in chapter 2, an analysis of different converter configurations that are suitable for our system can be made. This chapter starts by looking into the basics of DC/DC converters before some different topologies are discussed in order to find a suitable topology for further investigation.

3.1.1 Non-Isolated Unidirectional DC/DC Converters

The type of converter that is used in the shipboard system is determining the power flow characteristics of the battery energy and is therefore playing a vital role in the overall performance of the electrical grid[40]. The simplest topologies of DC/DC converters do not provide bidirectional power flow capability or galvanic isolation. This is due to the presence of diodes, allowing only for power flow in one direction and the lack of an isolating transformer. A very simple configuration of a unidirectional, non-isolated DC/DC converter is shown in figure 16. The converter is only capable of transferring power in one direction and the figure thus also show the transition from a non-controllable, unidirectional converter to a controllable bidirectional converter by replacing the diodes with controllable switches as seen in figure 16c. However, the replacement of diodes with controllable switches will increase the complexity of the converter, introducing more requirements to the control system as will be shown later. There is thus a trade-off between a simple topology with low requirements to control systems and more complex systems with better ability to control the power flow.

Figure 16: Simple (a) buck- and (b) boost-converters with diodes. (c) shows the same topology utilizing controllable switches, allowing for bidirectional power flow[39].

The number of components in the converter can also vary depending on the requirements regarding efficiency, ripple values and cost. An inductor can for example be placed in the low-voltage side as see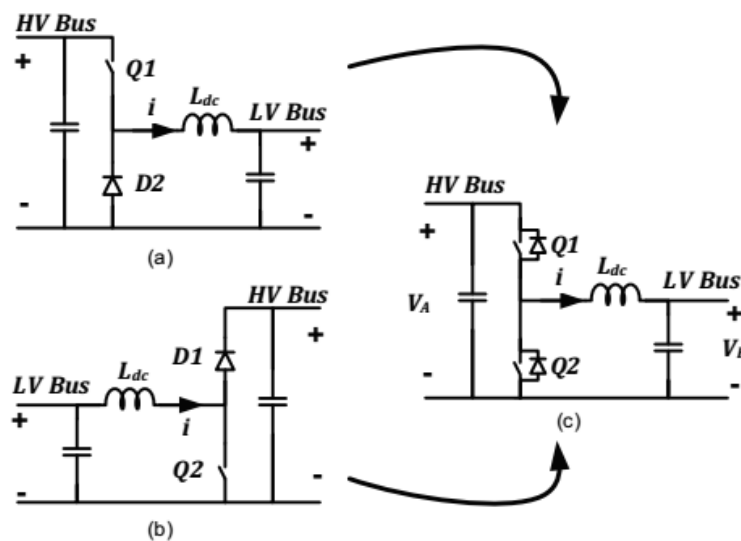n in figure 16 in order to smooth the current, which can be advantageous when charging or discharging batteries with regards to efficiency and lifetime[39]. Regardless of the number of components and types of switches that are used, some systems also require a galvanic isolation, often in terms of a transformer, in order to remove the direct connection between different systems, introducing the concept of an isolated DC/DC converter.

3.1.2 Isolated DC/DC Converters

When multiple sources are included in a high-power shipboard system, galvanic isolation is a requirement according to standards[39]. A transformer can be used in order to provide this galvanic isolation in addition to voltage matching. However, line-frequency transformers are large and bulky, and the utilization of high-frequency (HF) transformers have therefore become popular. In addition to the isolating properties it also provides voltage matching between different systems, determined by the turns ratio. The high-frequency transformer can also lead to avoiding the current and voltage waveform distortions that can occur for line-frequency systems and thus eliminate the problems related to core saturation of the transformer[41]. The isolation transformer will also contribute to a lower noise, increased personnel safety as well as improved operation of the protection systems. By placing the transformer in the DC/DC conversion stage, an isolated bidirectional DC/DC converter can be designed.

Common for all different DC/DC converter types operating at high power levels is the bridge structure, utilizing controllable switches such as Insulated-Gate Bipolar Transistors (IGBTs) or Metal-Oxide-Semiconductor Field-Effect Transistors (MOSFETs), illustrated as S_1-S_4 in figure 17. Among the two transistor types, IGBTs are most commonly used in high power systems[17]. The advantage with the controllable switches is their ability to operate fast in order to produce different voltages as well as to limit the currents in case of a short-circuit. Most converter topologies also need filters on the DC-side due to the harmonics that are created, where a capacitor and an inductor are often used in order to avoid resonance with high frequency.
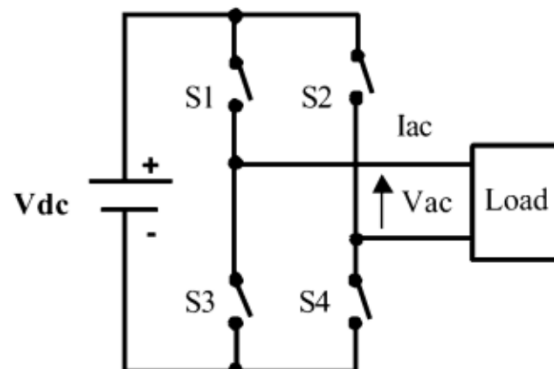
Figure 17: Full-bridge topology with controllable switches[42].

For high-power applications, the most generic way to represent a DC/DC converter can be as shown in figure 18[43]. The input and output voltages V_1 and V_2 can be at different voltage levels, where the connection of a battery to a grid is a typical example of this since the battery has traditionally been operating at lower voltage levels than the grid in order to reduce the amount of series connected cells. The battery side of the converter has a voltage-fed HF inverter/rectifier that is connected to a voltage-fed HF rectifier/inverter through a HF isolation transformer. Two different types of switching converters can be used, where the first one is referred to as a current-fed structure, having an inductor in series at its input terminal, yielding a stiff current characteristic similar as a current source[39]. The second type, referred to as a voltage-fed structure, has a capacitor in parallel at its input terminal, acting like a voltage source with its stiff voltage characteristic. Whether type to use depends on the system application and

can to a large extend affect the current and voltage waveforms of the converter. The inverter/rectifier units on both sides of the transformer can also be variations of either a half-bridge, full-bridge or a push-pull topology. However, the push-pull topology has some challenges related to the requirement of a center tap on the transformer for high-power applications and is therefore not commonly used for such systems[38]. Therefore, due to their simplicity and reliability in high-power systems, the half-bridge and full-bridge topologies are commonly used.
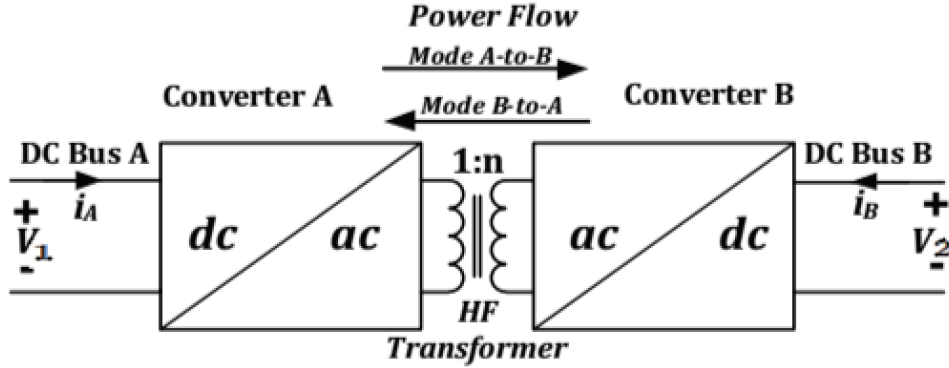
Figure 18: A generic illustration of a high-power bidirectional DC/DC converter[39].

As an example an isolated bidirectional DC/DC converter is shown in figure 19. The converter utilize a HF transformer in order to be able to handle both high currents and voltages in systems with a large difference between the low-voltage and the high-voltage side of the converter[18]. In addition, the turns ratio of the transformer will introduce an additional degree of freedom by means of making a step in the voltage, simplifying the connection between systems operating at different voltages. The disadvantage of having the HF transformer is related to cost and losses, and in order to meet the bidirectional criteria of the isolated DC/DC converter, controllable switches must be used in both bridges. This will increase the cost of the converter but also the complexity of its operation. Also, when the amplitude of the voltages on the two sides of the transformer are unequal, the circulating currents will increase, leading to a decrease in efficiency. It is thus seen how the complexity of the converter increase due to the need for an AC-link in order to transfer power via a magnetically isolating media and due to more controllable switches in order to achieve bidirectional power flow.
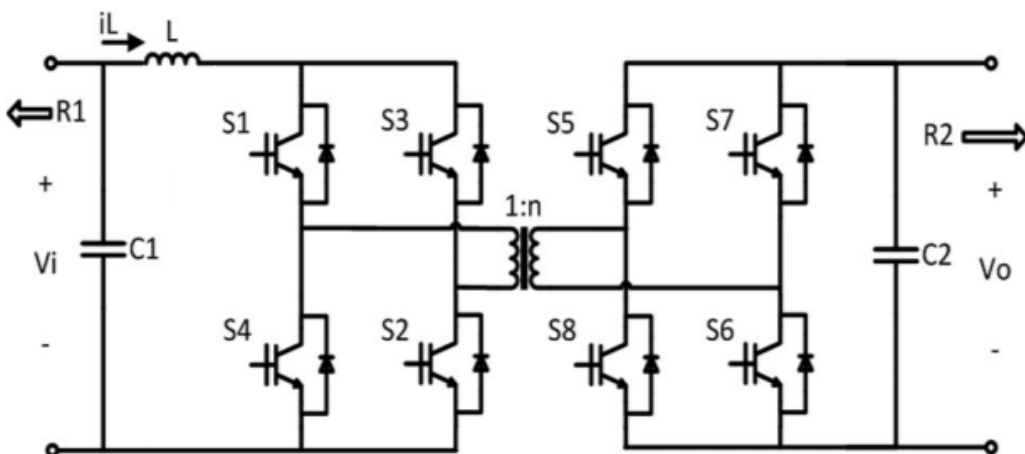
Figure 19: Structure of a bidirectional DC/DC converter[21].

The principle of having two active bridges like this is referred to as a Dual Active Bridge (DAB) converter. One of the bridges work as an inverter bridge, inverting the input DC voltage to a high-frequency square-wave AC voltage, and the other bridge rectifies the AC voltage to a DC output. The two bridges are connected through a high-frequency transformer and each bridge can consist of a different amount

of switches. The two bridges changes role for power flow in the opposite direction. The main advantage of this converter is related to the fact that it has a galvanic isolation, removing the direct connection between different parts of the electrical system and is thus meeting the requirement of isolation between unequal ground potentials[44]. Other advantages with the HF transformer are its high efficiency and small size due to the inverse proportional relation between frequency and size of the passive components, making it suitable for the transport industry where weight and space are limiting constraints. Among the main challenges related to the isolation transformer is the leakage inductance of the transformer, resulting in voltage spikes during transition between different operating switches[45]. Also, the ability to transfer power through the HF transformer is depending on the value of the leakage inductance and the switching frequency. An increase in both the switching frequency and the leakage inductance will for example lead to a reduced power transfer capability[46]. Therefore, the component ratings should be carefully calculated in order to achieve an optimal operation. However, the focus in this thesis will be on the two bridges and their operation, and the transformer will be assumed ideal in order to simplify the analysis. In the following section the commonly used half-bridge and full-bridge configurations will be discussed.

3.2   Half- and Full-Bridge Topologies

As mentioned, the half- and full-bridge topologies will be further discussed due to their simple and reliable design and their great applicability in DAB converters. Which of the two topologies is the better for the given application can be shown by comparing the full-bridge (FB) and half-bridge (HB) configurations as seen in figure 20. In figure 20a a full-bridge topology is shown where a high-frequency square-wave output voltage is produced with values of $+V_{dc}$ and $-V_{dc}$. This means that the full voltage V_{dc} is applied to the switches and the current stress on each switch will be equal to the load current I_{ac}. In comparison, the half-bridge topology utilize half the number of switches as seen in figure 20b. It also produce a high-frequency square wave output voltage of $+V_{dc}$ and $-V_{dc}$ when switch S_1 is on and off, respectively. But, due to its voltage boost capability that is doubling the voltage when operating at a duty cycle of 50%, the voltage stress on each switch will be twice the input voltage.

Figure 20: (a) Full-bridge and (b) half-bridge comparison[42].

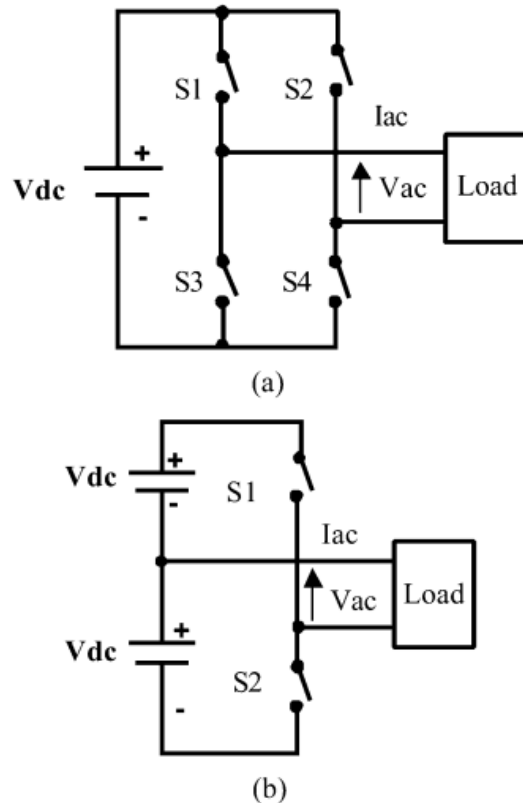The main difference between the half- and full-bridge topologies is the different amount of switches. Thus, when two of the transistors from the full-bridge configuration are removed, a half-bridge topology with less components can be created[42]. In the half-bridge topology shown in figure 20b two voltage sources of $V_{dc}/2$ could also have been connected as input to the half-bridge. The voltage stress on each switch would then have become lower but with the trade-off being a lower output voltage. For the half-bridge the amplitude value of the supply voltage to the isolation transformer will be half of the supply voltage compared to the full-bridge voltage, and thus the half-bridge current will be twice the full-bridge current. Therefore the switches must have higher ratings, questioning the total price and size of the converter. The half-bridge topology will thus have a collector peak current through its transistors with a value of

$$I_{Cpeak,HB} = \frac{P_{out}}{U_{DC}} \tag{3.1}$$

where P_{out} is the rated output power of the converter and U_{DC} is the input voltage to the half-bridge. For the full-bridge topology, assuming that the operation occur at an equal output power of 1 p.u., the current will be

$$I_{Cpeak,FB} = \frac{P_{out}}{2U_{DC}} \tag{3.2}$$

which is half of the current in the half-bridge transistors. The duty cycle will be set to 50% in the discussion in order to make an easy case study, and due to the fact that it won't exceed 50% for rated load and nominal voltage it is a reasonable choice for topology analysis[42]. Equation 3.3 and 3.4 shows the average current through the inverter for the half- and full-bridge topologies, respectively:

$$I_{Cav,HB} = \sqrt{\int_0^{0.5} (I_{Cpeak,HB}^2) dt} = 1.414 p.u. \tag{3.3}$$

$$I_{Cav,FB} = \sqrt{\int_0^{0.5} (I_{Cpeak,FB}^2) dt} = 0.707 p.u. \tag{3.4}$$

It is seen that the currents in the full-bridge topology are lower for the same power levels since twice the voltage levels at the transformer primary windings are applied. This means that a full-bridge topology can have switches with lower ratings compared to a half-bridge topology for the same power level, leading to smaller size of devices in addition to lower losses[42]. Also, the full-bridge can generate a zero output voltage, introducing the possibility to utilize improved modulation schemes. The disadvantage with the full-bridge is the higher requirement to gate drivers and a higher component count. However, for high-power applications, the higher efficiency of a full-bridge configuration would outweigh the higher component count.

Among the advantages with the half-bridge topology is a low-ripple DC current on the low voltage side, which is desirable when connected to for example a low voltage battery. However, the battery in this project will operate at the same voltage level as the DC grid. Also, for switches with the same current and voltage ratings, the power capability of the converter is proportional to the number of switches in the converter[41]. This means that a converter with eight switches can transfer twice the amount of power compared to a converter with only four switches. Therefore the full-bridge topology is seen to provide certain advantages that are beneficial for the given application. What should also be noticed is that several switching devices may have to be connected in parallel in order to meet the current ratings of the switches. This higher component count will also introduce an increase in both the cost and complexity of the system. When it comes to regulating the converter output, a duty cycle control is among the easiest methods to control the power switches, where the output voltage is proportional to the duty cycle[17]. However, this method causes high switching losses, and for high-power systems this is unacceptable. Another method is the phase-shift control, where each leg is individually controlled and this method will be further discussed in chapter 4.

3.3 Dual Active Half-Bridge

By connecting two half-bridges together through a HF transformer a Dual active Half-Bridge (DHB) converter can be designed as shown in figure 21. The converter consists of a current-fed side (side A) and a voltage-fed side (side B), where the current-fed side can include a storage device such as a battery in which a low ripple current is desired. The switches Q_1 and Q_2 have two roles in both the operational modes. For battery discharge-mode, meaning power transfer from A to B, they are first boosting the voltage from the input voltage level V_A to V_M at the auxiliary bus. They also perform an inversion of V_M from the input DC voltage to a square-wave AC voltage. This high frequency AC voltage allows for small passive components in the transformer due to the inverse proportional relation between frequency and size of filter components. On the voltage-fed side, the switches Q_3 and Q_4 function as a rectifier,
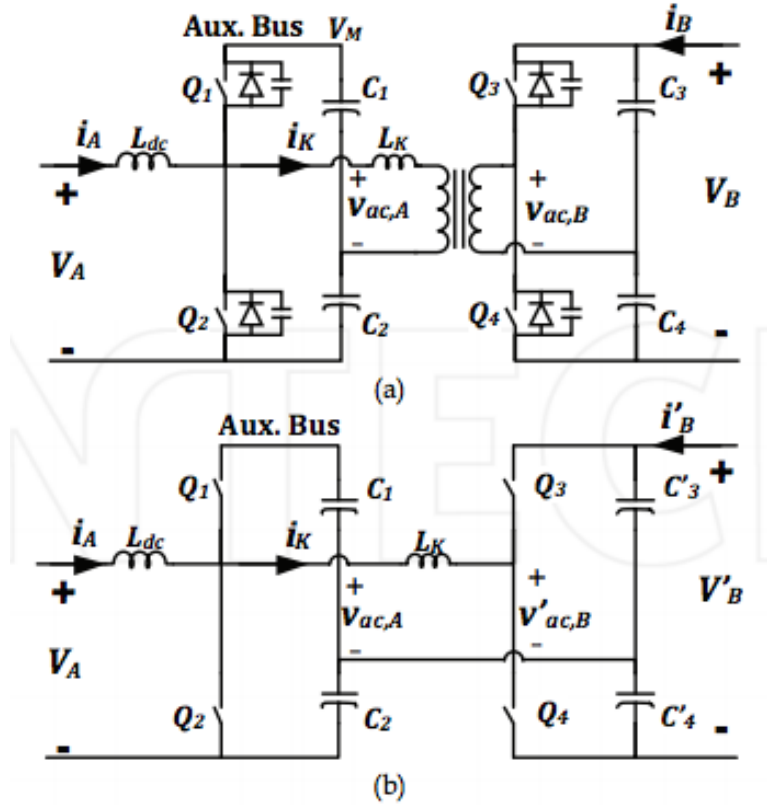
Figure 21: Dual half-bridge topology. (a) Circuit diagram and (b) idealized model[39].

supplying DC current to the DC-link of the grid side of the converter. Q_3 and Q_4 also have to switch in order to provide the phase shift between the A- and B-side voltages. The soft switching of Q_3 and Q_4 is also dependent on this phase shift[39]. For power flow in the other direction, meaning that the battery is charged, Q_3 and Q_4 inverts the AC voltage V_B before Q_1 and Q_2 both rectify the AC voltage and make a step in the voltage in order to meet the low-voltage level V_A from the auxiliary bus voltage level V_M. By having an inductor on the low voltage side of the converter, the current is smoothed before the voltage is stepped up, and therefore this half-bridge topology can be advantageous compared to the full-bridge topology as the voltage step will contribute to a lower current stress on the primary side of the transformer. In addition to this, a lower number of components is achieved for this half-bridge topology. The actual amount of power that is transferred from one side of the transformer to the other is determined by the phase shift between the square-wave voltages that are generated at each half-bridge.

Figure 22 shows the waveforms with 50% duty cycle for operation in both directions of the dual half-bridge topology. As seen in the figure, the phase shift has different polarity in the two directions, leading to opposite power flow directions. The current through the input inductor is thus negative in B to A mode. Equation 3.5 shows the average power transfer, where the bidirectional power range is achieved by varying the phase shift angle ϕ between -90 and +90 degrees[41]. Also, the amount of reactive power

transferred through the transformer should be minimized in order to maximize the efficiency. Since high phase-shift angles are related to higher reactive power flows, the series inductance L_K should be rated so that the power rating of the converter can be achieved for a low phase-shift angle[39].

$$P = \frac{V_A V_B \phi (1 - |\phi|)}{2n\pi L_K \omega} \qquad (3.5)$$
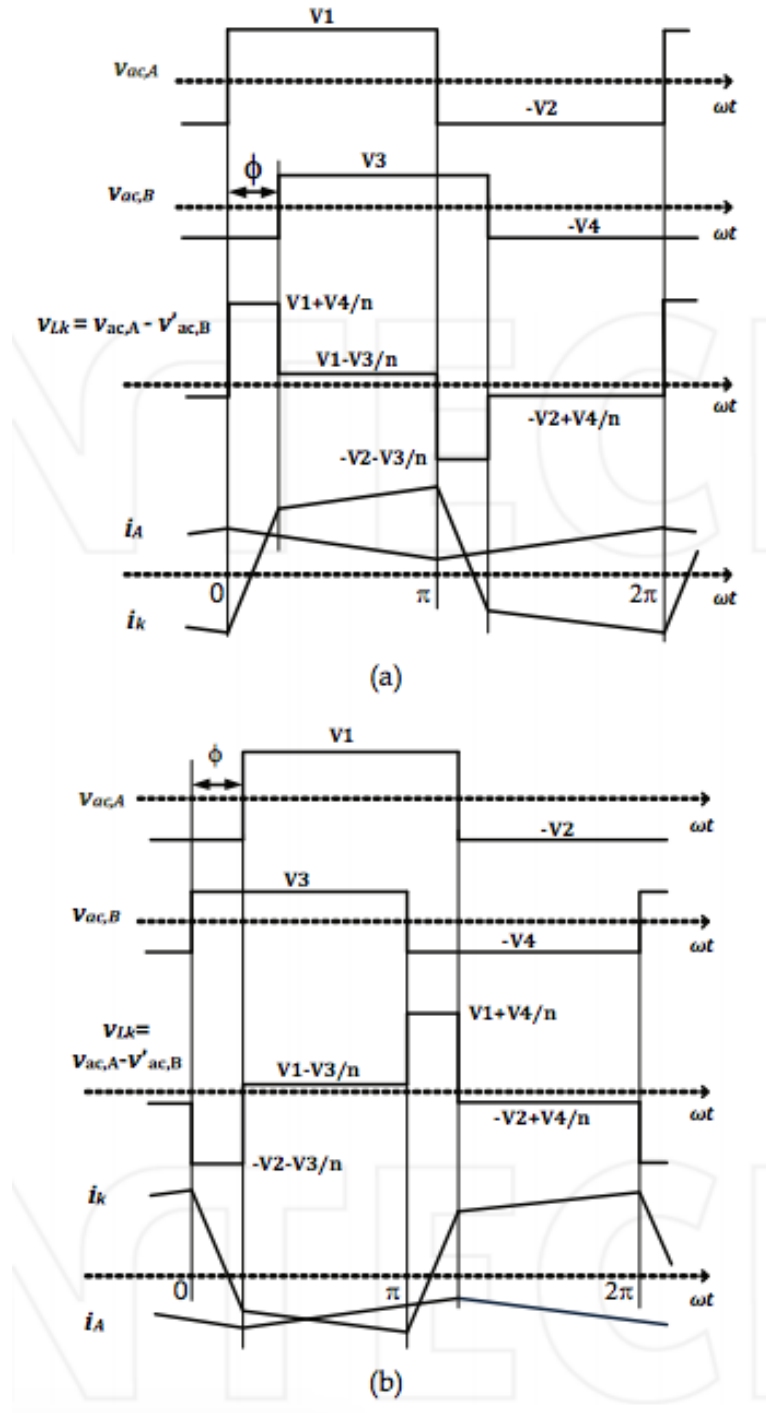
Figure 22: Dual half-bridge topology waveforms. (a) Power from A to B and (b) power from B to A[39].

Zero-Voltage Switching (ZVS) can also be achieved for all of the switches in this topology as long as the total current leaving a leg pole is lagging the voltage over the same leg. This will be explained in detail in chapter 4. For the converter given, this means that $(i_K - i_A)$ must lag the voltage over switch Q_2, namely V_{Q2}. In addition, $-i_K$ should lag V_{Q4}. Then the body diode will conduct while the switches

turn on and during turn off the voltage is close to zero due to the snubber capacitor, which includes the device parasitic output capacitance[39].

To summarize and conclude, this converter provide the following advantages:

- The number of switches is low compared to other topologies with the same power ratings;

- The range of bus voltages and loads is wide for soft-switching operation;

- Phase shift modulation control provides an easy control;

- The ripple current at the current-fed side is low, making connection of batteries appropriate.

The main disadvantages of the topology are related to ripple currents flowing in the splitting capacitors and unbalanced current stress between switches in the low-voltage side. The size and cost of the capacitors are also a drawback with the topology, especially for high power and voltage levels. Also, as mentioned in section 3.2, a half-bridge topology will operate at lower efficiency for higher power levels compared to a full-bridge converter. The discussion will therefore go on by looking at converters utilizing full-bridges on both sides of the HF transformer in order to achieve a higher efficiency for high-power systems.

3.4 Dual Active Full-Bridge

Another topology of isolated bidirectional DC/DC converters utilizing more switches in order to operate at a higher efficiency is the dual active full-bridge converter as shown in figure 23. In this topology the current will be flowing in both positive and negative directions during each half cycle, taking advantage of the negative portion of the hysteresis loop as well and reducing the chances of transformer saturation[47]. By using soft-switching techniques and phase-shift strategies of the voltage waveforms, the power transfer between the DC-buses can be controlled. By properly designing the snubber capacitors across the switches and the leakage inductance L_K, ZVS can be achieved and thus a high-frequency operation is appropriate. The anti-parallel diodes are also important components in order to achieve ZVS and their operational principle in combination with the snubber capacitor will be discussed in chapter 4. The phase shift ϕ
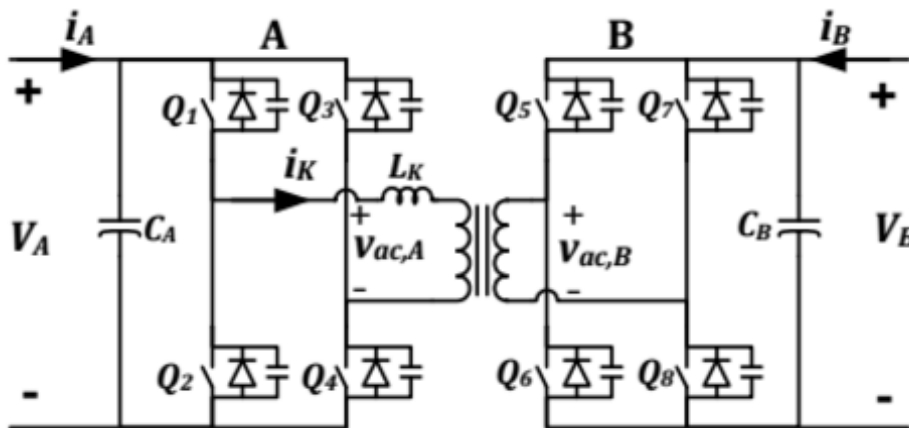
Figure 23: Dual active full-bridge topology[39].

determines the amount and direction of power for a fixed frequency operation mode[39]. The switches in each bridge operates in pairs, where switches placed diagonally (Q1,Q4 and Q2,Q3 for example) are turned on for half of the switching period each. This 50% duty cycle along with a controlled phase shift between the voltages in two legs lead to a nearly square-wave voltage that is transferred across the transformer. By properly controlling the switches, the phase shift between the converter voltages can be controlled, thus controlling the power flow. The average power that is transferred from one side to the other is determined by the input and output voltages, the phase shift, the switching frequency and the leakage inductance of the transformer. It is to be noted that the 50% duty cycle ignores the dead time of the switches. Figure 24 shows the waveforms of the Dual Active Bridge Isolated Bidirectional DC/DC (DAB-IBDC) topology.
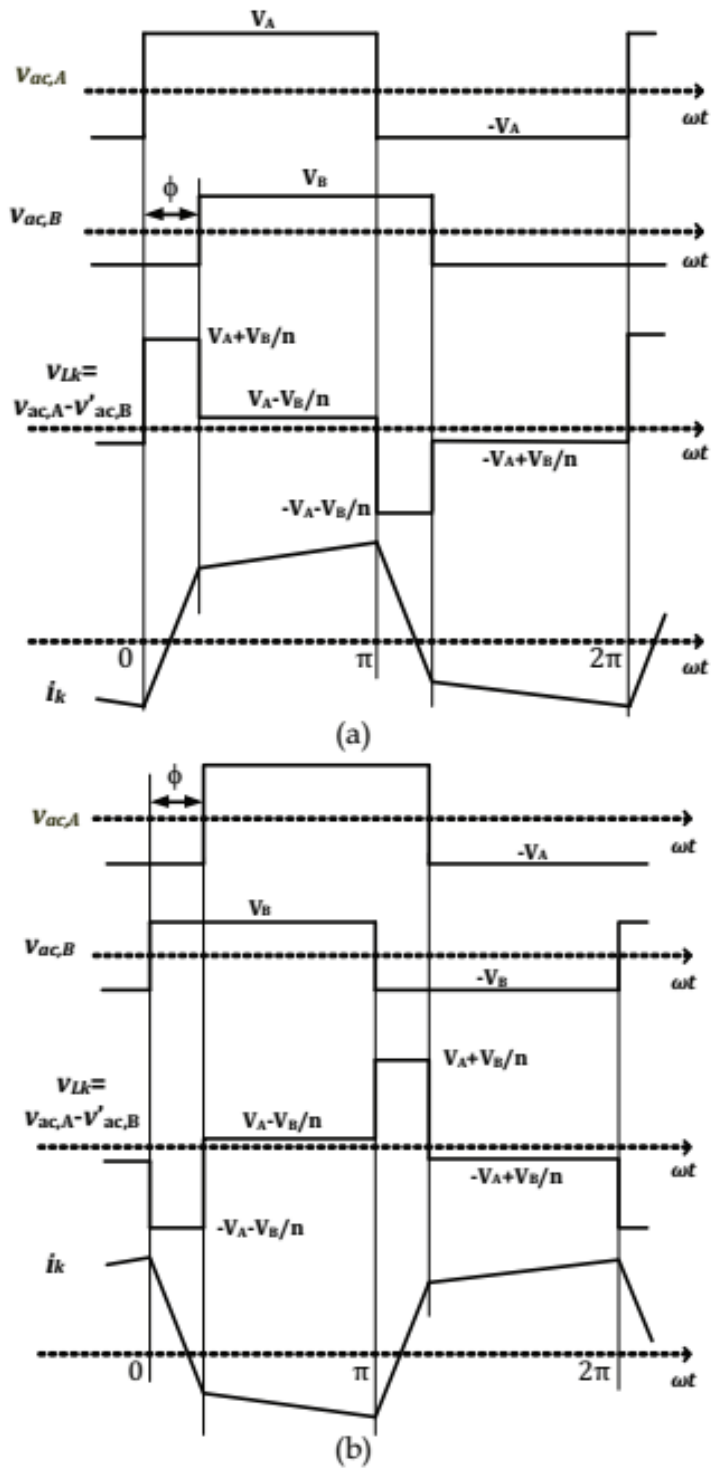
Figure 24: Dual active full-bridge topology waveforms. (a) Power from A to B and (b) power from B to A[39].

Among the advantages with the full-bridge topology is the fact that the capacitor ripple problems in the half-bridge are no longer present. This is due to the fact that the inductor current i_L now flows through the active switches and their freewheeling diodes instead of through the DC capacitors. In addition to this it has capacitors connected in parallel with the switching devices in order to achieve soft switching. These capacitors work as a snubber without losses, contributing to a soft switching. Also, the efficiency of the full-bridge converter is higher, which is an important feature when operating at high power levels. Thus, the full-bridge DAB-IBDC converter proves to perform well when operating at high power levels in addition to being reliable and power-dense.

3.5 Dual Active Full-Bridge with Input Inductor

Another configuration of the full-bridge DAB converter can be made by utilizing a current-fed full-bridge topology at the A-side as shown in figure 25. The leakage inductance of the transformer can lead to overshoots during current commutation and the smoothing inductor can contribute to reducing these transients. Figure 26 shows the operating waveforms, operating as an isolated boost-converter when power is transferred from A to B, and as a buck-converter when power is transferred from B to A. When power is transferred from B to A, the voltage-fed converter (Side B) is the active inverter. Switches Q_5 to Q_8 will then operate with ZVS. More details on the switching operation can be found in [48].
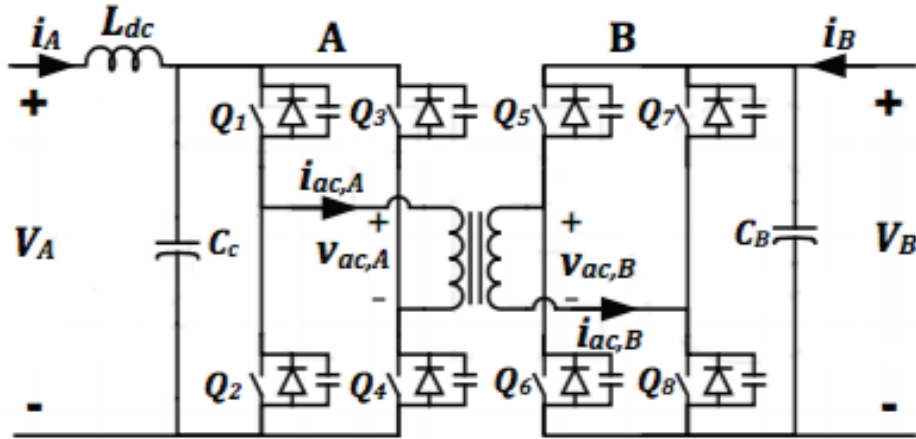
Figure 25: Dual active full-bridge topology with input inductor[39].

Among the advantages of having a current-fed topology are the following[39]:

- Protection against over-currents and short-circuits;

- The converter is not sensitive to transformer saturation;

- Low ripple input current, which makes it suitable for battery applications.

However, the disadvantages are:

- The input inductor is big and bulky;

- Potentially high losses and voltage spikes due to the leakage inductance of the transformer;

- High-quality capacitors are required due to high ripple on output current;

- Semiconductor switching devices need to be rated at a higher level than the operating DC voltage due to voltage spikes and boost operation.

In general, the component count and cost will be higher for the full-bridge converters compared to a half-bridge converter. For all of the topologies seen above, the voltage ratio between the two sides of the transformer can be defined as

$$d = \frac{V_B}{nV_A} \tag{3.6}$$

where V_A and V_B are the voltages on the A and B side respectively and n is the transformer turns ratio. Due to variations in both the input- and output-side voltages, this ratio will affect the converters ability to operate at ZVS. For a bridge leg, ZVS is achieved by letting the current leaving one leg pole lag the respective pole voltage[39]. This means that the voltage should cross zero before the current does, and according to the literature this can be achieved in all of the switches for a voltage ratio equal to 1[49]. The turns ratio n of the transformer should therefore be chosen in a way that fulfills this ratio. For values of d unequal to 1, the soft-switching capabilities of the converter will be reduced for lower load levels, and therefore the converter will operate less efficient for loads slightly higher than the average

load demand of the vessel. There are also reasons for not having a value of d equal to one. One of them is related to non-linear currents for high values of d, where a value of $d = 0.35$ is seen as a limit[50]. The flow of reactive currents through the converter will also increase for high values of d, and thus there is a trade-off in the design process between a high d-value with large ranges of ZVS and low switching losses or lower d-values where the conduction losses and reactive current flows are reduced. In this phase shift converter there are also more circulating currents and thus more conduction losses than in the traditional hard-switched Pulse-Width Modulation (PWM) converter. However, due to the reduced losses at high-frequency operation with soft-switching, the overall efficiency improves as the conduction losses are over-weighted by the improvement from soft-switching.
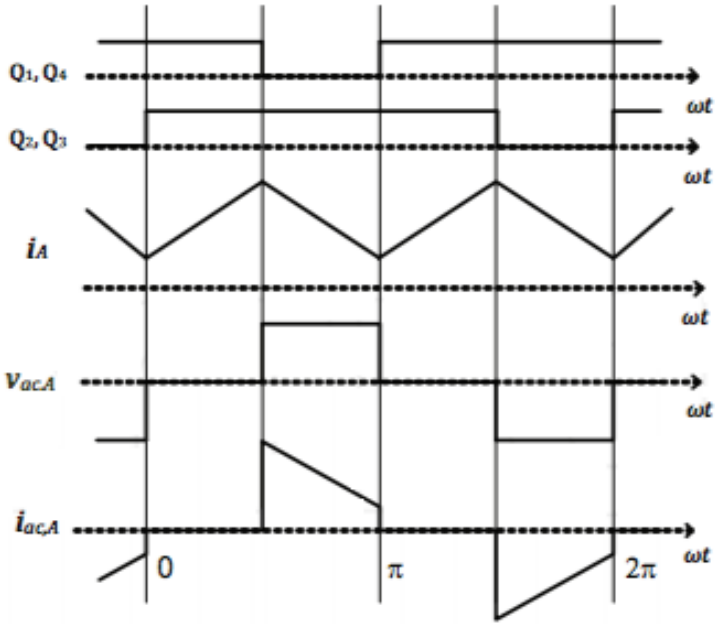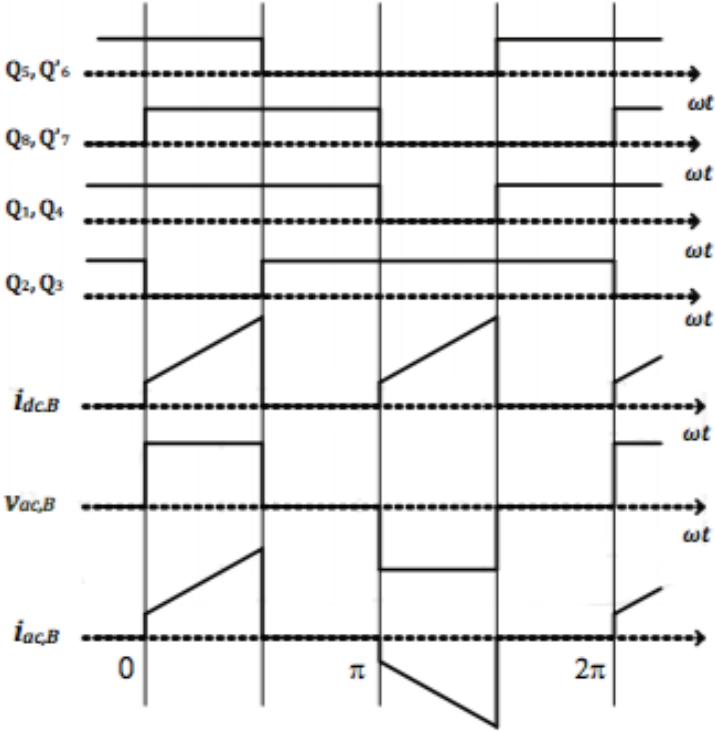
Figure 26: Operating waveforms. (a) Power from A to B and (b) power from B to A[39].

28

3.6 Three-Phase Dual Active Bridge Converter

The DAB topologies discussed till now have all been single-phase configurations. As was mentioned in section 3.2, the power transfer capability of a converter is proportional to the number of switches in the converter and therefore it can be interesting to analyze a converter utilizing even more than eight switches in order to further increase the efficiency. By using three half-bridges on both sides of the HF transformer, a three-phase converter can be designed. Three inductors and three high-frequency transformers are also needed. Thus, the changes made on a single-phase converter in order to analyze a three-phase DAB converter is relatively small since the setup is otherwise similar. However, the change in performance and utilization of the different components can be significant, both with regards to the passive components and the semiconductor devices.

Figure 27 shows a three-phase dual active bridge converter. As seen, each bridge consists of six switches and the operational principle is the same as for the single-phase converter. By letting each switch in a bridge operate at a duty cycle of 50% but with a 120 degree inner phase shift to the switches in the other two legs and with an outer phase-shift compared to the switches in the other bridge, power can be transferred through the high-frequency transformer.
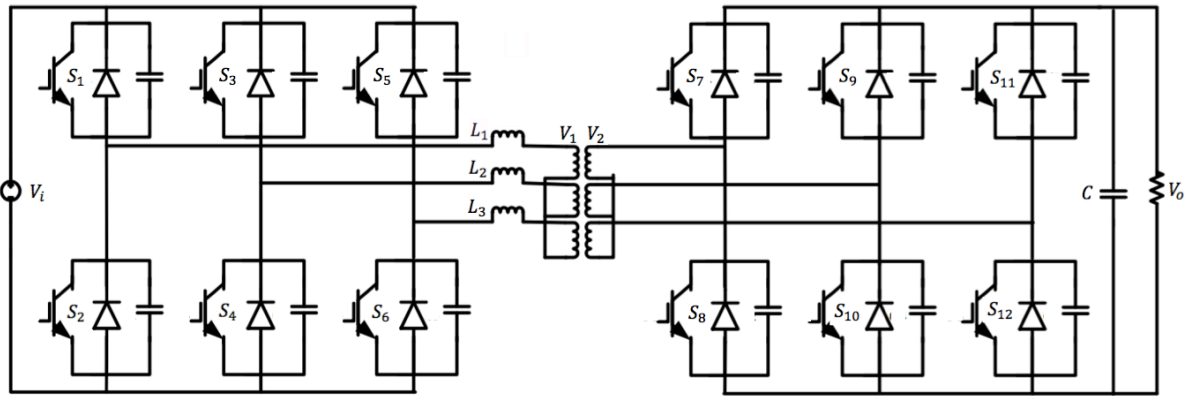
Figure 27: Three-phase dual active bridge converter[51].

The transferred power through the converter is given as

$$
P_0 = \begin{cases} \frac{V_i^2}{\omega L} d\phi(\frac{2}{3} - \frac{\phi}{2\pi}), & 0 \le \phi \le \frac{\pi}{3} \\ \frac{V_i^2}{\omega L} d(\phi - \frac{\phi^2}{\pi} - \frac{\pi}{18}), & \frac{\pi}{3} \le \phi \le \frac{2\pi}{3} \end{cases} \tag{3.7}
$$

where V_i is the input voltage, L is the total leakage inductance, ω is the frequency and ϕ is the phase shift between the two square-wave voltages [51]. The waveforms of the three-phase DAB converter is shown in figure 28.

Due to the fact that the current is distributed across several phase legs, lowering the current through each switch, the conduction losses in the three-phase DAB converter is also lower than in the single-phase topology[52]. The device ratings can also be lower for the same output power compared to the full-bridge single-phase topology. However, even though lower rated switches can lead to lower switch costs and efficiency benefits, the higher component count will contribute to a more complex converter.

The structure of a three-phase DAB converter predicts an efficient operation with advantages such as[53]:

- a reduced current stress on the switching devices as a result of the current sharing between several phase legs;

- cancellation of the flux in a balanced system due to the 120° offset between the phases, leading to a smaller transformer core material requirement;

- constant power operation due to the 120° phase shift that cancels the AC-component of the energy flow. Thus, the DC-link capacitor do not need to absorb the oscillations that occur in a single-phase converter and can therefore be designed with lower ratings;

- a transformer with low VA-rating can be used.
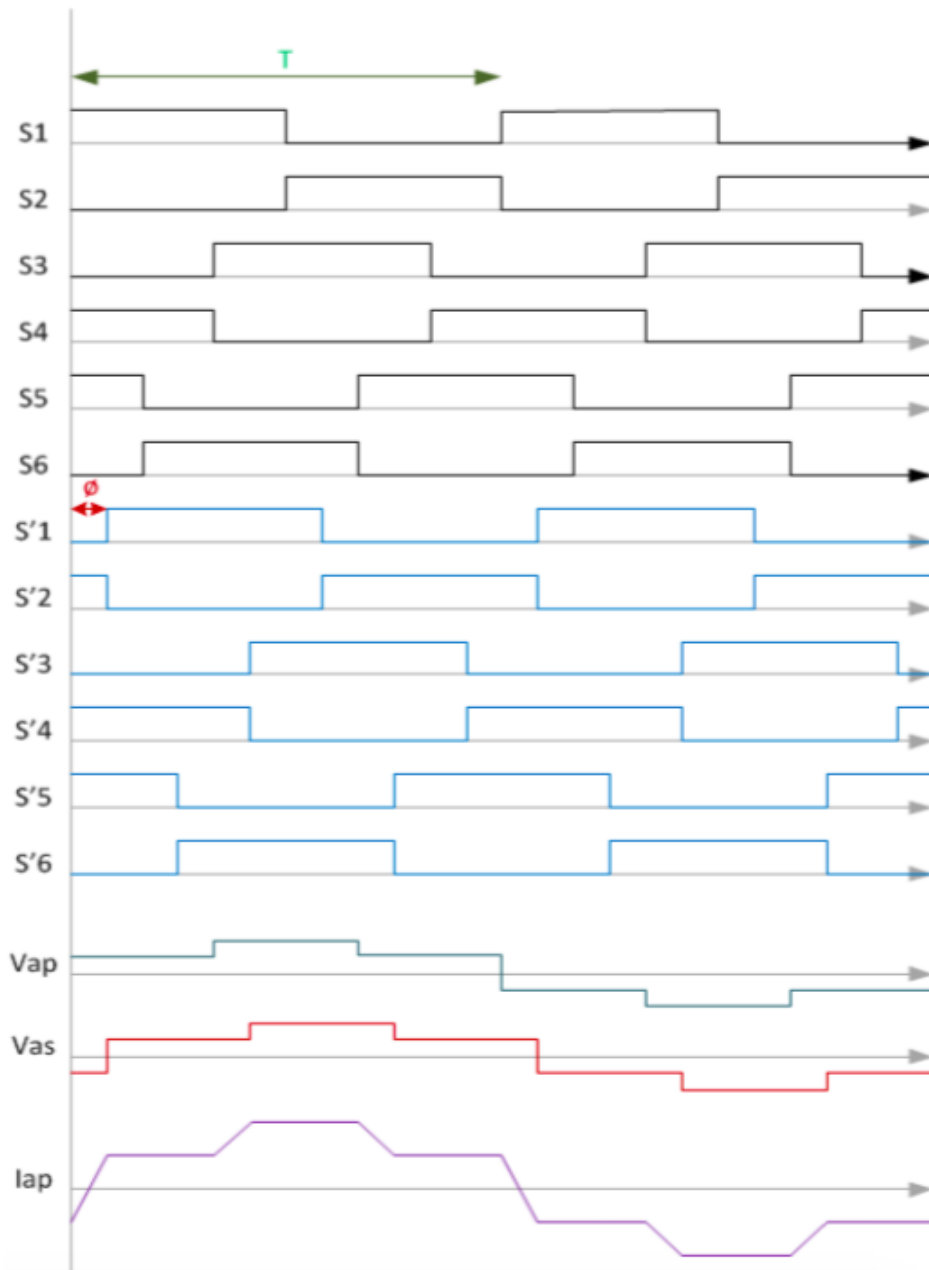
Figure 28: Three-phase dual active bridge converter waveforms[51].

It is therefore seen that the theoretical benefits of the three-phase DAB converter are superior to the single-phase converter with regards to both efficiency and device stress. However, conclusions drawn from earlier evaluations state that the theoretical advantages of three-phase DAB converters do not apply for practical implementation[52, 54, 55]. By lowering the current stress on each device, the benefits from an increased efficiency is negated by a higher component count, even though there is a lower peak current in the three-phase topology. In addition, the reduction of the three-phase transformer core lead to thermal challenges, as the smaller surface area leads to an increased ohmic and magnetic loss and is not capable of efficiently dissipating the generated heat. Therefore, based on the discussion that is made till now, the single-phase dual active bridge converter utilizing full-bridges is considered the most promising topology and will be further discussed in chapter 4 after briefly discussing some of the fault handling capabilities that are present with power electronic converters.

3.7 Fault Handling with Power Electronic Converters

As mentioned in the introduction, there are some challenges with regards to the protection of DC systems. The technology for AC systems is well-developed, but for DC systems the technology is relatively new, leading to the need for a new protection scheme in DC grids. This is related to the lack of a natural zero-crossing of the direct currents, the cost of DC circuit breakers (CB) in general as well as the lack of suitable DC breakers for marine vessels[56]. In DC grids, very fast current interruption is needed in order to avoid high stress on the semiconductor devices in the power converters and to avoid large parts of the electrical grid to be affected in case of a fault. Due to the low impedance of the DC cables, fault currents can become several magnitudes larger than the normal system currents within a few milliseconds and therefore it is important to have a good fault detection system in order to clear the fault as fast as possible.

In general, any protection system should contribute to handling faults in a way that makes the system operate as close to normal as possible even though some parts of the system are affected by a fault. Fuses have been used in AC systems for a long time due to their simple way of operation and low cost[57]. However, in low inductance DC systems where the current rate of change is high, the anticipated fault currents will be correspondingly high and thus the lifetime of the semiconductors as well as other components are highly vulnerable to faults. The slow operation of fuses also introduce challenges in achieving a well-protected DC system and therefore fuses are not commonly used in DC grids.

An advantage of the power electronic converters is related to the fact that the switches have a turn-off capability that provides full control of the currents through them[58]. The switches can be for example IGBTs, Gate Turn-Off thyristors (GTOs) or MOSFETs. By either turning the switches completely off or actively limiting the fault current, power converters can contribute to an active protection of the system during faults. The current will then be lower than a specific limit that is set in advance by the Fault-Current Limiter (FCL). When the breaker opens, the current from the source will be eliminated at once. However, the current on the load side will not cease instantaneously due to the energy stored in for example load filters and busbars. This energy will dissipate into the fault, and after the fault current on the load side is driven to zero, switches such as circuit breakers that are not rated to break high fault currents can physically isolate the faulty section from the rest of the system[58]. Such switches should be rated according to the efficient operation at rated values of current in the system, where examples of such operation can be bus-tie switches for split-mode operation or bus segmentation of the power grid. It is therefore seen that the absence of a power converter and a DC breaker can lead to very large short circuit currents, leading to damage of equipment.

Having a breaker based on solid-state technology can interrupt a current in microseconds[57]. They can also limit currents to a specified value or even force the current to zero by sensing the value of the current in order to find out when the current is too high. There are different types of FCLs, where the ones based on power electronics can provide advantages such as easy control, small physical sizes and a fast response. Figure 29 shows an example of how the DC/DC converter can be used as a FCL, controlling the current to the DC-bus and loads and thus being an important part of the protection system as well. In general, for any protection system, some design criteria are[57]:

- Reliability - the protection system should be predictable in the sense that it does not trip spuriously;

- Speed - the protection system clears the fault within a specified amount of time in order to avoid damage to personnel and equipment;

- Performance - says something about to which degree the loads are supplied during a fault. A higher performing protection system will have more loads operational during a fault and no critical overvoltage across the breakers. A well-performing system will therefore have a high redundancy to faults;

- Economics - cost of the protection system. The price of a high performance system will in general be higher than for a low performance system;

- Simplicity - how complex the system is. It depends on, among others, the amount of protection zones and number of parts.

In order to handle a fault current properly it must first be detected by the system. The detection of a fault is important both in order to quickly limit the amplitude of the current, but also in order to isolate only the necessary parts from the rest of the system in order to keep as much as possible of the system operational[58]. For alternating current systems the protection schemes are well-developed, utilizing differential current relays, distance relays, overcurrent relays and minimum voltage relays. For a DC system, some of these relays can also be used if they are installed correctly. By taking advantage of the low-impedance sources in the system that are able to provide large fault currents, tripping of the relays can be achieved if necessary. Among the challenges with a shipboard power system including energy storage is the fact that a bus section may be supplied from multiple sources. As long as the sources are connected through controllable power converters, this is not necessarily a big problem with regards to damage of equipment as each converter can limit their contribution to the fault current. However, when the currents are reduced to amplitude and rate of change levels similar to the normal operation currents, the detection of fault currents can be a challenge and thus new protection schemes are needed for DC distribution systems.

Figure 29: Power electronic converter used as fault current limiter.

For AC systems the protection schemes used have been based on the fact that AC currents have a natural zero-crossing every half period, making the extinguish of the arc in the mechanical circuit breaker feasible. This is something that does not happen with DC fault currents. Magnetic arc blowers and chutes can be used in DC circuit breakers in order to extinguish arcs by cooling them down and forcing the current to zero[58]. Therefore, faults in DC systems with arcs are specifically harmful as they do not necessarily self-distinguish. In order to interrupt such fault currents, the voltage across the interrupting device needs to be higher than the system nominal voltage and the voltage across the device should also be large enough to impose a high negative rate of change in the current that flows in the system. For power converters that consist of semiconductor devices, this increased voltage may lead to a breakdown of components if they are not designed to handle these increased voltages.

Also, even though power converters reduce fault currents, these reduced currents can be a challenge in some systems[58]. The higher alternating currents, which can be in the range of 10-100 times higher than the rated values helps in the operation of the arc chute of the CB. If the power converter in a DC system limit a fault current, the system may not even detect the fault, which can lead to more faults and cascade effects. The current-limiting effect of power converters may also lead to difficulties in separating normal operation and faulty conditions due to the fact that the reduced fault currents may not be that much larger than the normal operating currents are. This lead to the need for new methods of detecting faults. Also, due to the more expensive direct current circuit breaker in combination with mechanical isolating switches, alternative approaches, involving a combination of fuses, isolating switches and controllable power electronic converters should be used[10]. This means that in the future the solution to clear DC faults is to either use a hybrid concept consisting of a mechanical circuit breaker (similar to the ones used in AC systems) in combination with power electronic circuits, utilizing both of their advantages such as low losses and fast switching speeds or to use a purely semiconductor-based breaker, with the disadvantage of higher on-state losses[40].
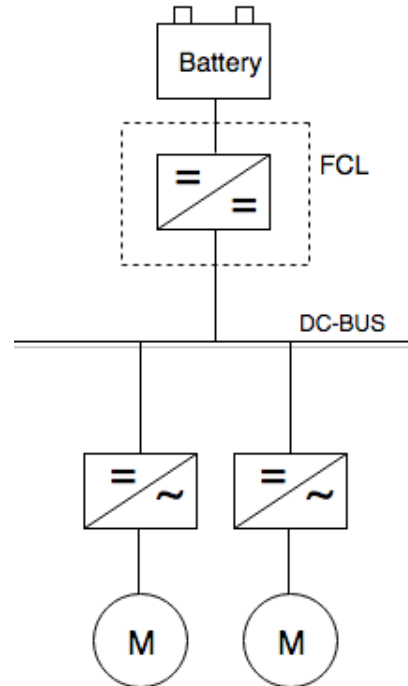
Another challenge in the detection of DC system faults is related to the lack of a fundamental frequency. For AC systems the frequency is used as a variable in order to measure the impedance in which the relays are given as input[58]. For direct current systems this is not possible and therefore introduce a challenge in the detection of fault currents. Some other methods have been proposed by the literature, where one method is based on the injection of a current in order to measure the voltage and then calculate the impedance. However, this is a time consuming measurement and computation method. Within power electronic converters the components also heat up during operation and therefore introduce losses. This heat will have to be removed, especially for high-frequency switching, and special cooling requirements or even limitations in switching speed may have to be introduced in order to avoid thermal breakdown. However, with regards to fault handling, a high switching frequency is desirable as it contributes to a lower breaking time.

From the aforementioned discussion, it can be seen that the combination of DC circuit breakers and power electronic converters can lead to an improved fault handling capability of the DC grid. The CBs are thus needed in order to clear the DC fault in the future for selective operation of the different parts of the grid. The converters will act quickly in order to make the grid de-energized before lower rated switches open in order to isolate faulty sections without handling large currents. This means that when a fault occurs and is detected by the system, the current is limited by the power converters that feed the faulty bus section. Then the relevant switches open in order to isolate the faulty section and reconfigure the system in an optimal way. Power converters will then reset and deliver power to the system again with the faulty section disconnected from the rest of the system. A great advantage with this protection scheme is related to the amount of energy that is dissipated into the fault. This is limited mainly to the energy stored in the filter components of the converter and in the DAB topology the amount of filter components are low, yielding good fault characteristics. Faults can therefore be cleared within a short amount of time, keeping the power grid operational for as much time as possible. However, it should be noted that this is only true for converters using controllable switches. As an example, for the AFE converter the diodes will conduct the current and the fault current is therefore left uncontrolled in this topology.

4 Steady-State Operation of the Full-Bridge DAB Converter

As discussed in chapter 2 and 3 it is seen that the requirements to the converter are the following:

- It must be able to operate in both directions for charge and discharge of the battery;

- It must be able to handle high power;

- It should operate with high efficiency;

- Isolation is required;

- A low component count and weight is beneficial;

- It should utilize a simple and reliable topology;

- Soft-switching is desired and will thus require additional components such as snubber capacitors in parallel with the switches and additional inductance in series with the transformer.

Among the different topologies the single-phase DAB converter proves to be the most promising topology for implementing a battery in a shipboard electrical power grid as it can provide these features while still being a relatively simple converter. This chapter will discuss the steady-state operation of the single-phase DAB-IBDC converter, starting with an ideal model without losses before the model is expanded in order to include losses.

4.1 Lossless DAB Model

Due to the promising operation of the DAB converter with respect to efficiency and volume, its steady state operation is analyzed. The converter consist of two voltage-controlled full-bridges connected together through a high-frequency transformer as shown earlier, and the power transfer is performed by having two phase-shifted time varying voltages across the equivalent inductance of the transformer plus any additional inductance needed for energy transfer[11]. This means that a simplified model of the dual active bridge converter can be made as shown in figure 30. The model represents the two square-wave voltages as two varying voltage sources v_{AC1} and v_{AC2}, where assumptions made in the model are:

1. no losses are present;

2. the magnetizing inductance and parasitic capacitance of the transformer are neglected;

3. the supply voltages V_1 and V_2 are considered constant.
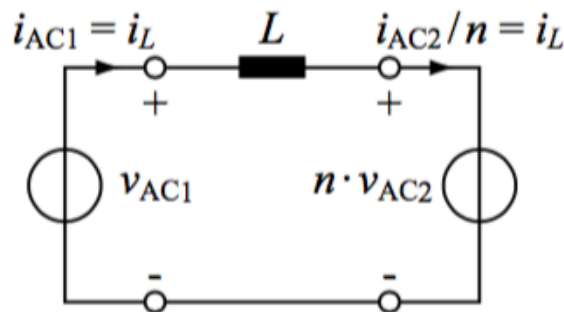
Figure 30: Lossless model of the DAB converter[11].

4.1.1 Current and Power in the DAB Converter

The voltage levels at the primary side are $+V_1$, 0 and $-V_1$ depending on the state of the switches in the primary bridge. For the secondary bridge the possible voltage levels are $+V_2$, 0 and $-V_2$. This means that the voltage across the inductor is equal to

$$v_L(t) = v_{AC1}(t) - nv_{AC2}(t) \tag{4.1}$$

where n is the transformer turns ratio. This leads to a current through the inductor at time t_1 equal to

$$i_L(t_1) = i_L(t_0) + \frac{1}{L} \int_{t_0}^{t_1} v_L dt \quad \forall \quad t_0 < t_1 \tag{4.2}$$

with an initial current of $i_L(t_0)$ at time t_0. The delivered or received instantaneous power of the two voltage sources can then be expressed as

$$p_1(t) = v_{AC1}(t) i_L(t) \tag{4.3}$$

and

$$p_2(t) = nv_{AC2}(t) i_L(t) \tag{4.4}$$

As seen from equation 4.2, the calculation of $i_L(t_1)$ is easier if the interval between t_0 and t_1 has a constant voltage level of $v_{AC1}(t)$ and $v_{AC2}(t)$, which should be kept in mind when finding an interval to integrate the voltage in order to determine the inductor current. Since the model is assumed to be lossless, $P_1 = P_2$ and the average power during one switching cycle can be found as

$$P_1 = \frac{1}{T_s} \int_{t_0}^{t_0+T_s} p_1(t) dt \tag{4.5}$$

and

$$P_2 = \frac{1}{T_s} \int_{t_0}^{t_0+T_s} p_2(t) dt \tag{4.6}$$

where $T_s = 1/f_s$ is the switching period. It is thus seen how the power transfer can be adjusted by either changing

- the phase shift $\phi = \phi_2 - \phi_1$ between the voltage sources $v_{AC1}(t)$ and $v_{AC2}(t)$, being in the range between $-\pi/2$ and $+\pi/2$,

- the duty cycle of $v_{AC1}(t)$ or $v_{AC2}(t)$, D_1 or D_2, with values between 0 and 0.5 or

- the switching frequency f_s.

Since both the switching frequency and the duty cycle is constant in this work, the power transfer is adjusted by changing the phase shift, ϕ. However, an expression for the instantaneous power can also be inserted in equation 4.5 and 4.6 as will be shown in the following section. The control parameters discussed till now are shown in figure 31.
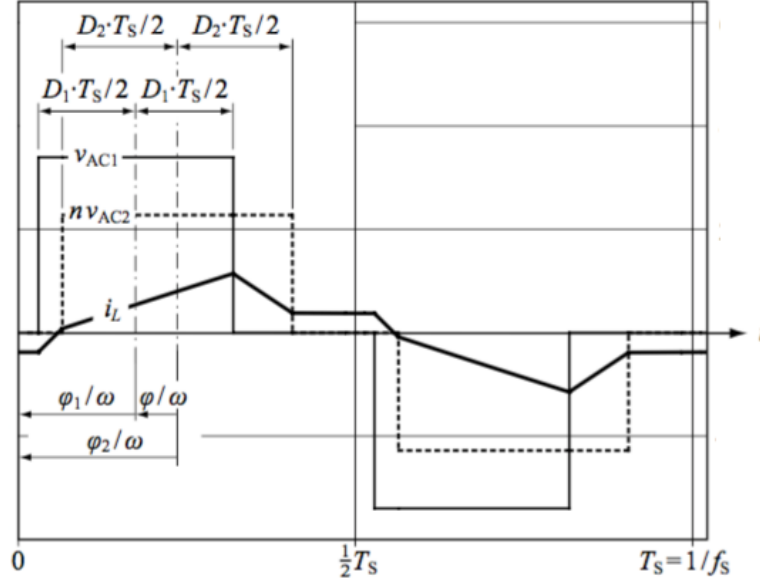
Figure 31: DAB control parameters[11].

4.1.2 Phase Shift Modulation

The power flow through the converter will be explained using the full-bridge DAB-IBDC converter as shown in figure 32 as example[59]. One of the bridges will work in the inversion mode while the other one works in the rectification mode. The two bridges are controlled in order to produce a high-frequency AC square-wave voltage at the terminals of the transformer, and by having a phase-shift between the two voltages the current magnitude and direction through the leakage inductance of the transformer and thus the power flow through the converter can be controlled. The input and output voltages are V_1 and V_2, respectively, when the converter transfer power from bridge H_1 to H_2. The switching frequency is f_s and the turns ratio of the transformer is n. In addition to the internal inductance of the transformer, some additional inductance may be needed for energy transfer, and the equivalent leakage inductance is shown in the figure as L.
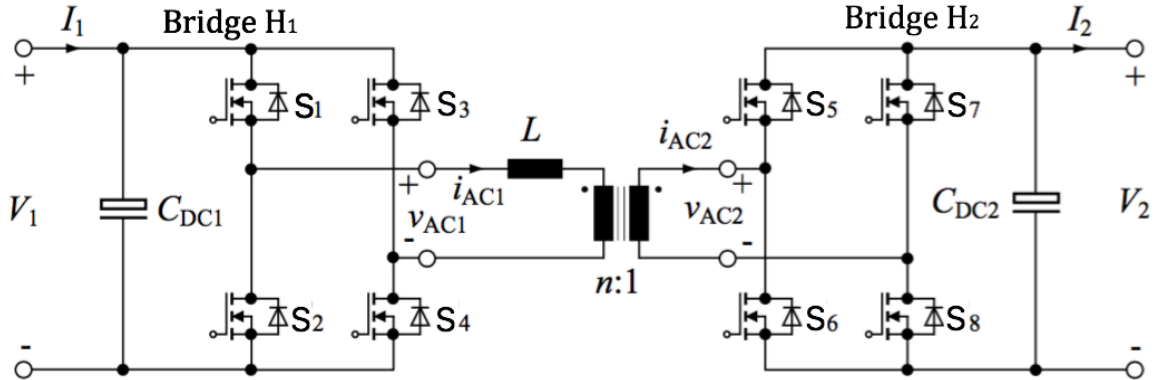
Figure 32: Topology of DAB-IBDC[11].

As mentioned previously in this section the converter will be operated with a constant switching frequency and duty cycle. The effect of deadband must also be included in the control in order to avoid a short between switches placed in the same leg of the converter[41]. However, this will not be discussed in detail in this thesis and the pulse width in percentage of a period will be set to 49.5% during simulations in order to avoid both switches in a leg to conduct at the same time. This means that there is a time (in total 1% of a switching period) where all of the switches in the bridge are turned off and the inductor current will oscillate at a value close to zero with the associated chance of varying the output voltage polarity[42]. These varying voltage waveforms may lead to Electromagnetic Interference (EMI)

and should therefore be avoided by the use of filters.

However, in this analysis the duty cycle will be regarded as maximum, equal to $D_1 = D_2 = 0.5$, thus avoiding the effect of deadband. The two switches in a phase leg is then operated for half of the switching period each. The voltage across the transformer can then be determined by properly controlling the phase shift between these two square-wave voltages and different combinations of primary and secondary voltages can be used to shape the current through the transformer and thus the magnitude and direction of power flow as well. Thus, the phase shift ϕ is the only parameter that is used to control the power transfer and is defined as positive when the primary voltage leads the secondary voltage, transferring power from bridge H_1 to H_2. This modulation principle is referred to as phase shift modulation and is the most common method used for DAB converters[11]. The value of the voltage sources is then either $-V_1$ or $+V_1$ for $v_{AC1}(t)$ and $-V_2$ or $+V_2$ for $v_{AC2}(t)$ as seen in figure 33. Due to the constant level of V_1 and V_2 during a switching period, the steady-state values of the voltage sources and the current through the inductor equals

$$v_{AC1}(t+T_s/2) = -v_{AC1}(t)$$
$$v_{AC2}(t+T_s/2) = -v_{AC2}(t) \tag{4.7}$$
$$i_L(t+T_s/s) = -i_L(t)$$
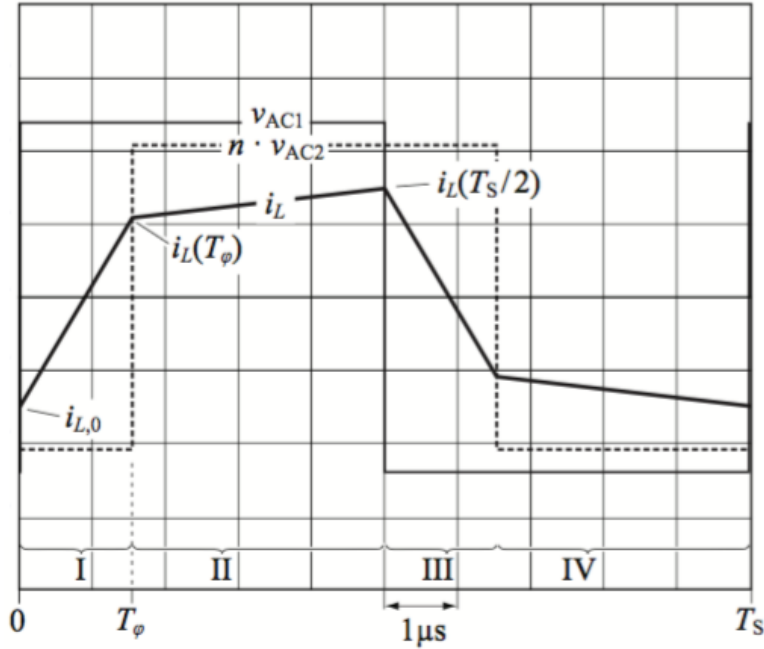
Figure 33: Inductor current and transformer voltages[11].

The fact that the voltages are constant during each half-cycle makes the calculation of the power transfer easier as only the first half-cycle needs to be considered and it can be found as

$$P_1 = \frac{1}{T_s}\int_0^{T_s} p_1(t)dt = \frac{2}{T_s}\int_0^{T_s/2} v_{AC1}(t)\dot{i}_L(t)dt = \frac{2V_1}{T_s}\int_0^{T_s/2} i_L(t)dt \tag{4.8}$$

From equation 4.8 it can be seen that the inductor current needs to be found in order to determine the power P_1. In the period where $0 < t < T_s/2$ (period I and II in figure 33), the current has two expressions for operation in steady-state. The first time interval gives

$$i_L(t) = i_{L,0} + (V_1 + nV_2)t/L \quad \forall \quad 0 < t < T_\phi \tag{4.9}$$

and the second interval gives

$$i_L(t) = i_L(T_\phi) + (V_1 - nV_2)(t-t_1)/L \quad \forall \quad T_\phi < t < T_s/2 \tag{4.10}$$

37

where the phase shift ϕ is assumed to be positive and L is the leakage inductance of the transformer plus other series inductance needed for energy transfer. By writing T_ϕ as $\phi/(2\pi f_s)$ where f_s is the switching frequency and by using the symmetry shown in equation 4.7, the inductor current can be written as

$$i_{L,0} = \frac{\pi(nV_2 - V_1) - 2\phi nV_2}{4\pi f_s L} \tag{4.11}$$

for a positive phase shift and a transformer turns ratio n. However, this will also apply for a negative phase shift, and thus an expression for the transferred power can be found as

$$P = \frac{nV_1V_2\phi(\pi - |\phi|)}{2\pi^2 f_s L} \quad \forall \quad -\pi < \phi < \pi \tag{4.12}$$

where ϕ is related to the duty cycle as $D = \phi/\pi$. It can therefore be seen that V_1 should lead V_2 in order to transfer power from bridge H_1 to H_2 in figure 32. This is for a positive phase shift ϕ between the two bridges. The average input current is found as

$$I_{av} = \frac{nV_2}{2\pi^2 f L_K}\phi(\pi - |\phi|) \tag{4.13}$$

and this current will be determining the switch-ratings of the converter for the phase angle that gives the maximum power transfer ($4MW$). For the phase-shift modulation control, special attention should also be given to the value of the transformer leakage inductance and turns ratio. This is due to the fact that the phase shift ϕ, for a constant switching frequency, is the only parameter that can be used to reduce the Root Mean Square (RMS) currents of the transformer since this current solely depends on the DC-voltages as well as the phase shift[60]. By calculating the derivative of the power with respect to the phase shift angle ϕ, the maximum power transfer is found for

$$\frac{\delta P}{\delta \phi} = 0 \tag{4.14}$$

with a solution

$$|P_{max}| = \frac{nV_1V_2}{8f_s L} \quad for \quad \phi = \pm\pi/2 \tag{4.15}$$

Equation 4.15 also show the relation between the maximum power transfer and the value of the converter inductance, where it is seen how a change in the inductance value affects the maximum power transfer capability of the converter for a fixed-frequency operation. For a given power level, the required phase shift can be found by rearranging equation 4.12 into

$$\phi = \frac{\pi}{2}\left[1 - \sqrt{1 - \frac{8f_s L|P|}{nV_1V_2}}\right]sgn(P) \quad \forall \quad |P| < |P_{max}| \tag{4.16}$$

where sgn(P) refers to the sign of the power, giving a positive phase-shift value for a positive power transfer and a negative phase-shift value for a negative power transfer. When it comes to actual phase-shift control strategies of the DAB-IBDC, the methods for single phase-shift (SPS), extended phase-shift (EPS) and dual phase-shift (DPS) will be discussed based on the DAB-IBDC topology shown previously in figure 32.

Figure 34 shows the square-wave signals from switches $S_1 - S_4$ in bridge H_1 and $S_5 - S_8$ in bridge H_2 with a duty ratio of 50%. The alternating output voltages on each side of the transformer are shown as v_{AC1} and v_{AC2} and i_L is the inductor current. The period of switching is shown as T_{hs} and therefore DT_{hs} is the phase-shift angle. The SPS control method lets diagonal switches operate in pairs, meaning (S_1, S_4) and (S_2, S_3) on the H_1-side and (S_5, S_8) and (S_6, S_7) on the H_2-side in order to produce two two-level square-wave voltages with a phase-shift as seen in figure 34a. Advantages with this control method is related to its highly dynamic control, small inertia and good soft-switching capabilities. The phase-shift ratio is denoted by D, where $D = \phi/\pi$ and thus by adjusting ϕ the voltage across the leakage inductance of the transformer is controlled. This single phase-shift ratio is thus the only parameter that is varied in order to control the active power flow, and thus the reactive power flows are not controllable in this method. This is seen as one of the main disadvantages of the method as the transformer leakage

inductance leads to circulating currents for unequal voltages on the two sides. This can be seen as the yellow area in figure 34a and is a result of the primary current not being in phase with the primary voltage. This will make a portion of the power, called backflow power, being sent back to the voltage source instead of crossing the inductance, thus not doing any useful work and leading to a reduced efficiency of the converter[61]. Also, the ZVS range is limited, leading to high power losses and thus the need for more optimal control methods if the load is to be varied within a large power range.
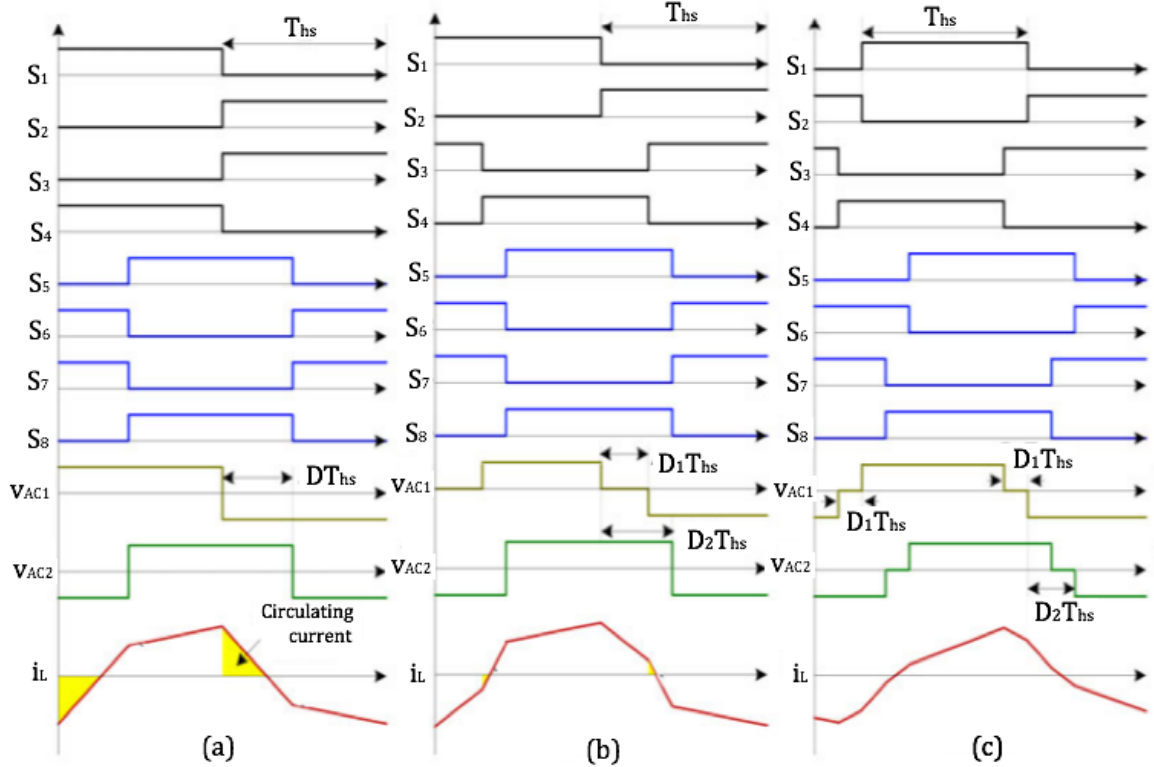
Figure 34: (a) SPS control. (b) EPS control. (c) DPS control. It is to be noted that the average values of v_{AC1} and v_{AC2} are zero for one switching period in steady-state operation in order to avoid transformer saturation[41].

The EPS method shown in figure 34b can improve the efficiency of the converter in addition to improving the weakness related to the limited ZVS range of the SPS method. This leads to less current stress in addition to a more flexible regulation. The switching pattern in the EPS control is different from the SPS method in the sense that the switches in one bridge switch in pairs and the other bridge is switched with an inner phase-shift ratio D_1 between the two legs, leading to a three-level square wave from one bridge and a two-level square wave from the other as seen by v_{AC1} and v_{AC2} in figure 34b. This will also lead to reduced circulating currents. The outer phase-shift ratio D_2 is the phase shift between the primary and secondary sides and is used to control both the magnitude and the direction of the power flow while D_1 is used to limit the circulating currents and to achieve a useful ZVS range. Thus, the disadvantages of the SPS control method seems to be improved in the EPS method. However, the disadvantage of implementing this method is related to the change of power flow direction and the need for a change in operating states of the bridges in order to keep the circulating currents low.

The last method is referred to as the DPS control method and is shown in figure 34c. Here, both bridges are switched with an equal inner phase-shift ratio D_1 and with an outer phase-shift ratio D_2 between the primary and secondary sides. This leads to a three-level square-wave AC voltage from both the bridges with a low current stress, a large ZVS range, high efficiency and a the need for a small output capacitance[41]. The sum of D_1 and D_2 must be less than or equal to one since D_2 will not be able to control the power flow for a sum higher than one, leading to a converter out of control[62]. If the losses

in the converter are neglected, the power flow at DPS control is found as

$$P = \begin{cases} -\frac{nV_1V_2(D_1^2+2(-1+D_2)D_2)}{4Lf_s}, & D_1 < D_2 \\ -\frac{nV_1V_2D_2(-2+2D_1+D_2)}{4Lf_s}, & D_1 \geq D_2 \end{cases} \tag{4.17}$$

with a constraint being that

$$D_1 + D_2 \leq 1 \tag{4.18}$$

From this it can be seen that when D_2 increase, the operation region of D_1 decrease. Thus, there is a trade-off between having small circulating currents and being able to transfer a large amount of power. The fact that both of the bridges operate at the same switching pattern makes the operating states in both directions the same and the challenge in the EPS method related to change of power flow is thus solved. The DPS control method can therefore offer a good performance in addition to an easy implementation.

To conclude, the requirement to change the operating state for different power flow directions makes the EPS method difficult to implement. Since the shipboard converter needs to operate efficiently in both directions and the power flow direction can change rapidly and often, the SPS and DPS control methods are seen as good control methods due to their high efficiency, easy implementation and good performance. As one of the advantages with the DPS control is that it can achieve ZVS for several switches when the converter operates at different voltage ratios, a justification of the use of SPS control is made due to the 1:1 voltage ratio of the used converter in this thesis[63]. For a transformer with voltage ratio equal to 1, ZVS is achieved for all of the switches in a dual active bridge converter operating with the SPS control and thus a high efficiency can be achieved for operation at high switching frequencies. This is also a reason to design the battery pack in order to achieve a voltage level that matches the voltage level of the DC-grid.

4.1.3 Soft-Switching

The soft-switching range and capabilities of DAB converters are also depending on the component choice and configuration. Since the converter efficiency will decrease rapidly as a result of circulating currents and unequal amplitude of the two AC voltages, these components should be chosen carefully[41]. The correct component choice can lead to improved performance and different topologies have been discussed in the literature for increased soft-switching performance. The solutions vary from simple LC-type resonant configurations to more advanced asymmetric and symmetric CLLC types. The parasitic components of the switching devices can be taken advantage of, but if these are too low to achieve ZVS in the required load range, additional components must be added. This can be by means of placing capacitors in parallel across the switches and by having an inductor in series with the transformer.
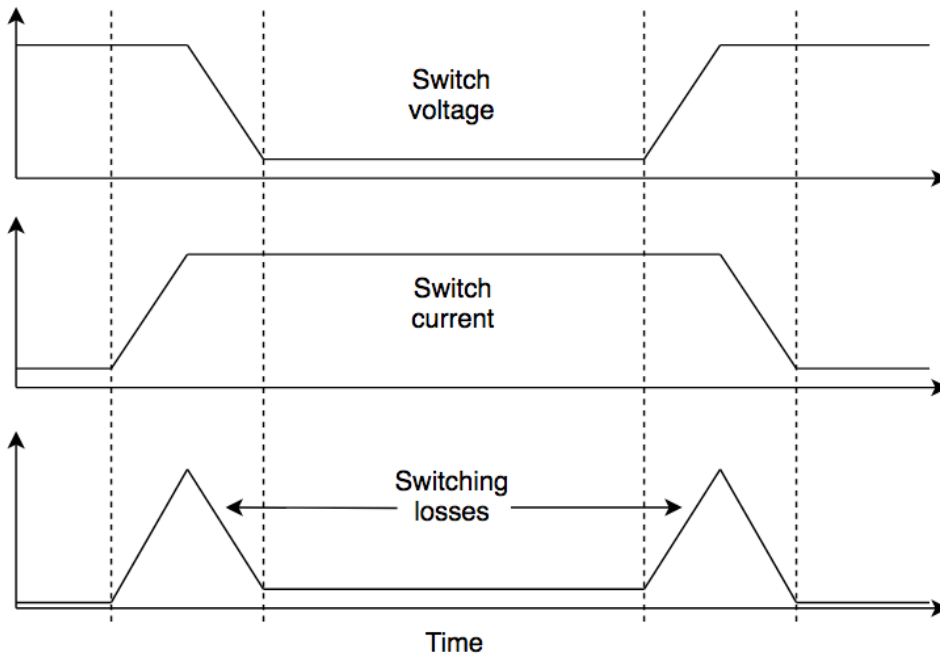
Figure 35: Switching losses during hard switching.

Figure 35 shows the switching losses that occur for a hard-switched converter. As seen, both the current through and the voltage across the switching device are non-zero at the same time, leading to a short time of losses referred to as switching losses. These turn-on and turn-off switching losses will occur once every switching period, leading to large losses for high-frequency operation. A solution to this problem is to use a resonant circuit as seen in figure 36, where a simple LC series resonant tank is illustrated and can be used to shape the voltage and current in order to provide ZVS and/or Zero-Current Switching (ZCS). Since the load is in series with the resonant tank, the converter appear as a current source to the load and is thus not suitable for several-output systems.
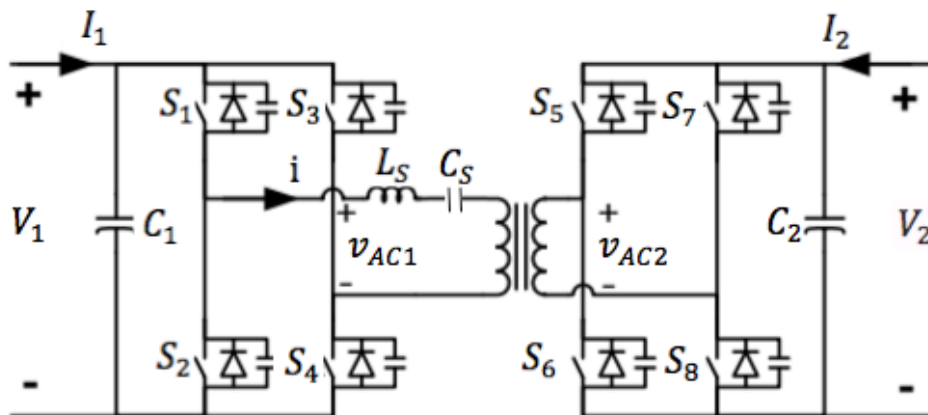
Figure 36: DAB-IBDC with LC-type resonant[39].

Figure 37 shows a symmetric CLLC resonant tank where the power and output voltage are often controlled by a variable-frequency modulation technique[41]. It can provide a wider soft-switching range than the LC filter and can thus be interesting in some application areas where this is crucial. However, for a system where the loads are fluctuating with fast changes between the power flow direction, an LC-type with a fast bidirectional transition speed is beneficial due to its simple phase-shift control. Thus, the resonant components will lead to more optimal operational frequencies and the efficiency of the converter will increase as a result of this.

Another option is to use resonant switches, utilizing resonant elements in order to shape the voltage across and current through the switches. This can be capacitors connected across a switch in order to

achieve ZVS or the transformer stray inductance in order to achieve ZCS. The parasitic elements of the switches can sometimes be large enough, but additional components will have to be added otherwise, such as for an IGBT where the capacitance is too low, introducing the need for a snubber capacitor in parallel with each IGBT as is also shown in figure 37. The snubber capacitors will then charge through the energy stored in the leakage inductance and from the source[64, 65]. Due to this, additional series inductance may have to be added to the transformer leakage inductance in order to achieve a large enough stored energy so that soft-switching can be achieved in the converter. The snubber capacitor will lead to an increased voltage rise time and thus lower losses at turn off since both high current and voltage at the same time is avoided. The capacitors should also be discharged in advance of the turn-on of the switches in order to avoid large currents through the switches and thus large turn-on losses[66]. By properly choosing these component ratings, the switching losses can be very low as will be explained in the following.

Figure 37: DAB-IBDC with symmetric CLLC-type resonant tank[39].

In order to reduce the losses related to the switching actions, the conducting and non-conducting time of the switches should be carefully controlled. These transitions between different switch-states can occur in two different ways referred to as linear transitions and resonant transitions. By assuming ideal devices, the snubber voltage across a switch will change linearly at 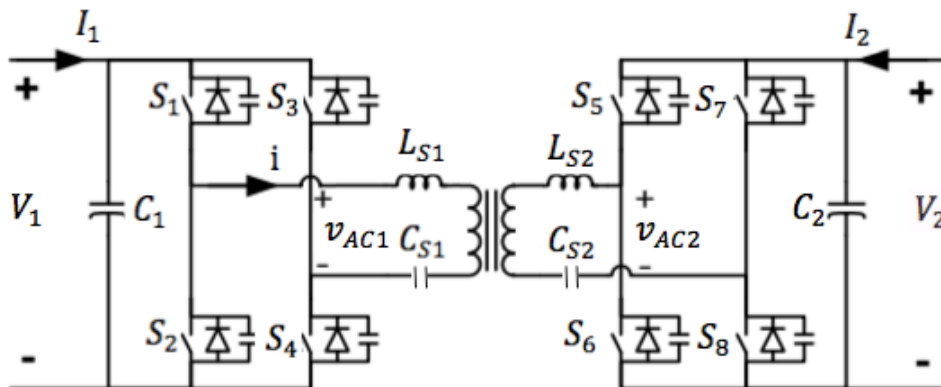the end of a power transfer period when the snubber capacitor takes over the current in the respective leg. When a snubber capacitor, let's say the one connected to S_8 in figure 32, is fully charged the voltage across it equals the input voltage and the voltage across the other switch in the same leg (S_7) is zero. This allows for low switching losses at the turn-on of switch S_7 since the parallel diode of S_7 clamps. For a small amount of time, the power transfer through the transformer is then zero since the voltage on the primary is zero and the primary inductor energy starts circulating between switch 1 and 3, flowing in the diode of switch S_3. When the diode of switch 3 stops conducting after this freewheeling period, switch S_5 is turned off. A resonant circuit is then created by the primary inductance and the snubber capacitors of switch S_5 and S_6. The voltage across switch S_5 will be zero at the end of this period if the snubber capacitor and primary inductance ratings are chosen appropriately. The voltage across S_6 will be equal to the input voltage and thus the input voltage is applied across the primary inductor. The diodes of switch S_6 and S_7 will conduct the primary current even though these switches have positive gate signals and switch S_6 can be turned on in this interval. When the current reverses, switch S_6 and S_7 starts conducting.

What should be noticed from this is that all of the switches are turned on while their parallel diodes are conducting. Therefore, the turn-on losses are eliminated as a result of the resonance between the snubber capacitance and leakage inductance of the transformer being tuned in order to have switching actions during the zero-crossings. The snubber capacitors across the switch also lead to an increased rise-time of the voltage, keeping the voltage low during transitions and thus the turn-off losses are also very low. The linear transition makes the charging of the capacitors easy as the full load current is applied also for light loads. Circulating currents in the primary bridge (H_1) during the freewheeling intervals in the resonant transition may also introduce the need for additional inductance in series with the leakage

inductance of the transformer, requiring careful calculations in order to have a low-current transition. The challenge lies in determining the resonant components and the determination of these components will be further discussed in chapter 5. However, if the components are rated properly, the converter can operate at high switching frequencies in order to reduce the size of the magnetic components and still have negligible switching losses. The main challenge is then related to the conduction losses in the switches.

Among the disadvantages with these resonant structures is that they introduce additional components with their respective increase in system size and cost. There is thus a trade-off between having good soft-switching capabilities with the CLLC type and a more simple and fast LC resonant tank with less components operating at a high frequency. Literature has, however, shown that hard-switched converters are more efficient at lower switching frequencies but for applications where the transformer size matters, high-frequency operation with soft-switching achieves a higher efficiency[67]. For high-power systems, this will compensate for the higher costs and more complex system. It is thus seen that by using a LC switch resonance, one of the major drawbacks with the conventional topologies are removed, namely the switching losses. By having a combination of inductance and capacitance in the circuit, the resonance tank inductance is used for a voltage shift and the capacitance is used for a current change in order to achieve soft-switching. This results in a converter that can operate efficiently at high switching frequencies while still being in the safe thermal region. Table 4 shows a summary of the above discussion by means of a comparison of the different solutions.

Resonant network structure	Power control	Duty cycle	Soft-switching characterization	Soft-switching range	Additional component	Bidirectional transition speed
Traditional type	Phase-shift modulation	50% duty cycle for all switches	ZVS for few switches	Narrow	No	Fast
LC-type for ZVS	Phase-shift modulation	50% duty cycle for all switches	ZVS for all switches	Narrow	A capacitor across each switch and an inductor in series with the transformer	Fast
LC-type series resonant tank	Phase-shift modulation	50% duty cycle for all switches	ZVS for primary switches, ZCS for secondary switches	Narrow	A capacitor	Fast
CLLC-type asymmetric series-parallel resonant tank	Frequency modulation	50% duty cycle for inverter switches, additional resonant signal for rectifier switches	ZVS for inverter switches, ZCS for rectifier switches	Wide	Two capacitors and an inductor	Slow
CLLC-type symmetric resonant	Frequency modulation	50% duty cycle for inverter switches, turn off for rectifier switches	ZVS for inverter switches, soft communication for rectifier switches	Wide	Two capacitors and an inductor	Slow

Table 4: Comparison of soft-switching solutions[41].

4.2 DAB Model with Conduction Losses

The converter models shown till now are assumed ideal and will therefore operate with no losses. In reality losses will occur in the converter, and these are primarily related to conduction losses, switching losses, auxiliary gate driver losses and core losses in the magnetic components[11]. Due to the introduction of resonance elements and thus soft-switching operation at a voltage ratio of $d = 1$ as mentioned in section 3.5, losses related to the transition between different switching states are very low in the DAB topology and can therefore be neglected. Also, the power needs to the gate signals of the IGBT switches are very low and thus these losses are also neglected. Further, the transformer is assumed ideal as analyzing the core losses in the magnetic components is a large study and will not be the focus in this thesis. The remaining losses are therefore the conduction losses, primarily related to the switches in the two bridges of the converter. An explanation of the conduction losses will thus be given in order to obtain a more accurate model while still being simple to analyze.

Figure 38 shows the primary side of the converter with the resistances representing the conduction losses in the switches. The conduction losses are losses that are present when the IGBT or the freewheeling diode is conducting current and they are determined by the RMS current through the switches, their on-state voltage as well as the length of the conduction interval for each switch. The resistance of all the switches are assumed to be equal, and thus all switch resistances are represented as R_{S1} in figure 38.
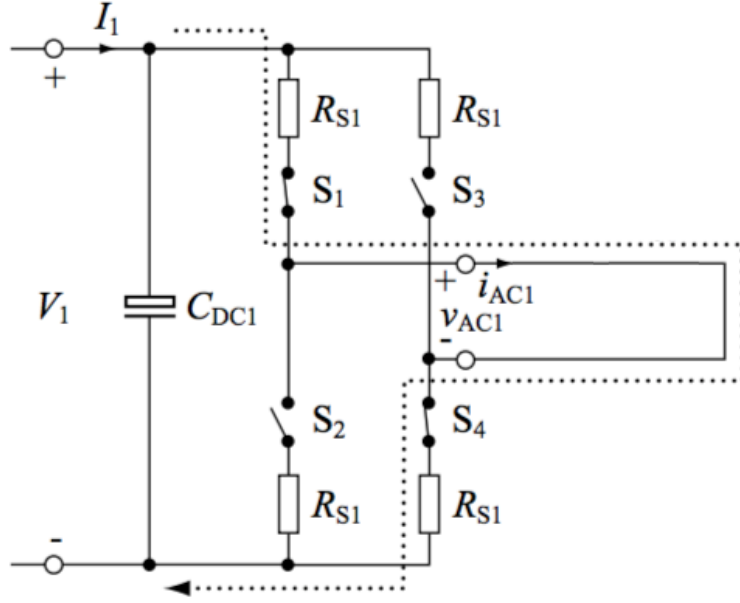
Figure 38: Full-bridge circuit with conduction losses[11].

The internal on-state resistance of the diode is non-linear and will change for different forward currents I_F. For a diode the conduction losses can be found as

$$P_{cond,diode} = I_F V_F = \frac{1}{T_s} \int_0^{t_{on}} v_F(t) I_F(t) dt = V_D I_{D,av} + R_D I_{D,RMS}^2 \qquad (4.19)$$

where $I_{D,av}$ is the average current through the diode, $I_{D,RMS}$ is the RMS current through the diode, R_D is the on-state resistance and V_D is the on-state voltage drop. The conduction losses for the IGBT are found in a similar way as for a diode. For an average collector-emitter voltage and collector current the average power loss in one IGBT can be found as

$$P_{cond,igbt} = I_C V_{CE} = \frac{1}{T_s} \int_0^{t_{on}} v_{CE}(t) I_C(t) dt = V_{ce,sat} I_{av} + R_{on} I_{RMS}^2 \qquad (4.20)$$

with $V_{CE,sat}$ being the collector-emitter on-state saturation voltage, I_{av} being the average current, R_{on} is the on-state resistance and I_{RMS} is the RMS current.

For steady-state operation each of the eight switches will conduct current for half a switching cycle T_s with a repeating negative current waveform as was seen in figure 34. This means that $i(t) = -i(t - T_s/2)$ and the RMS and average current values through each switch can be found by looking at the current waveforms and using the formulas for RMS and average values for triangular and square-wave waveforms as given in appendix 8.2. Thus, for all of the eight switches, the total conduction losses will be

$$P_{s,cond} = 8(P_{cond,diode} + P_{cond,igbt}) \qquad (4.21)$$

The currents and operation times are found by calculations and simulations and the next chapter will discuss the current and component values in order to build a model of the DAB converter and determine the conduction losses. The reverse recovery losses are also included for the maximum power transfer of $4MW$ in order to show a more realistic value of the converter efficiency operating at full load.

45

5 Design of Single-Phase DAB Converter

From the discussion made till now it is seen that high efficiency, high power density, a high level of safety and low emissions are required in a shipboard power system. By implementing a battery through a DC/DC converter all of these features can be achieved. Different converter topologies have been discussed and the single-phase dual active bridge converter is seen to be a promising topology. Among the main parameters that should be determined in order to design the converter are the input and output voltages V_1 and V_2, the switching frequency f_s, the auxiliary inductance including the transformer leakage inductance, the transformer turns ratio 1:n, snubber capacitors and output filter values. In order to have a good current control of the converter in a large part of the soft-switching range, the transformer turns ratio should be equal to the ratio between input and output voltages. By taking into account constraints such as maximum load power, current stress in components, bearable RMS current values, power density and efficiency, the auxiliary inductance and switching frequency can also be determined[41]. This chapter will discuss the design of the DC/DC converter with its components and their ratings according to the characteristics of the shipboard grid. The converter that is investigated will have the following specifications:

- Input voltage: 1100V

- Output voltage: 1100V

- Transformer turns ratio: 1:1

- Output power: 4MW

5.1 Switching Frequency

Converter component ratings should be chosen carefully in order to have an efficient connection between the expensive storage system and the shipboard grid. The switching frequency is among the parameters that are determining the rating of the magnetic components and should thus be chosen in a way that avoids large internal losses and excessive battery heating. Due to skin and proximity effects, a too high switching-frequency will lead to increased battery impedance and conduction losses and meeting the insulation requirements is thus difficult[68, 69]. In addition to this, both the natural resonant frequency of the transformer and the need for a high driving power will be constraints, leading to justification of a somewhat lower switching frequency than the maximum allowable. On the other hand, having a too low switching frequency will lead to a slow dynamic response of the converter control and a large size of the magnetic components, especially the transformer, thus leading to a trade-off between choosing a high or low frequency, where it is seen that volume and weight are low-frequency constraints while thermal limitations are present for high frequencies. For hard-switched converters, the switching losses will also be high at high switching frequencies.

Another important parameter that is dependent on the switching frequency is the power transfer capability of the converter. As shown earlier in equation 4.12 and 4.13, a higher switching frequency, keeping everything else constant, leads to a lower power rating, thus being a constraint on the maximum power transfer capability of the converter. Both the dynamic response of the converter and its ability to charge and discharge the battery fast are also in favor of a high switching frequency and it is thus seen how the switching frequency affects very much of the converter operation[34]. Based on this the switching frequency is chosen to be $10kHz$, referred to as a medium switching frequency. Since the transformer magnetizing inductance becomes negligible at this high frequencies, the transformer can be modelled by its leakage inductance and due to the fact that the switching frequency is kept constant, potential EMI issues in the converter are also reduced[11].

5.2 IGBTs and Diodes

The maximum voltage that will be applied to each switch will equal the input voltage. Since the input and output voltage are equal, this will be $1.1kV$ for operation in both directions for all of the switches in both of the two full-bridges. By taking into account the rated power of $4MW$, the load current will be approximately $3.6kA$.

The switches that are used in both of the active bridges will be IGBTs, assumed to operate at a junction temperature of $125°$C. These transistors combine the best features of MOSFETs and Bipolar Junction Transistors (BJTs), achieving a low voltage drop in the on-state as well as a fast switching characteristic[17]. In general, both conduction losses and switching losses needs to be considered for an IGBT switch. The conduction losses are due to the voltage drop that occurs across the switch in the on-state as a result of its inherent resistance and the resistance of the parallel diode in the freewheeling period. The switching losses occur due to the turn-on and turn-off of the IGBT. However, for soft-switched applications, the switching losses are very low and in this thesis the switching losses will thus be neglected.

When determining the IGBTs to be used, potential voltage spikes should also be taken into consideration in order to avoid damage of the switch during transients. The value of the voltage spikes can be high, and for a di/dt of for example $300A/\mu s$ and leakage inductance of $1.5\mu H$, the voltage spike will be

$$V = L\frac{di}{dt} = 1.5\mu H * 300\frac{A}{\mu s} = 450V \tag{5.1}$$

The chosen IGBTs should therefore be able to withstand voltages higher than the system voltage, which has the disadvantage of having to chose a switch with both higher losses and cost. In order to have a safety margin for the IGBTs, the operating voltage of $1100V$ should not exceed approximately 65% of the collector-emitter breakdown voltage, and therefore the 5SNA 3600E170300 IGBT module from ABB HiPak is chosen for this converter with a breakdown voltage of $1700V$[70]. Also, as will be explained in the next chapter, simulations have shown that the switch current reach RMS values as high as $5.65kA$. Since the continuous current capability of one switch is $3.6kA$ as seen in the data sheet shown in appendix 8.1, two IGBT modules will have to be parallel connected. The on-state characteristics of the IGBT are shown in figure 39 and by taking into account that two switches are parallel connected, the on-state resistance can be found by looking at the relationship between the collector-emitter voltage and the collector current of the switch as follows

$$R_{igbt,on} = \frac{\Delta V_{CE,on}}{\Delta I_C} \tag{5.2}$$

which is equal to the slope of the curve at the intersection between the collector current and the collector-emitter voltage.

For the anti-parallel diode the current ratings should be the same as for the IGBT. The IGBT pack from HiPak with a parallel diode connected takes care of this by having a parallel diode with the same current capability as the transistor. The forward characteristics of the parallel connected diode are shown in figure 40 and the resistance is found similarly as for the IGBT switch.
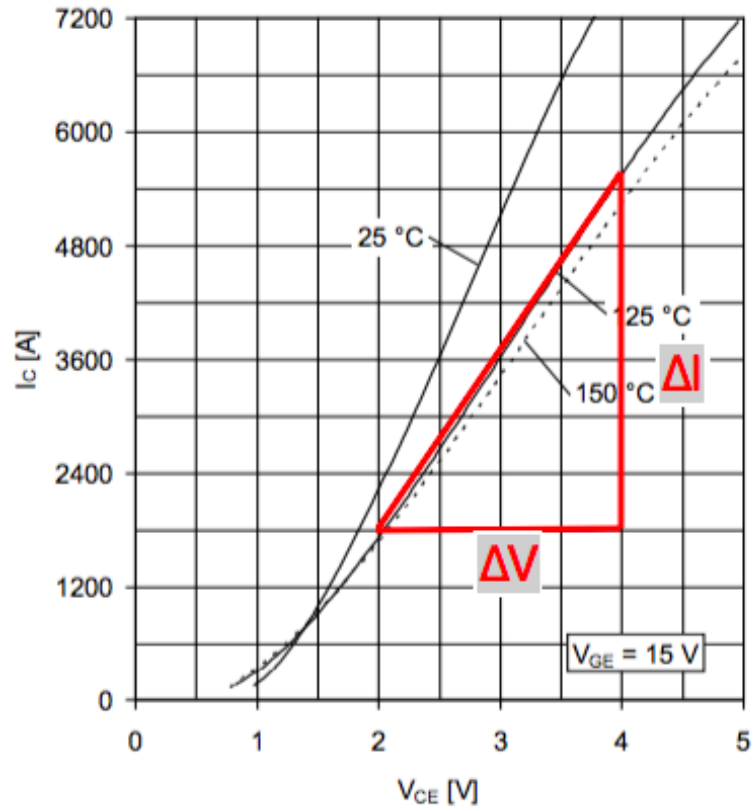
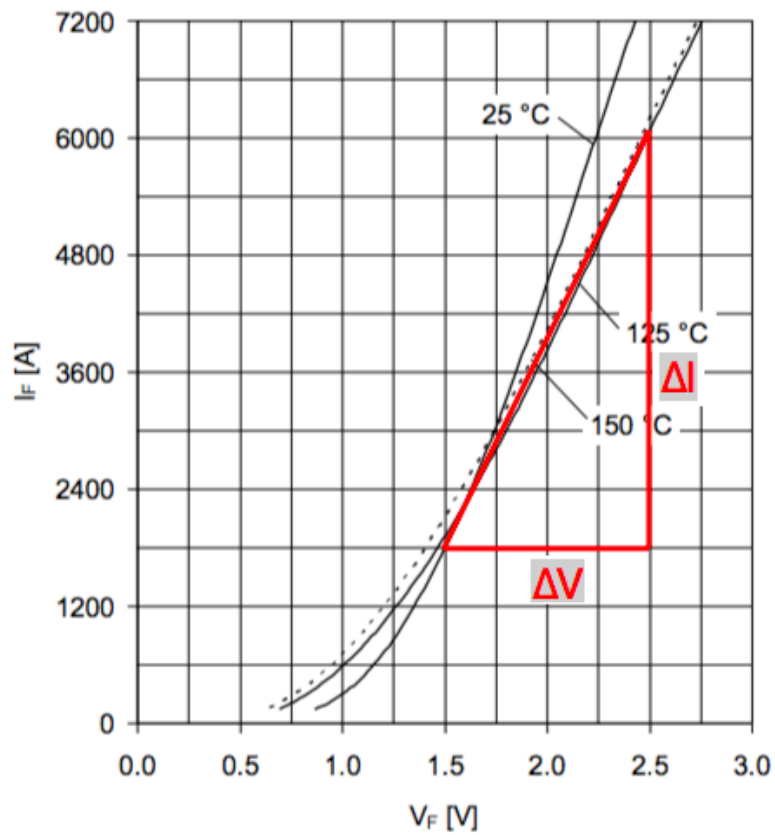Figure 39: On-state characteristics of the IGBT[70].

Figure 40: On-state characteristics of the diode[70].

5.3 Snubber Capacitors and Leakage Inductance

In order to design the snubber circuit and design a soft-switched converter, some design criteria should be taken into account[65, 71]:

- The snubber capacitance should be large enough so that the charging time is longer than the fall time of the current through the IGBT. This is in order to avoid large currents and voltages at the same time. For this project the capacitor charging time is chosen to be 5 times larger than the current fall time.

- Due to high duty cycle losses, a maximum value of the leakage inductance of the transformer should be found.

- The maximum value of the snubber capacitance in the lagging leg should be determined based on the maximum value of the leakage inductance.

- In order to charge the capacitors as calculated in the previous item, a minimum value of the inductance must be determined.

- Lastly, the value of the leading leg snubber capacitors can be found based on its charging time.

The input current i_{in} is assumed to be constant during on-state, and equation 5.3 and 5.4 shows how to determine the phase-shift ratio and the input current to the converter.

$$D = \frac{V_{load}}{V_{in} n} \tag{5.3}$$

$$i_{in} = \frac{P_{in}}{V_{in} D} \tag{5.4}$$

n is the transformer turns ratio, which is equal to 1 in this project. Due to the fact that several IGBT modules can be connected in series and parallel in order to meet the voltage and current ratings, the voltage, current and capacitance of a single IGBT module will be

$$V_{mod} = \frac{V_{total}}{n_s} \tag{5.5}$$

$$I_{mod} = \frac{I_{total}}{n_p} \tag{5.6}$$

and

$$C_{mod} = C_{total} \frac{n_s}{n_p} \tag{5.7}$$

where n_s and n_p are the number of series- and parallel connected modules in each switch. The total energy that is stored in a snubber capacitor can then be found as

$$W_{cap} = n_s n_p \frac{1}{2} C_{mod} V_{mod}^2 = n_s n_p \frac{1}{2} C_{total} \frac{n_s}{n_p} \frac{V_{tot}^2}{n_s^2} = \frac{1}{2} C_{tot} V_{tot}^2 \tag{5.8}$$

The snubber capacitor should increase the rise-time of the voltage across the switch during turn-off. The switch current will decrease at the same time as the voltage starts to rise, and therefore the voltage rise time should be somewhat larger than the fall time of the current in order to avoid large turn-off losses. In the calculation of the minimum snubber capacitance, a voltage rise time that is 5 times larger than the current fall time is used. Equation 5.9 can then be used to calculate the minimum snubber capacitance

$$C_{S,min} = \frac{i_{in} \Delta t}{V_{in}} \tag{5.9}$$

where Δt equals 5 times the current fall time which is equal to the voltage rise time of the IGBT. Both these values can be found in the IGBT data sheet[70].

The maximum value of the transformer leakage inductance can then be determined. Since the current reversal time will be large for a large inductor value, the inductor value should be kept below a maximum

value in order to achieve soft-switching. With a switching frequency of $10kHz$, the switching period will be $100\mu s$. Due to two current reversals in each period and a five times difference in voltage rise time and current fall time, Δt should be kept below $10\mu s$ in order to avoid high duty cycle losses. By determining a maximum current reversal time of 10% of the period, the maximum leakage inductance can be calculated as

$$L_{max} = \frac{0.1V_{in}}{2f_{sw}i_{in}} \tag{5.10}$$

The maximum value for the lagging leg snubber capacitance can then be calculated based on this maximum inductance value by setting the maximum leakage inductance energy equal to the capacitor energy as follows

$$C_{S,max} = \frac{1}{2}\frac{L_{max}i_{in}^2}{V_{in}^2} \tag{5.11}$$

Thus a lower and an upper limit is found for the lagging leg snubber capacitors. A minimum value of the leakage inductance should also be found since the lagging leg snubber capacitors are being charged by the energy stored in this inductor. This minimum inductance value can then be found based on the fact that the inductance energy should be at least equal to the energy stored in the capacitors. It will also have to be taken into account that two snubber capacitors are connected in series in each phase-leg for the full-bridge topology, where one is charging and the other is discharging. Equation 5.12 shows the calculation of the minimum leakage inductance.

$$L_{min} = 2\frac{CV_{in}^2}{i_{in}^2} \tag{5.12}$$

where the value of the leakage inductance is a trade-off between having a high output power with high transformer and IGBT current stress and having lower output power but with lower transformer and IGBT current stress. Lastly, the snubber capacitance value of the leading leg can be found as

$$C_{S,lead} = \frac{\Delta t i_{in}}{V_{in}} \tag{5.13}$$

In this thesis, an assumption is made that 2% of the whole period can be utilized for charging the capacitors. This means that equation 5.13 can be rewritten as

$$C_{S,lead} = \frac{0.02i_{in}}{f_{sw}V_{in}} \tag{5.14}$$

The results from calculating the component values with the equations given above and the input data as presented in the beginning of this section are given below in table 5. Since the value of $C_{S,lead}$ is in the interval between $C_{lag,min}$ and $C_{lag,max}$, the value of C_{lag} is chosen to be 6.6115μF in order to simplify the model and have all the snubber capacitances at equal values. Also, with the assumption of infinite magnetizing inductance and zero core losses in the transformer, the transformer can be modelled by its leakage inductance.

Component	Value
i_{in}	3636.36 A
$C_{lag,min}$	1.0248 μF
L_{max}	1.5125 μH
$C_{lag,max}$	8.2644 μF
L_{min}	1.2100 μH
$C_{S,lead}$	6.6115 μF

Table 5: Calculated values of snubber components.

5.4 Output Capacitor

In addition to the actual converter components, some filter components are also normally included in order to keep the output ripple within the required limits. A normally accepted value of the output voltage ripple is 1% of the average load voltage and thus a capacitor should be connected at the output of the converter in order to reduce the voltage ripple[6]. Also, the connection to a DC grid with four diesel generators will contribute to a more stable output voltage, and thus the output capacitor is chosen to have a large value in order to model this. That means that the voltage is held steady by the capacitor and the control system, leading to a steady operation of the DAB converter for varying load demands as will be shown in the next chapter. The output capacitor is chosen to be $100mF$ based on a trial and error method in Simulink.

6 Performance Evaluation

6.1 Model Description

Even though the inclusion of power electronic components bring in a lot of benefits to the system with regards to control and conversion in the system, it also introduce extra complexity as a result of the switching characteristics of the semiconductor devices[18]. This, in addition to their non-linear behavior, leads to a complex system including both mechanical and electrical components with very different characteristics. An example of this is the time constants of the system, where some power electronic semiconductor device can have a time constant in the range of nanoseconds, while for ship hydrodynamics the time constant can be tens of seconds. Making a simulation model of the whole system will then be highly complex and therefore only the connection of the batteries to the DC grid with a load is analyzed in this simulation setup in order to evaluate the converter performance.

The time averaged load, P_{avg}, that the system demand is given by equation 6.1. By calculating this based on the simple load profile given in section 2.5, the average power is found to be $6MW$. The diesel gensets will thus deliver this average power to the DC grid, and by including a battery storage system, the peak power ($10MW$) can be supplied from the diesel gensets and the storage system together. It is to be noticed that an assumption is made that the battery is large enough to deliver the required power without having large voltage fluctuations and that the battery is charged when the demand is lower than the average power.

$$P_{avg} = \frac{\int_0^t P_{load}(t)}{t} \tag{6.1}$$

First, a simplified model of a single-phase DAB converter was built in Matlab/Simulink in order to analyze the switching pattern of the IGBTs. Components are chosen from the Simscape package in Simulink, allowing for a connection between physical component models. The model consists of two full-bridges with four ideal IGBTs each connected in parallel with a freewheeling diode and a snubber capacitor. The snubber capacitor is connected in parallel to the switches in order to achieve ZVS switching as discussed in chapter 4. By having an ideal transformer, it is modelled simply by its equivalent inductance plus any additional inductance needed for energy transfer. In addition to having ideal components the output voltage is locked to the shipboard grid voltage of $1100V$, which is a model of the steady output voltage of the diesel gensets to the DC bus. Figure 41 shows the converter model built in Simulink.

As seen in the left part of figure 41, the Li-ion battery is modelled as a constant voltage source in series with a small resistance. In order to have the current rating to deliver a maximum power of $4MW$ at an operating voltage of $1100V$, several batteries must be connected together in series and parallel as was previously shown in table 3. This leads to a continuous discharge rate of 6C for the battery at maximum load. With the energy level of one battery module being $6.7kWh$, the battery will have a total energy of $660kWh$.

The load is modelled as a resistance connected in parallel across the output of the converter, which also represents a load connected to the shipboard DC-grid. By representing the load as a resistance with a constant voltage across it, it is basically a constant current source which can be modelled as a Constant Power Load (CPL)[72]. The value of the current is given as the ratio between a reference power and the voltage at the DC-link:

$$I_{load} = \frac{P_{ref}}{V_{DC}} \tag{6.2}$$

It is to be noted that the currents found are an average value for a specific load condition that is in steady state. The transients in the model is therefore not taken into account.
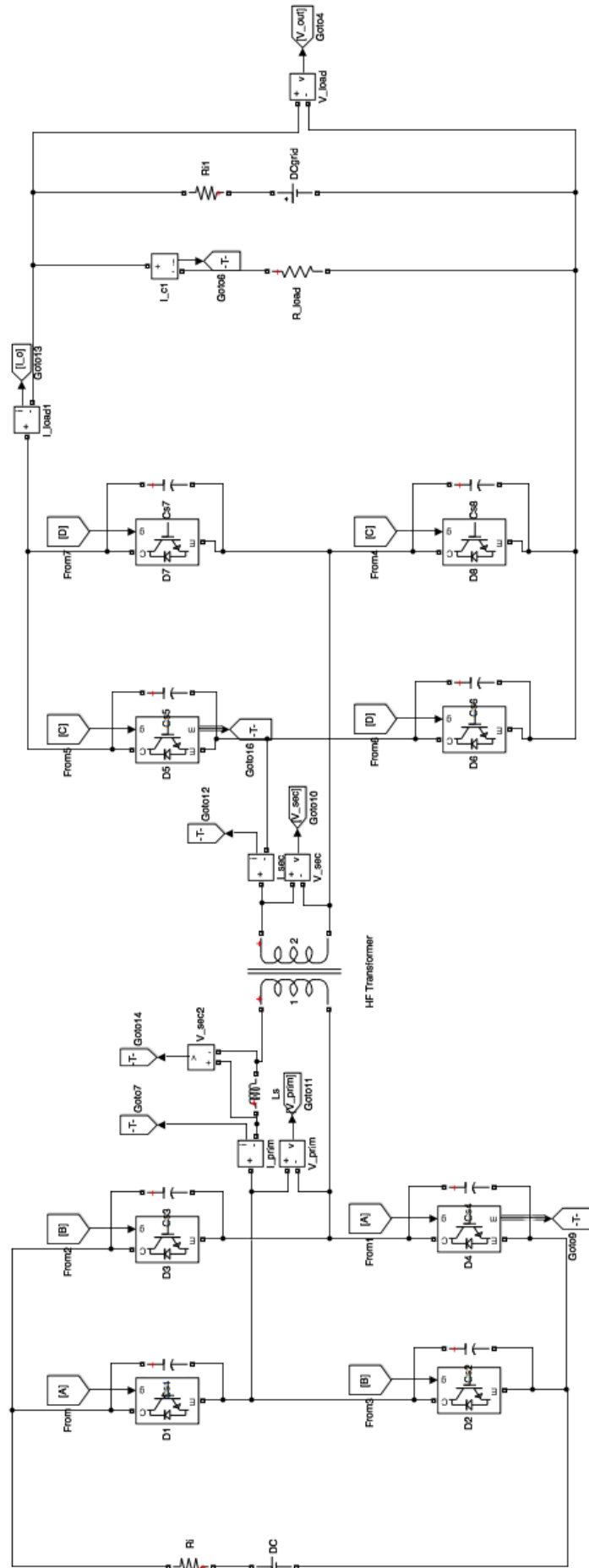
Figure 41: Simplified Simulink model of the single-phase DAB converter.

In order to model a more realistic converter, the model is expanded to include a variable load, which is fed by the given load profile as explained in chapter 2. The CPL resistance is calculated as

$$R_{CPL} = \frac{V_{DC}^2}{P} \tag{6.3}$$

where V_{DC} is the system voltage of $1100V$ and P is the load level, varying from 1 to $4MW$. This means that the CPL is represented by a resistance parallel and thus different load levels are achieved by changing the value of the resistance. The current through the load is found as

$$I_{CPL} = \frac{P}{V_{DC}} \tag{6.4}$$

where P is the power flowing through the converter and V_{DC} is the system voltage of $1100V$. Thus, the operating points of the converter will change during simulation, representing different load demands. In addition to this, the fixed voltage source is removed, introducing the need for a control system in order to keep the output voltage at a steady level.

Due to the power imbalance that will occur at the output of the converter during transitions, the output voltage of the converter will in reality vary for changing load demands. Depending on how much the voltage is varying, distortions in the grid current will occur and the stress on the switching devices will increase along with the increase in voltage fluctuations. This variation may be unacceptable and since the diesel generators can not be assumed to be a stiff grid, especially not for large power fluctuations, a PI controller is implemented as seen in figure 43. The implemented control system operates at constant frequency and constant duty-ratio, controlling the output voltage of the converter to be steady at $1100V$ for varying load demands. The input to the controller is then based on the difference between a reference voltage V_{ref} and the actual output voltage V_{out} of the converter, where the controller calculates the required phase shift based on the relation between transferred power P and phase shift angle ϕ as shown previously in the power transfer equation for the DAB converter (equation 4.12). Regarding the tuning of the PI controller, a transfer function for the system would have eased the calculation of the control parameters. However, due to the complexity of the electric devices and the whole system with time constants ranging from nanoseconds to tens of seconds, a transfer function was not made and the tuning was done by a trial and error method.

In order to realize a phase-shift modulation control of the converter, a gate signal generator is made. It is based on four square-wave pulses that are sent to the cross-connected switch pairs in each converter bridge, where the phase-shift ϕ from the PI controller is added to the signal as a delay after being scaled and normalized according to the switching period. Thus, a positive phase-shift angle will delay the gate signals to the secondary bridge switches, transferring power from the leading to the lagging side. Since only a positive delay can be applied to a gate pulse, power transfer in the opposite direction is achieved by delaying the gate signals to the primary side switches. However, for power transfer with a positive phase shift angle, the primary side gate signals are not delayed. The non-ideal behaviour due to the deadtime between the gate signals must also be taken into consideration in order to avoid shoot-through with its according chance of damage of components and thus the pulse width of a gate signal is set to 49.5%. The gate signal generator is shown in figure 44. As the switches are turned off during the deadtime, the freewheeling diodes are forced to conduct the current and thus the voltage across the phase leg is equal to either the positive or negative bus voltage. Without a proper control system, this would have lead to an error in the value of the output voltage. Also, because of the symmetry of the converter, the control system can be designed for power flow in one direction and be simply mirrored to the other bridge in order to transfer power in the opposite direction. Thus, the converter allows for bidirectional power flow, showing equal characteristics in both directions. This is also one of the advantages with the phase-shift modulation technique, showing good performance and easy implementation of bidirectional power flow. The model has also replaced the ideal combined IGBTs and diodes with separate IGBTs and diodes, allowing for a more accurate investigation of their performance and losses at a given operating point.

Figure 42: Simulink model of the single-phase DAB converter with variable load and non-ideal switches.
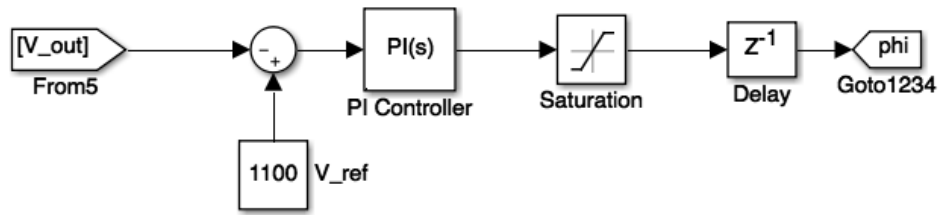
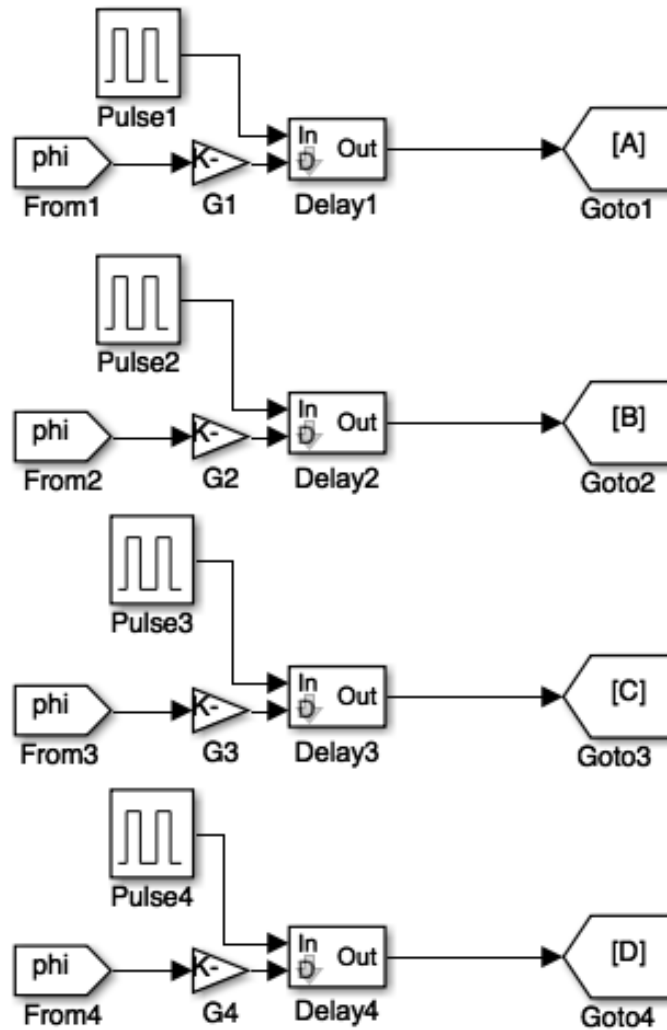Figure 43: PI controller for the single-phase DAB converter.

Figure 44: Phase-shift modulation generators for the single-phase DAB converter.

6.2 Tuning of Parameters

After running the simulation model for the given load profile it was seen that the inductor current had very high peak levels. These currents would have been harmful for the switches and thus a decision was made to tune the parameters of the converter in order to achieve better performance of the converter by means of lower peak currents and thus less stress on the switching devices. This will also lead to a more safe operating converter with lower chance of failure due to excessive currents. However, as mentioned earlier, one of the disadvantages with the phase-shift modulation technique using a single-phase shift control is related to high current levels and thus these currents were expected to occur. Figure 45 show the primary side IGBT currents in the transition from a $1MW$ load to a $4MW$ load. It is seen that in addition to having a conduction interval in approximately half of each switching period there are also peak currents with extremely high values and these would have lead to damage of the switches. However, the response of the controller is seen to be fast and the new steady-state operation occurs within 5 switching periods.
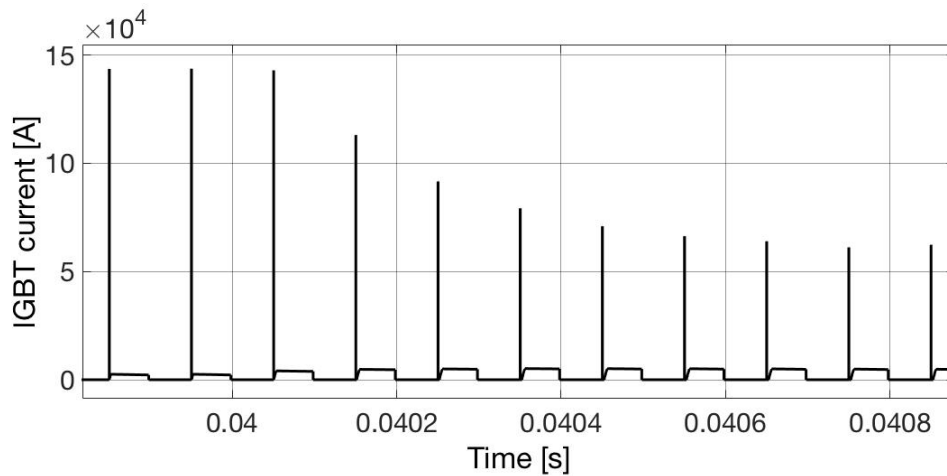
Figure 45: Current peaks and transition from a $1MW$ load to a $4MW$ load.

Figure 46 shows that high peak currents through the switches occur for all the load levels. At most, the peak current reach values of more than $144kA$.
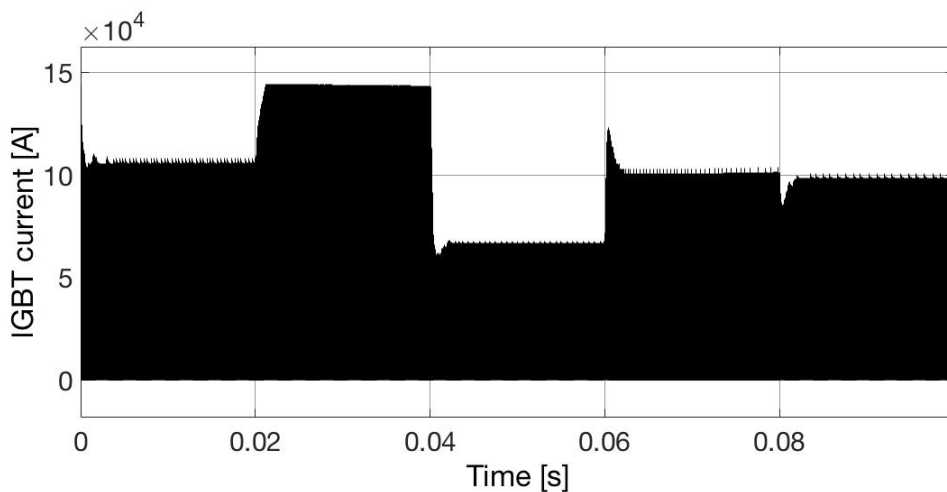
Figure 46: Current through the IGBT switches.

The high peak currents are seen to result from the discharge of the snubber capacitors and therefore a decision was made to tune the snubber capacitors in order to avoid the large current discharge while still having a converter that operates with soft-switching. Figure 47 show these high capacitor currents, and by comparing figure 46 and 47 it is seen that the current from two snubber capacitors are discharged

through the conducting switch for the whole operation time.

Figure 47: Current through the snubber capacitance in parallel with a switch.

Since the two snubber capacitors in a phase leg discharge through the conducting switch, leading to very high peak currents, smaller snubber capacitors are chosen in order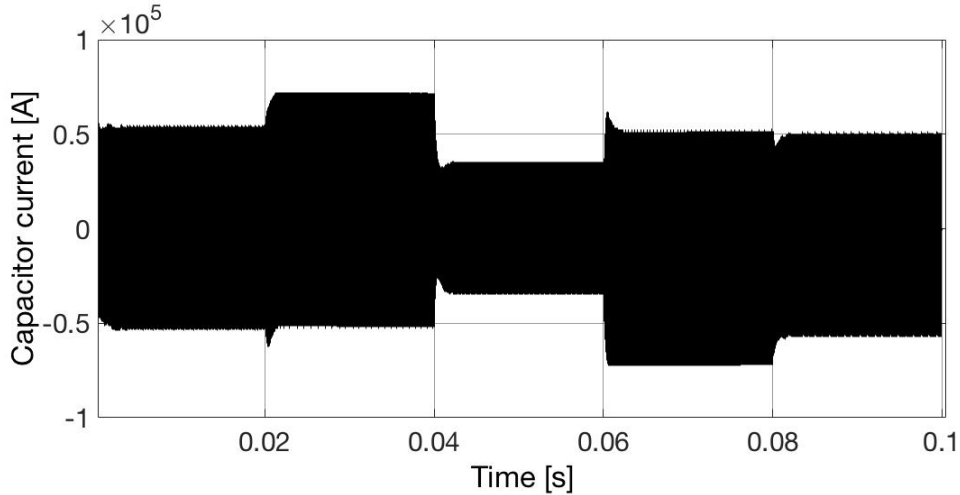 to reduce these currents. The new capacitors are chosen to be $0.72nF$ based on a combination of a trial and error tuning in Simulink and the converter equations presented earlier. These new capacitor values also introduce the need for a new leakage inductance value. The tuning is based on the power equation for the DAB converter, shown again here in equation 6.5.

$$P = \frac{nV_1V_2\dot{\phi}(\pi - |\phi|)}{2\pi^2 f_s L} \quad \forall \quad -\pi < \phi < \pi \tag{6.5}$$

As seen in the power flow equation, for a fixed switching frequency, the power flow capability of the converter is proportional to the phase-shift angle ϕ and inversely proportional to the size of the leakage inductance L, and thus a new leakage inductance will change the power flow capability. This means that either a new switching frequency should be utilized or the converter must operate at lower phase-shift angles for a given power transfer. By using equation 5.9-5.14 with the new snubber capacitance value, a leakage inductance value is found to be $1.1\mu H$. Due to the small change in leakage inductance, the switching frequency can be kept at $10kHz$ and the power transfer capability will remain at $4MW$ for a smaller operating phase-shift angle compared to with a larger leakage inductance value. As mentioned in chapter 4, the circulating currents will be higher for a high operating phase-shift value and thus the circulating currents (and the reactive power, leading to losses) will be reduced as a result of lowering the phase-shift angle ϕ. The disadvantage with this tuning is related to higher RMS currents in the switches, leading to higher conduction losses.

6.3 Simulation Results

The Simulink model is run with the load profile as explained previously and with the new component values. The loads vary within a range between 1 and $4MW$, and by running the simulation model with loads according to the load profile the performance of the converter can be analyzed for different output levels. It is to be noticed that the converter is only run in one direction for simplicity reasons, and due to the 1:1 turns ratio of the transformer and thus similar operation in both directions this is a reasonable choice.

6.3.1 Steady-State Operation

Figure 48 shows the output power of the converter for the given load demand. It is seen that the converter must be able to handle large steps in output power and thus its performance should be evaluated in order to see how it responds. One of the parameters that will be affected of a change in power demand is the output voltage of the converter. The voltage fluctuations are shown in figure 49 and it shows that for a large load step from $1MW$ to $4MW$, such as the one that occurs at $t = 0.04s$, the voltage fluctuation is approximately 0.36% ($4V$), proving a good response from the PI controller. For smaller load steps the voltage fluctuation is even lower. A special case is for a total load demand of $6MW$, where the diesel gensets deliver exactly the same amount of power as the load demand and thus the converter will not deliver or consume any power from the grid. However, even though the converter is not doing any work in that condition it should be noted that an output power of zero do not equal zero currents. This is due to the circulating currents that are still present in the converter, leading to losses in the devices. Thus, for a constant duty-ratio operation, zero reactive power for an active output power of zero is not possible. However, this is not analyzed in detail in this thesis and the operating profile as shown here will be used.
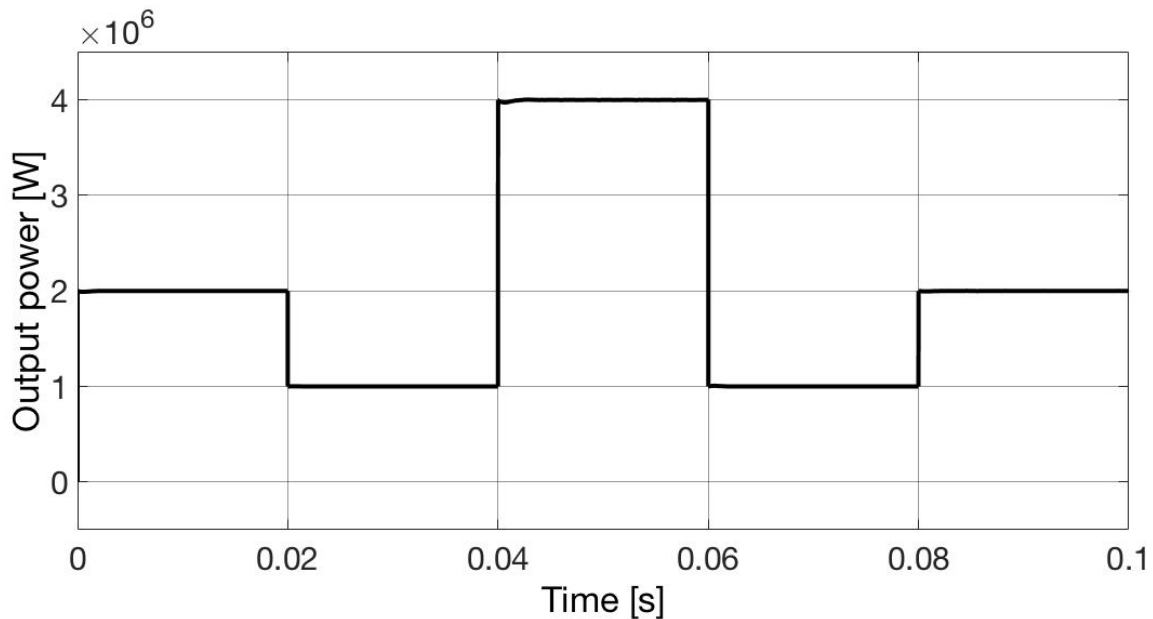

Figure 48: Output power of DAB converter according to the load profile.
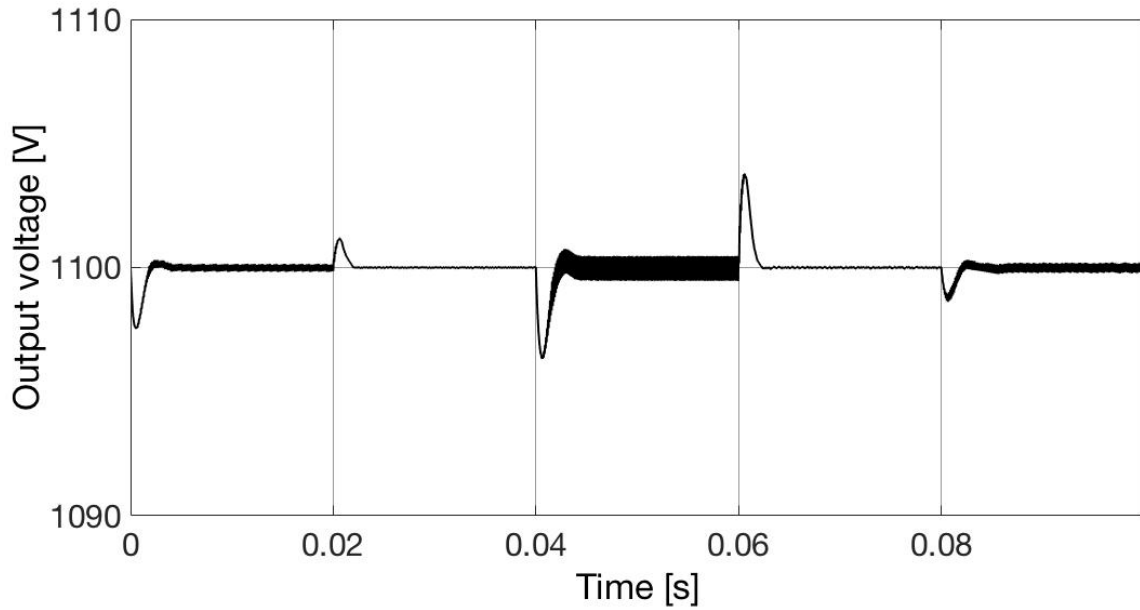
Figure 49: Output voltage of DAB converter.

The current through the IGBTs and diodes for the primary side at a $2MW$ load are shown in figure 50 and 51, respectively. It can be seen from the IGBT and diode currents that the primary bridge is working in inversion mode and the secondary bridge is working in rectification mode. Therefore, for each operating point when power is transferred from the primary to the secondary side, the four IGBTs on the primary side and four anti-parallel diodes on the secondary side are conducting the main current. The primary side diodes and secondary side transistors are only conducting in the transition between on- and off-state in order to handle the reversing current due to the deadtime where none of the IGBTs in a leg are conducting. It is also to be noticed how the switch only conducts current during the first half switching period, while the cross-connected switch conducts during the second half of the switching period with a small deadtime in between. Figure 52 shows a zoom-in of the primary side diode current shown in figure 51.
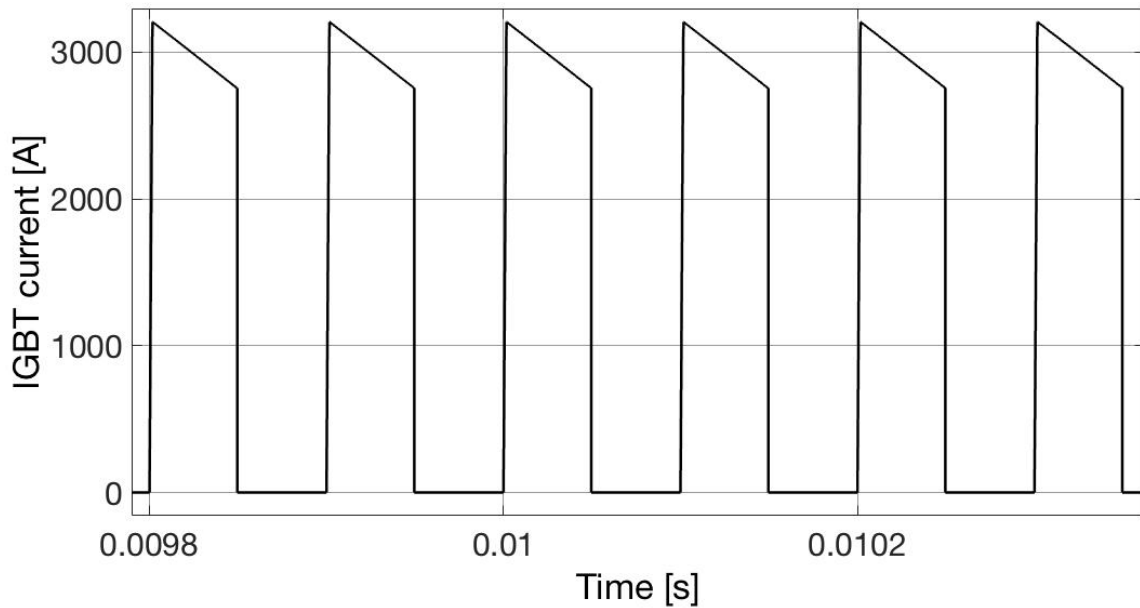
Figure 50: Primary side IGBT current.
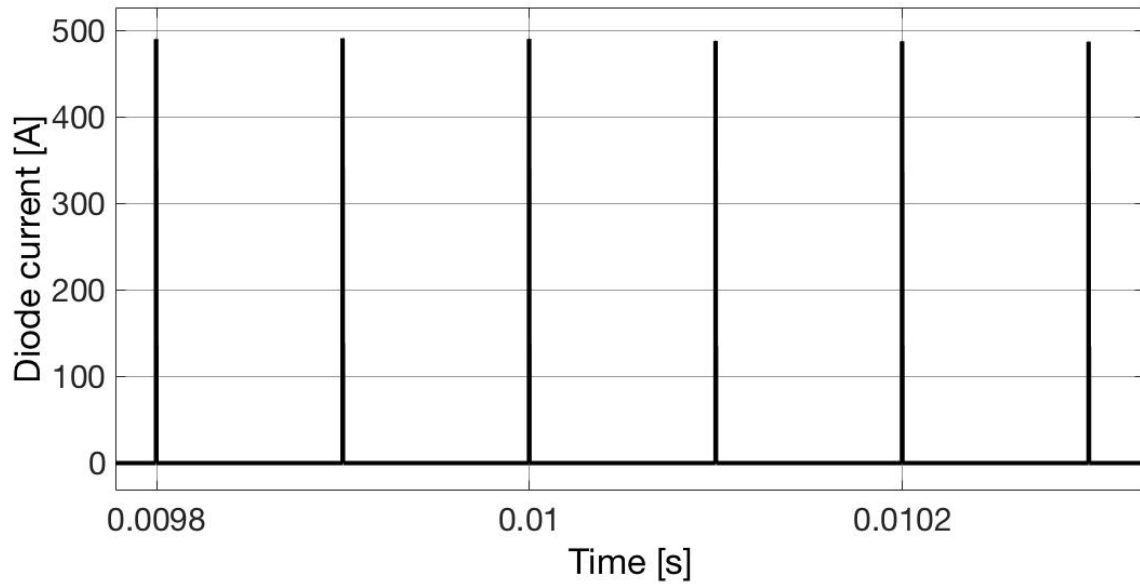
Figure 51: Primary side diode current.
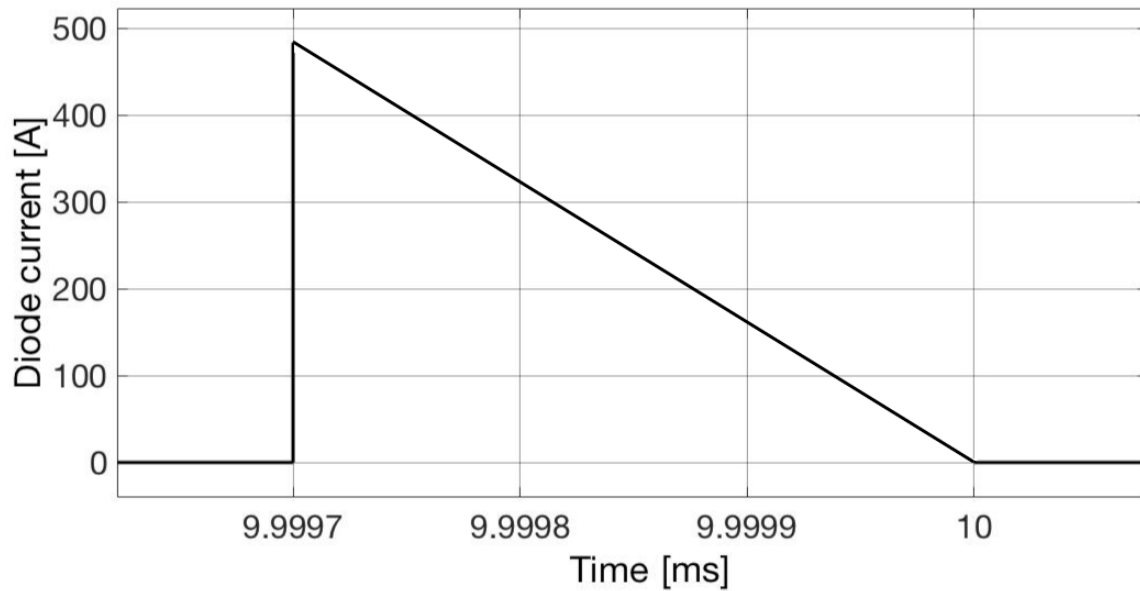
Figure 52: Primary side diode current zoom-in of one peak shown in figure 51 above.

For the same load demand of $2MW$, the secondary IGBT and diode currents are shown in figure 53 and 55, respectively. The secondary side switches are operating in rectification mode where the role of the transistors and diodes have changed compared to the primary side, where the diodes are conducting most of the current on the secondary side. Figure 54 shows a zoom-in of the secondary side IGBT current shown in figure 53.
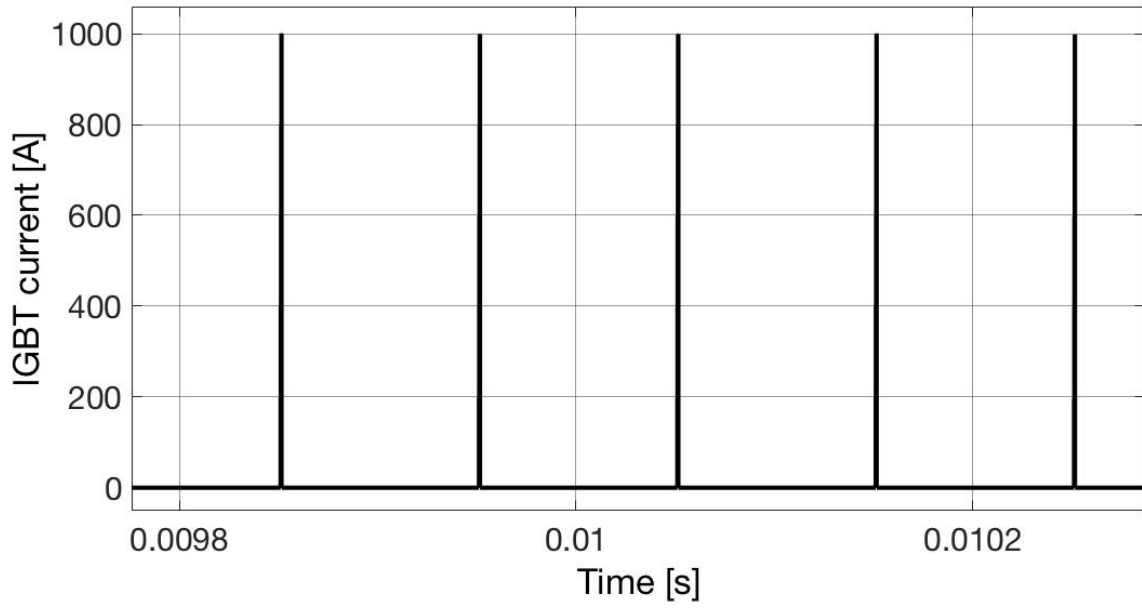
Figure 53: Secondary side IGBT current.
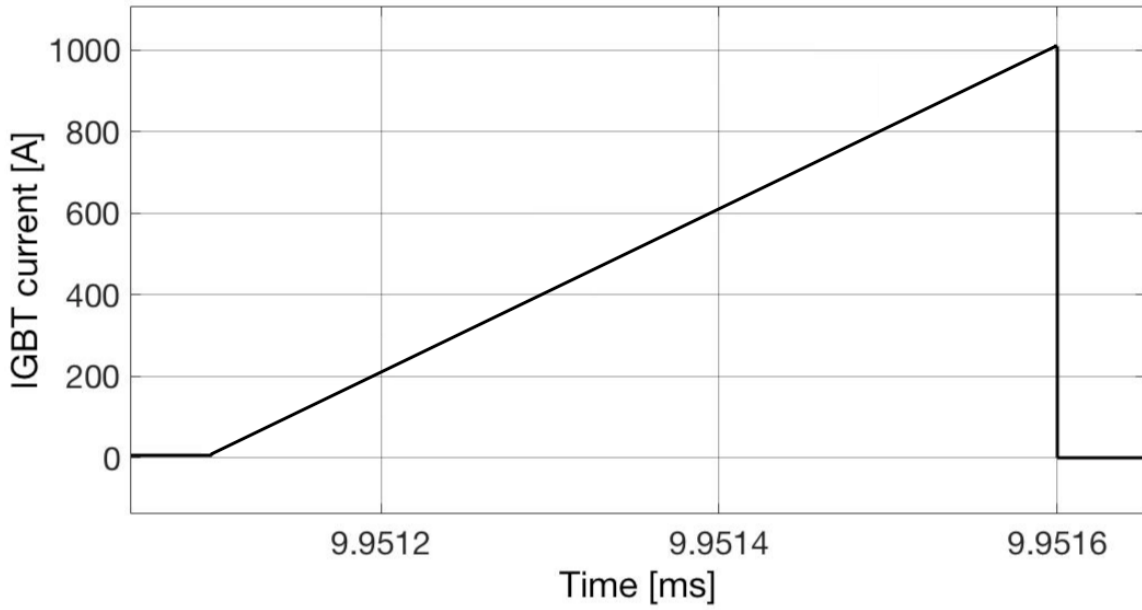
Figure 54: Secondary side IGBT current zoom-in of one peak shown in figure 53 above..
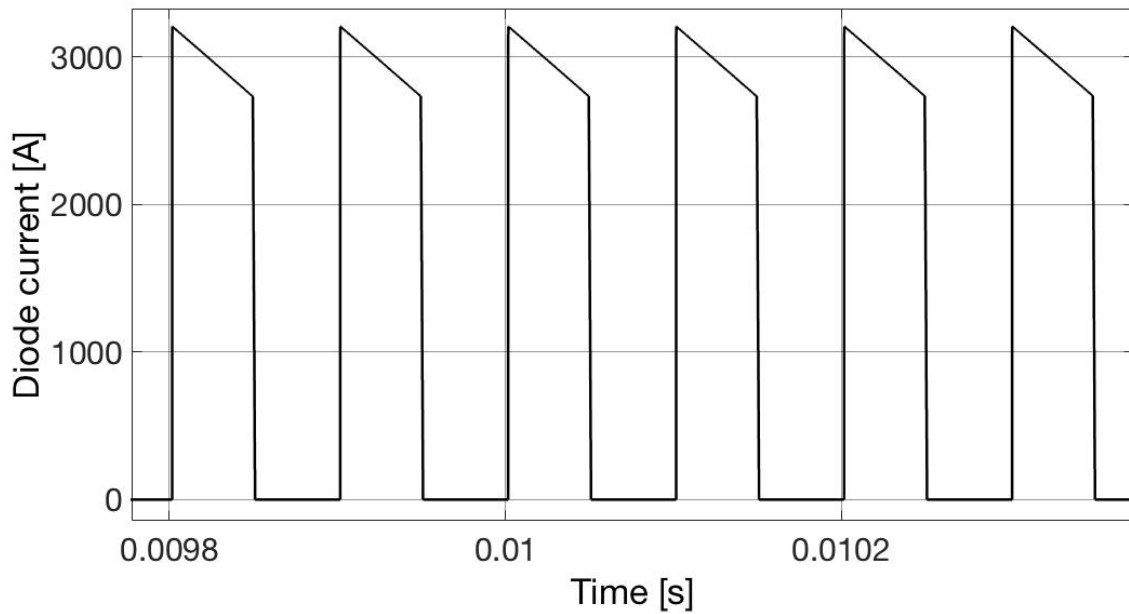
Figure 55: Secondary side diode current.

From the above presented figures it can be seen that the switches on the primary side are conducting most of the current, and that less current is flowing through the diodes. However, for the secondary side, most of the current is flowing through the diodes, and the switches are only conducting a small fraction of the total load current. Also, one of the main advantages with the DAB converter is related to the presence of ZVS. The conduction interval starts with the freewheeling diode conducting the current, and the current through the diode decrease to zero while the voltage across it, and thus also across the transistor, remains at zero. Thus, the transistor can turn on while the voltage is at zero, providing a soft-switched transition as seen in figure 56.
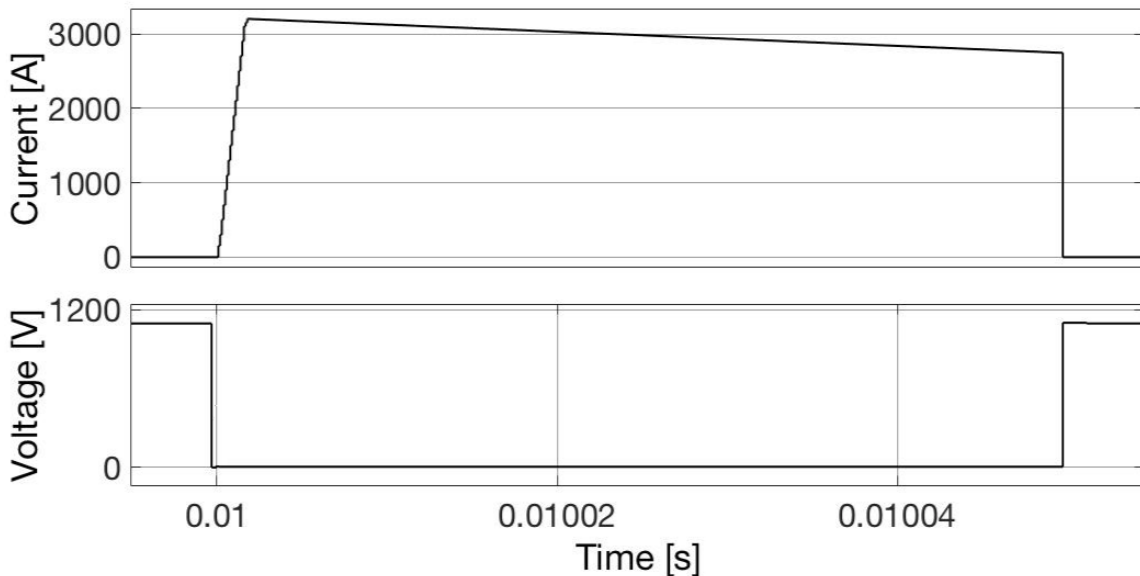
Figure 56: Voltage fall and current rise waveforms of an IGBT with snubber.

When the IGBT conducts, the current through the transistor is equal to the leakage inductance current. When the switch is to be turned off, the current starts to decrease immediately since the current can flow through the parallel capacitors. These capacitors will be charged when a current flows through them, increasing the voltage across the switch. The current which charge the capacitor will equal the difference between the load current and the current that flows through the IGBT. When the capacitor is fully charged the voltage across the switch is at its maximum value and the diode starts to conduct.

When the switch is turned off and the transistor stops conducting, the rise time of the voltage across the snubber capacitance allows the current to decrease before the voltage starts rising, avoiding operation at both high current and voltage at the same time. This leads to a soft-switched turn-off and thus avoids high instantaneous power loss.

It is seen that when the IGBTs turn on the voltage across the parallel capacitance has reached zero, and thus the switch can turn on with zero switching loss. At turn-off, the voltage across the switch increase according to the charging characteristics of the capacitor, and thus by using capacitors as calculated previously, the switching losses can be neglected. The losses that need to be considered are then the conduction losses and these will depend on how much power is transferred through the converter. As mentioned in chapter 4, the phase shift between the primary and secondary square-wave voltages leads to a voltage across the leakage inductance. This will further lead to a current flowing through the transformer and thus power is being transferred from the leading to the lagging side. Figure 57 shows the voltage across the leakage inductance.
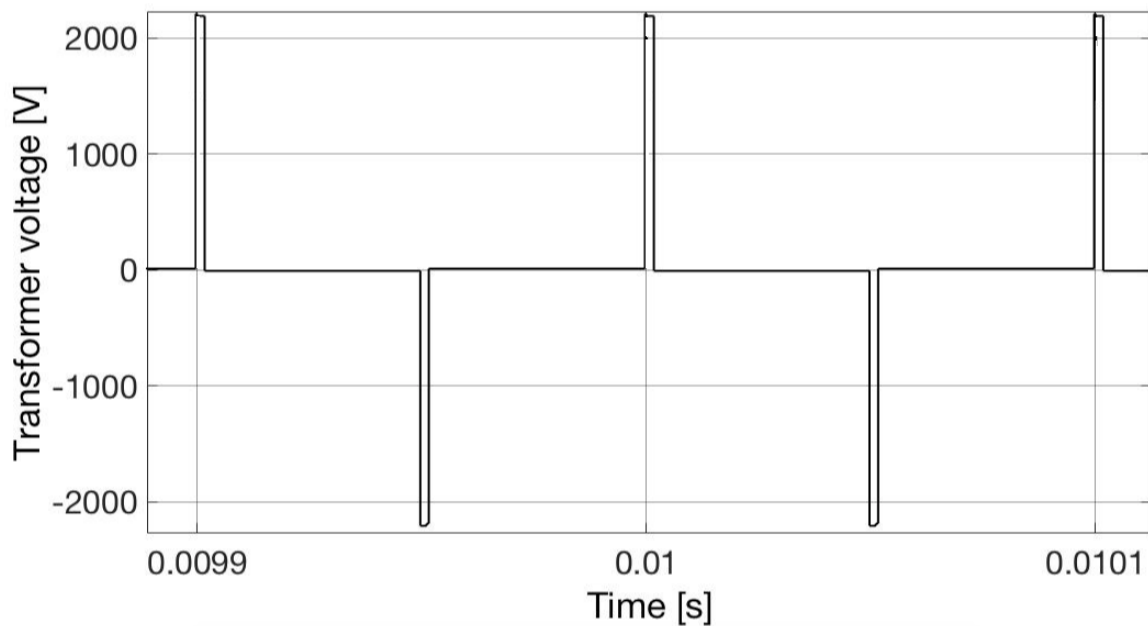
Figure 57: Voltage across the leakage inductance/transformer.

As mentioned previously in this section, the current through the converter will not be zero for zero active power, and the transformer currents for zero-power operation are shown in figure 58. This will introduce some losses in the converter even though it is not doing any useful work.
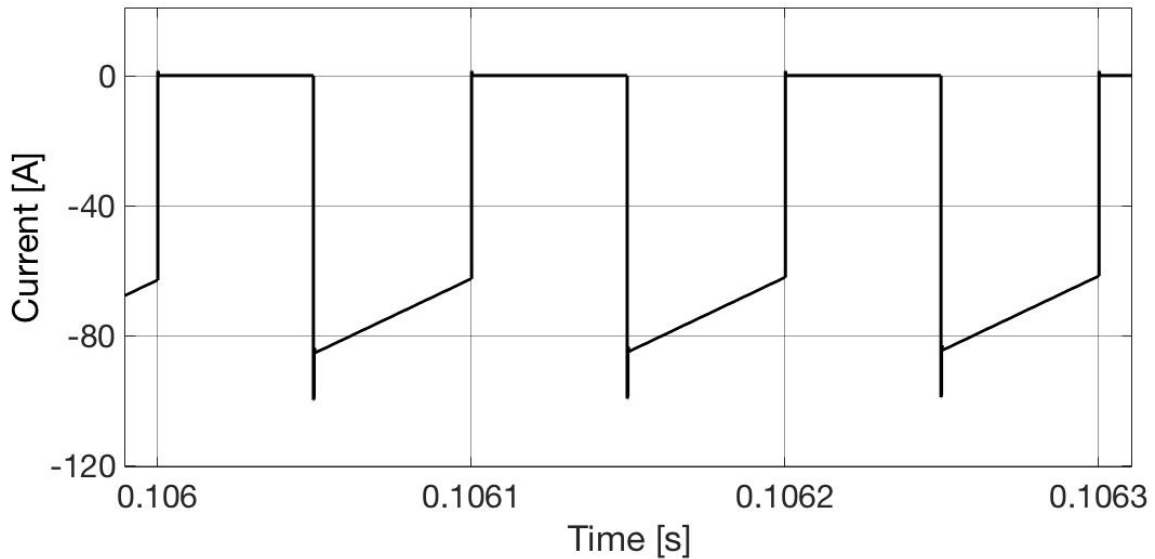
Figure 58: Transformer current for zero active power operation.

6.3.2 Converter Efficiency

By measuring the current through the IGBTs and diodes for different load levels in steps of $200kW$ from 0 to $4MW$ as shown in figure 59 the RMS and average current values can be calculated. Thus, the on-state resistance of the components can be found and the conduction losses are calculated for each load level as explained in section 4.2.
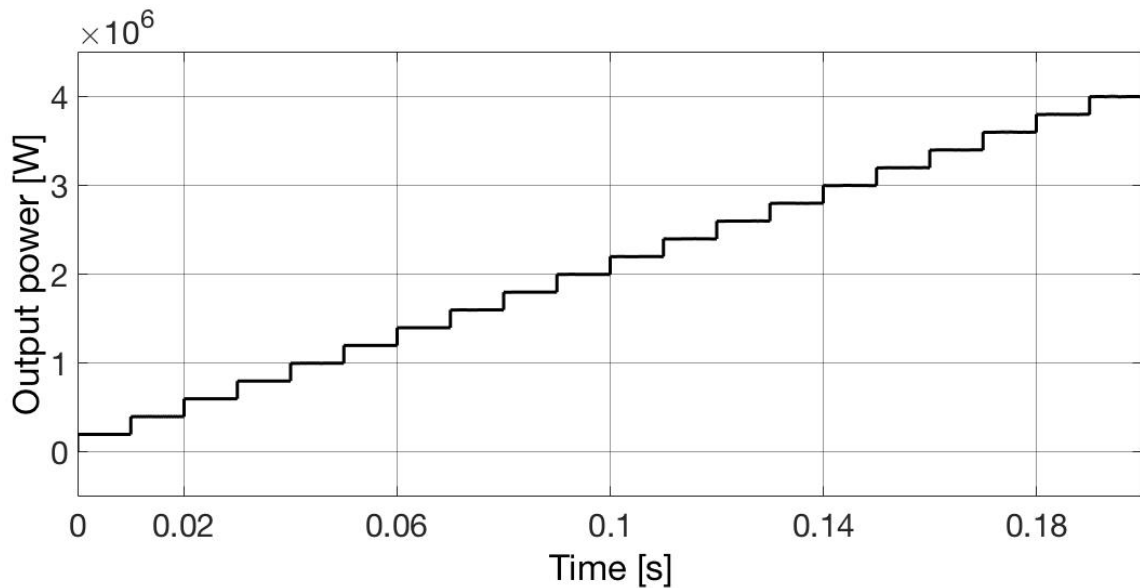
Figure 59: Output power increasing with steps of $200kW$ in order to calculate the efficiency at different load levels.

The peak values of the currents as well as their conduction interval time can be used in order to calculate the RMS and average currents through the switches and freewheeling diodes. Based on these calculations and results from the simulation the efficiency of the converter is plotted for the different load levels as seen in figure 60. As can be seen from the figure, the efficiency decrease at higher power levels due to the increasing load currents and thus increasing conduction losses. The efficiency at $4MW$ power transfer is found to be 97.2% and more than 99.5% for very low loads. By using the reverse recovery energy from the data sheet, the reverse recovery losses at an output power of $4MW$ and switching frequency of $10kHz$ will be $86.4kW$, and thus the efficiency at maximum power transfer is reduced to 95.1%. In addition to this it should be reminded that the losses related to the magnetic components, especially the

transformer, will lead to a somewhat lower total efficiency of the converter. The parameter values for the loss calculation are shown in appendix 8.3.
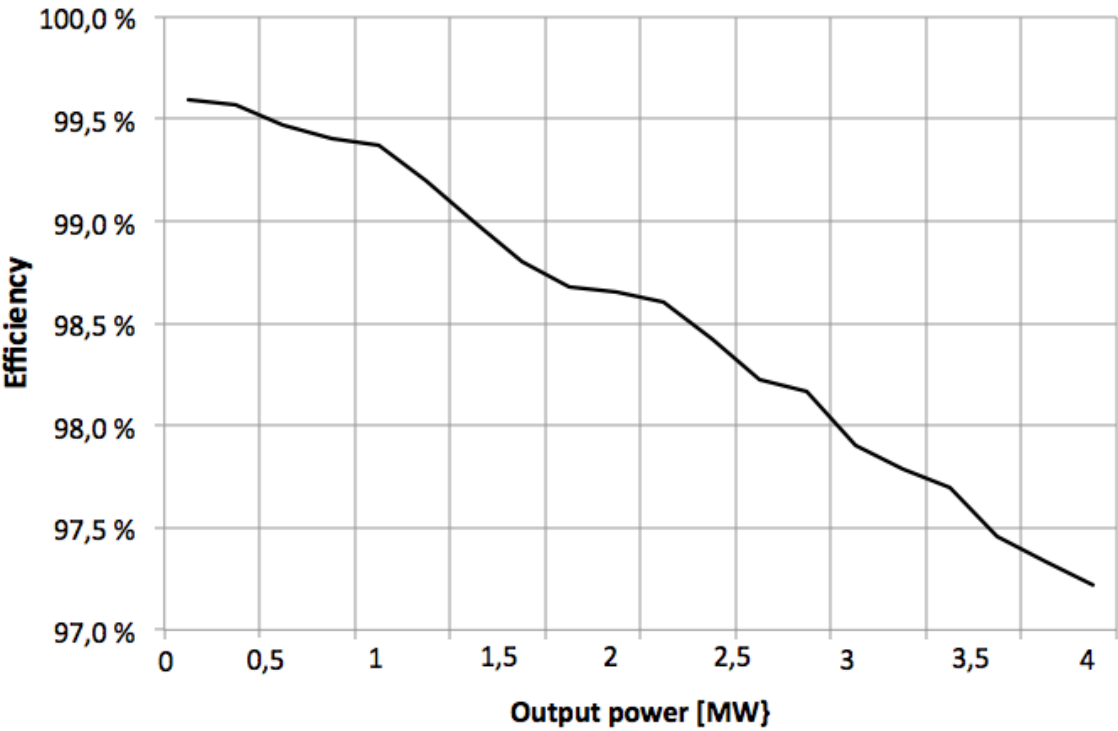
Figure 60: Converter efficiency for load steps of $200kW$ with a maximum output power of $4MW$.

7 Conclusion and Further Work

7.1 Conclusion

A shipboard power grid is explained by means of its energy suppliers, energy consumers and energy transfer elements. It is seen that an electrical grid is highly complex and the implementation of a battery increase the complexity even more. However, having a hybrid ship that combines the best features of fuel engines and batteries together can improve the performance of a ship significantly if implemented correctly, and the connection of a battery through a DC/DC converter allows for controlling the power flow as well as providing galvanic isolation between the grid and the battery. Due to the flexible connection between the battery, converter and the power grid by means of cables, the placement of the converter can be chosen as appropriate for the given ship. Thus the larger and more heavy components can be placed at lower decks. Regarding the size of the battery, this is seen to be of a comparable size as an already implemented battery pack on the ship Viking Lady. By placing the battery pack in a container, the proper safety and cooling systems are also taken care of inside the same enclosure, proving a good example for practical implementation. A dual active bridge converter utilizing two full-bridges is therefore designed, simulated and evaluated in order to investigate the connection of a battery to the shipboard power grid.

In order to design a converter that operates efficiently at high switching frequencies, attention has been given to the resonance components, meaning the snubber capacitors and the leakage inductance of the transformer. By having components that work in coherence with each other, soft-switching is achieved and thus a high switching frequency can be used in order to reduce the size of the magnetic components and achieve a high power-density of the converter. Also, a PI controller is implemented in order to maintain a steady DC-link voltage and to control the power flow through the converter for a fluctuating load demand. The dynamic behavior is thus improved by integrating a control system and the distortions in the grid current as well as the stress on each switch are reduced, leading to a prolonged lifetime of the converter and battery.

The steady-state operation of the converter is evaluated by making a model in Matlab/Simulink and its performance has been analyzed. It is seen that the converter responds fast to large power variations with a voltage fluctuation of less than $4V$ for a jump in power demand from 1 to $4MW$. This is only a 0.36% deviation in the voltage, meeting the requirement of less than 1% ripple in the output voltage of the converter. In reality, the connection to a DC grid with diesel generators and AFE converters keeping a stable output will lead a more stiff grid and thus contribute to less fluctuations in both voltage and currents. However, by only having a filter capacitor at the output of the converter, the dynamic response of the converter can be analyzed and it can be seen how the converter can be used as a voltage regulator, thus stabilizing the grid during load steps and other transients.

By looking at the waveforms of the currents through the IGBTs and diodes, it is seen that the converter operates as expected according to the theoretical models. Also, the efficiency at a load demand of $4MW$ is more than 95% when the reverse recovery losses are included. It is seen that the conduction losses are dominating at higher power levels and for a low power demand of $200kW$, the converter operates at an efficiency of more than 99.6%. These efficiencies does not take the transformer with its losses into account and the assumption of having an ideal transformer should also be considered in the analysis, where both the efficiency and performance will be less ideal with the transformer included in the model. It is also expected to have more voltage spikes in the converter during transition between different operating switches when the transformer is modelled more accurately. Also, when the parasitic components of the transformer are included in the model, high-frequency oscillations are assumed to be present, increasing the need for filter systems. However, the ideal transformer allows for having the inductor current and voltage seen as smooth waveforms without large distortions.

7.2 Further Work

The single-phase dual active bridge converter was chosen for further investigation in this thesis. However, it would be interesting to also model and test other DC/DC converters in order to evaluate their performance in a similar shipboard system. This could be the three-phase dual active bridge converter and other configurations of the single-phase converter utilizing other resonance networks than the resonant switch converter seen here.

In this thesis an ideal transformer is assumed where all losses related to this component are neglected. This is of course a simplification that leads to a less accurate model with higher efficiency than with the transformer included and further work should be focused on the improvement of the model by including a detailed analysis of the high-frequency transformer. Also, the losses related to auxiliary circuits such as the gate drivers have been neglected. For this thesis the focus has been on designing a soft-switching converter without overshoots and with a good performance, but the focus on the magnetic components and their design, weight, density and ratings could have been a natural continuation of this thesis. This would also have allowed for a more detailed discussion with regards to the switching frequency, finding an optimal relation between size of the magnetic components, power transfer capability and soft-switching capability.

An important characteristic with regards to the operation and conduction losses of both the IGBTs and diodes is the switching transients. The Matlab/Simulink software do not provide accurate and real models for these switches, and other software should therefore be used in order to model the switches more realistically. The author suggests to use ANSYS Simplorer. It would also have been interesting to investigate some other modulation schemes and phase-shift methods in order to see how the converter performance change. In specific, the dual phase-shift method seems interesting, and an analysis and comparison of the single phase-shift method and the dual phase-shift method would have been interesting to see implemented in a model.

Bibliography

[1] J. Lindtjorn et al. Demonstrating the benefits of advanced power systems and energy storage for dp vessels. *Dynamic Positioning Conf.*, Oct. 2014.

[2] A. K. Adnanes. Maritime electrical installations and diesel electric propulsion. *ABB AS Marine*, 2003.

[3] All-electric ship, siemens. `https://w3.siemens.no/home/no/no/sector/industry/marine/Documents/Orig.BDPC_16pages.pdf`. Accessed: 11-04-2017.

[4] R. Nilsen and I. Sorfonn. Hybrid power generation systems. *13th European Conference on Power Electronics and Applications*, 2009.

[5] Wärtsila, the lady recharges her batteries. `http://cdn.wartsila.com/docs/default-source/product-files/ea/systems/article-TW-2014-03-LLH.pdf?sfvrsn=8`. Accessed: 20-05-2017.

[6] M. Fazlali and M. Mobarrez. Design, simulation and evaluation of two different topologies for the 2.4 mw 4/6 kv dc-dc full-bridge converter, May 2012.

[7] M. Alifanov. Power electronic design of a multi mw dc/dc converter, 2013.

[8] R. Menis A. Tessarolo, S. Castellan and G. Sulligoi. Electric generation technologies for all-electric ships with medium-voltage dc power distribution systems. *IEEE*, 2013.

[9] Rodrigo A. F. Ferreira et al. Analysis of voltage droop control method for dc microgrid with simulink: Modelling and simulation. *IEEE*, 2012.

[10] Abb, onboard dc grid. `https://library.e.abb.com/public/b4f3f099e9d21360c1257a8a003beac2/ABB%20Generations_20%20Onboard%20DC%20grid.pdf`. Accessed: 07-03-2017.

[11] F. Krismer. *Modeling and Optimization of Bidirectional Dual Active Bridge DC-DC Converter Topologies.* PhD thesis, 2010.

[12] Fang Luo et al. A novel solid state fault current limiter for dc power distribution network. *IEEE*, May 2008.

[13] Gregory F. Reed et al. Ship to grid. *IEEE Power and Energy Magazine*, Nov/Dec. 2012.

[14] Z. Jin et al. Next generation shipboard dc power system. *IEEE Electrification Magazine, Aalborg University*, 4(2):45–57, 2016.

[15] B. Zahedi. *Shipboard DC Hybrid Power Systems.* PhD thesis, Oct. 2014.

[16] Assessing the potential of hybrid energy technology to reduce exhaust emissions from global shipping. *Energy Policy*, 40:204–218, 2012.

[17] Undeland Mohan and Robbins, editors. *Power Electronics Converters, Applications and Design.* John Wiley and Sons, Inc, 2003. ISBN 978-0-471-22693-2.

[18] B. Zahedi and L. E. Norum. Modeling and simulation of all-electric ships with low-voltage dc hybrid power systems. *IEEE Trans. on Power Electronics*, 28(10):4525–4537, Oct. 2013.

[19] Bill Drury and Austin Hughes, editors. *Electric Motors and Drives.* Elsevier Science, Newnes, 2013. ISBN 978-0-080-98332-5.

[20] Siemens drives, sinamics gl150. `http://www.industry.siemens.com/drives/global/en/converter/mv-drives/Pages/sinamics-sm150.aspx`. Accessed: 03-06-2017.

[21] O. C. Nebb B. Zahedi and L. E. Norum. An isolated bidirectional converter modeling for hybrid electric ship simulations. *IEEE*, 2012.

[22] Y. Patel L. Wei and C. S. N. Murthy. Active front end rectifier design trade-off between pwm and direct power control method. *IEEE*, pages 1015–1021, 2014.

[23] Siemens web page, active front end. `http://w3.siemens.no/home/no/no/sector/industry/marine/pages/active_front_end.aspx`. Accessed: 06-03-2017.

[24] O. C. Nebb. Use of energy storage in a lvdc distribution network for ships, Jun. 2012.

[25] I. Sorfonn. Power management control of electrical propulsion systems - design and control. *Dynamic Positioning Conf., Wärtsilä N.A. Inc.*, Oct. 9-10, 2007.

[26] M. B. Solberg. Fuel efficiency operation of dp thruster drives by use of supercapacitors. *Department of Electric Power Engineering, NTNU*, 2010.

[27] M. Uzunoglu M. C. Kisacikoglu and M. S. Alam. Load sharing using fuzzy logic control in a fuel cell/ultracapacitor hybrid vehicle. *Int. Journ. of Hydrogen Energy*, 34(3):1497–1507, 2009.

[28] Bu-808: How to prolong lithium-based batteries. `http://batteryuniversity.com/learn/article/how_to_prolong_lithium_based_batteries`, . Accessed: 02-03-2017.

[29] A. E. Trippe et al. Charging optimization of battery electric vehicles including cycle battery aging. *Innovative Smart Grid Technologies Conf. Europe (ISGT-Europe), IEEE*, pages 1–6, 2014.

[30] Jim McDowall. Understanding lithium-ion technology. *Saft America Inc.*, 2008.

[31] B. Perry. High capacity battery packs. *Corvus Energy*, Oct. 2012.

[32] Bu-205: Types of lithium-ion. `http://batteryuniversity.com/learn/article/types_of_lithium_ion`, . Accessed: 02-03-2017.

[33] Mathworks, generic battery model. `http://corvusenergy.com/wp-content/uploads/2016/03/AT6700-Module_-CORVUS-ENERGY_Specifications-Brochure-_Mar2016.pdf`, . Accessed: 26-02-2017.

[34] Vacon nx, design guide hybridization. `http://drivesliterature.danfoss.com/performCachedSearch.action?searchText=&languages=ALL&embedded=FALSE#`. Accessed: 09-03-2017.

[35] Bu-302: Series and parallel battery configurations. `http://batteryuniversity.com/learn/article/serial_and_parallel_battery_configurations`, . Accessed: 03-03-2017.

[36] Davide Andrea, editor. *Battery Management Systems for Large Lithium-Ion Battery Packs.* Arctech House, 2011. ISBN 978-1-60807-104-3.

[37] Corvus lithium-ion battery pack. `http://corvusenergy.com/viking-lady-offshore-supply-vessel-osv-eidesvik-offshore/`, . Accessed: 13-04-2017.

[38] J. S. Lai and D. J. Nelson. Energy management power converters in hybrid electric and fuel cell vehicles. *Proc. IEEE*, 95(4):766–777, Apr. 2007.

[39] H. R. Karshenas et al. Bidirectional dc-dc converters for energy storage systems. *Energy Storage in the Emerging Era of Smart Grids*, 2011.

[40] R. Bartelt V. Staudt and C. Heising. Short-circuit protection issues in dc ship grids. *IEEE*, pages 475–479, 2013.

[41] W. Liu B. Zhao, Q. Song and Y. Sun. Overview of dual-active-bridge isolated bidirectional dc-dc converter for high-frequency-link power-conversion system. *IEEE Trans on Power Electronics*, 29 (8):4091–4106, Aug. 2014.

[42] T. Jalakas D. Vinnikov and M. Egorov. Feasibility study of half- and full-bridge isolated dc/dc converters in high-voltage high-power applications. *IEEE 13th Int. Power Electronics and Motion Control Conf.*, pages 1257–1262, 2008.

[43] F. C. Lee K. Wang and J. Lai. Operation principles of bidirectional full-bridge dc/dc converter with unified soft-switching scheme and soft-starting capability. *IEEE*, 28(10):111–118, 2000.

[44] M. Balasingh J. B. Banu and S. Rajarajacholan. A non-isolated bidirectional dc/dc converter with lcd snubber. *Rev. Téc. Ing. Univ. Zulia*, 39(1):131–143, 2016.

[45] S. Rejitha and G. Sreedevi. Comparison of an isolated bidirectional dc-dc converter with and without a flyback snubber. *Journal of Electrical and Electronics Engineering*, 8(2):16–25, Dec. 2013.

[46] A. K. Rathore and X. Li. Comparison of zero-voltage-switching current-fed full-bridge and half-bridge isolated dc/dc converters with active clamp. *IEEE PEDS*, pages 133–138, Dec. 2011.

[47] A. Singh and V. S. Jabir. Voltage fed full-bridge dc/dc and dc/ac converter for high-frequency converter using c2000. *Application Report, Texas Instruments*, pages 111–118, Jun. 2015.

[48] K. Wang et al. Bidirectional dc to dc converters for fuel cell systems. *Power Electronics in Transportation, Dearborn MI, USA*, pages 47–51, Oct. 1998.

[49] M. N. Kheraluwala et al. Performance characterization of a high-power dual active bridge dc-to-dc converter. *IEEE Trans on Ind. Applications*, 28(6):1294–1301, Nov./Dec. 1992.

[50] A. R. Alonso et al. An overall study of a dual active bridge for bidirectional dc/dc conversion. *IEEE*, pages 1129–1135, 2010.

[51] M. S. Moeinian. Design and implementation of a proper modulation and control scheme for a single and three phase dual active bridge converter, May 2014.

[52] D. G. Holmes D. Segaran and B. P. McGrath. Comparative analysis of single- and three-phase dual active bridge bidirectional dc-dc converters. *Australasian Universities Power Engineering Conf. (AUPEC'08)*, 2008.

[53] D. S. Segaran. *Dynamic Modelling and Control of Dual Active Bridge Bidirectional DC-DC Converters for Smart Grid Applications.* PhD thesis, Feb. 2013.

[54] R. Doncker M. Divan and M. H. Kheraluwala. A three-phase soft-switched high-power-density dc-dc converter for high-power applications. *IEEE Trans. Ind. Appl.*, 27(1):63–73, 1991.

[55] D. Boroyevich X. Jing, F. Wang and S. Zhiyu. Single-phase vs. three-phase high density power transformers. *Proc. IEEE Energy Conversion Congress and Exposition (ECCE)*, pages 4368–4375, 2010.

[56] X. Wang. Feasibility and challenges in microgrids for marine vessels, Dec. 2016.

[57] R. M. Cuzner and G. Venkataramanan. The status of dc microgrid protection. *IEEE*, 2008.

[58] P. Calroll and R. A. Dougal. New horizons in dc shipboard power systems. *IEEE Electrification Magazine*, pages 38–45, Feb. 2014.

[59] C. Wang C. Mi, H. Bai and S. Gargies. Operation, design and control of dual h-bridge-based isolated bidirectional dc-dc converter. *IET Power Electron*, 1(4):507–517, Apr. 2008.

[60] J. Zhao. Distributed power conversion architecture for microgrids and integration of renewable energy sources, 2013.

[61] J. Jiang X. Shi and X-Guo. An efficiency-optimized isolated bidirectional dc-dc converter with extended power range for energy storage systems in microgrids. *ISSN Energies*, pages 27–44, 2013.

[62] X. Liu et al. Novel dual phase-shift control with bidirectional inner phase shifts for a dual-active bridge converter having low surge current and stable power control. *IEEE Trans. on Power Electronics*, 32(5):4095–4106, 2016.

[63] S-K. Sul M. Kim, M Rosekeit and R. W. A. A. de Doncker. A dual phase-shift control strategy for dual-active-bridge dc-dc converter in wide voltage range. *IEEE 8th Int. Conf. on Power Electronics - ECCE Asia*, pages 1–6, 364-371.

[64] V. Vlatkovic R. F. J. A. Sabate and B. H. Cho. Design considerations for high-voltage high-power full-bridge zero-voltage-switched pwm converter. *IEEE Peper*, 1990.

[65] A. B. Mehmet Timur Aydemir. A critical evaluation of high power hard and soft switched isolated dc-dc converters. *IEEE Paper*, 2002.

[66] D. Maksimovic and R. W. Erickson, editors. *Fundamentals of Power Electronics.* Springer Science, 2001. ISBN 978-1-47570-559-1.

[67] M. A. Bahmani M. Mobarrez, M. Fazlali and T. Thiringer. Performance and loss evaluation of a hard and soft switched 2.4 mw, 4kv to 6kv isolated dc-dc converter for a wind energy application. *IEEE*, 2012.

[68] C. Chen J. Wang, K. Zou and L. Chen. A high frequency battery model for current ripple analysis. *Applied Power Electronics Conf. and Exposition (APEC), Twenty-Fifth Annual IEEE*, pages 676–680, 2010.

[69] J. Liu et al. Design of high voltage, high power and high frequency transformer in lcc resonant converter. *IEEE*, pages 1034–1038, 2009.

[70] Abb hipak igbt module. `https://library.e.abb.com/public/521288a37504d63583257ca9002dbba2/5SNA%203600E170300%205SYA%201414-06%2002-2014.pdf`. Accessed: 03-04-2017.

[71] L. Max. *Energy Evaluation for DC/DC Converters in DC-Based Wind Farms.* PhD thesis, 2007.

[72] Tron Hansen Syverud. Modelling and control of a dc-grid hybrid power system with battery and variable speed diesel generators, Jun. 2016.

[73] Mastering electronic design, how to derive the rms value of a triangle waveform. `https://masteringelectronicsdesign.com/how-to-derive-the-rms-value-of-a-triangle-waveform/`. Accessed: 13-05-2017.

8 Appendix

8.1 Corvus Data Sheet AT6700

AT6700 Module

Voltage and Capacity

Voltage and Capacity		AT6700-100	AT6700-50
Voltage	Maximum	100.8 VDC	50.4 VDC
	Minimum	76.8 VDC	38.4 VDC
Maximum Pack Voltage		1100 VDC	
Capacity		75 Ah	150 Ah
Energy		6.7 kWh	
Scalability		6.7 kWh (1 module) to >10 MWh (1500 modules)	
Cycle Life		>8000 cycles, 80% DoD	

Power Performance

Power Performance		AT6700-100	AT6700-50
C-Rate – Peak[1]	Discharge	10C (750A)	10C (1500A)
	Charge	5C (375A)	5C (750A)
C-Rate – Continuous[2]	Discharge	6C (450A)	4C (600A)
	Charge	3C (225A)	3C (450A)
C-Rate – RMS[3]	Liquid Cooled	3C (225A)	3C (450A)
	Air Cooled	1.5C (110A)	1.5C (225A)

General Specifications

General Specifications		
Weight	Liquid Cooled	72 kg (158 lb)
	Air Cooled	70 kg (154lb)
Construction		Sealed marine grade aluminium enclosure
Dimensions		59x33x38 cm (26x13x15 in)
Ingress Protection		IP67
Vibration & Shock		UNT 38.3, IEC 60086-2-6
Racking		Included
Installation Flexibility		Configurable racking to fit any space
Connectors		Sealed / no exposed conductors

Battery Management System

Battery Management System	
State of Health	Included
State of Charge	Accuracy ±1% throughout current range
Temperature sensors	4 standard / 24 optional
Communications	J1939 standard (to Pack Controller) Modbus TCP (optional with Array Manager)
EMC/EMI	Compatible with maritime switchboards and gensets

Safety

Safety	
Safety	Integrated HVIL Thermal runaway anti-propagation BMS current control parameter Integrated over-temperature disconnect Fuses (in Pack Controller)
Voltage Isolation	4.5kV
Class Approvals	DNV-GL, LR, ABS, BV

[1] Peak – maximum rating for 10 seconds
[2] Continuous – single charge or discharge
[3] RMS – indefinite alternating charge and discharge

Specifications subject to change without notice.

ABOUT US
Corvus Energy manufactures the world's most durable Energy Storage Systems (ESS). Designed for heavy industrial applications, a Corvus ESS will reduce fuel consumption, maintenance, emissions & increase reliability. Contact us today to learn how Corvus energy storage can improve your bottom line:

CONTACT
Toll Free: +1 (888) 390-7239
Tech Support +1 (604) 227-1932

HEAD OFFICE
#220-13155 Delf Place
Richmond, BC V6V 2A2 Canada
info@corvusenergy.com

NORWAY
Corvus Norway AS
+47 918 25 618
sales@corvusenergy.com

2016-03-25

corvusenergy.com

8.2 RMS and Average Current Values

By looking at the current waveforms from the simulations it is seen that the IGBT and diode currents are of a square-wave and triangular waveform. Thus, the RMS and average values can be calculated by finding the peak values of the triangular waveforms and the height of the square-waves in addition to the length of the conduction interval. For the triangular waveforms, the RMS and average values are given as[73]

$$I_{rms,tri} = I_{peak}\sqrt{\frac{t}{3T}} \tag{8.1}$$

and

$$I_{avg,tri} = I_{peak}\frac{t}{2T} \tag{8.2}$$

where I_{peak} is the peak value of the waveform, t is the length of the conduction interval and T is the time of the switching period, which is $100\mu s$ for a switching frequency of $10kHz$. For a square-wave, the RMS and average values are given as

$$I_{rms,sq} = \sqrt{\frac{I_{peak}^2 t}{T}} \tag{8.3}$$

and

$$I_{avg,sq} = I_{peak}\frac{t}{T} \tag{8.4}$$

with I_{peak} being the peak current, t is the length of the conduction interval and T is the switching period. Therefore, the average and RMS current values can be found by using the peak values and the conduction time found from the simulations. The results are presented in appendix 8.3.

8.3 Loss Calculation and Parameter Values

The loss calculation is based on the equations shown in section 4.2, restated here in equation 8.5 and 8.6 for simplicity. The diode losses are found as

$$P_{cond,diode} = I_F V_F = \frac{1}{T_s}\int_0^{t_{on}} v_F(t)I_F(t)dt = V_D I_{D,av} + R_D I_{D,RMS}^2 \tag{8.5}$$

where $I_{D,av}$ is the average current through the diode, $I_{D,RMS}$ is the RMS current through the diode, R_D is the on-state resistance and V_D is the on-state voltage drop. For the IGBT, the losses are found as

$$P_{cond,igbt} = I_C V_{CE} = \frac{1}{T_s}\int_0^{t_{on}} v_{CE}(t)I_C(t)dt = V_{ce,sat}I_{av} + R_{on}I_{RMS}^2 \tag{8.6}$$

with $V_{CE,sat}$ being the collector-emitter on-state saturation voltage, I_{av} being the average current, R_{on} is the on-state resistance and I_{RMS} is the RMS current. The average and RMS currents in the diodes and IGBTs are found by using the results from the simulations as well as the formulas shown in appendix 8.2.

The average and RMS current values for the primary and secondary side are presented in table 6 and 7, respectively. Table 8 and 9 shows the on-state resistance for the diodes and IGBTs for the primary and secondary side, respectively. Lastly, table 10 and 11 show the on-state voltage for the diodes and IGBTs for the primary and secondary side, respectively. All parameter values are calculated for an output power in steps of $200kW$.

Output power[kW]	$I_{av,diode}$[A]	$I_{rms,diode}$[A]	$I_{av,igbt}$[A]	$I_{rms,igbt}$[A]
200	0.04	0.365	149	211.3
400	0.12	1.1	216	307
600	0.17	4.39	320	454
800	0.6	12.6	415	588
1000	0.9	19	512	726.8
1200	0.72	15.2	686	974
1400	0.63	13.3	893	1268.4
1600	0.534	11.3	1111	1579.7
1800	0.271	7	1290	1831.1
2000	0.69	14.5	1480	2098
2200	0.28	7.23	1680	2381.9
2400	0.28	7.23	1970	2800.9
2600	0.08	2.07	2270	3224.2
2800	0.34	8.78	2480	3521.4
3000	0.065	1.68	2780	3946.7
3200	0.017	0.439	2970	4221.4
3400	0.041	1.06	3160	4480.6
3600	0.041	1.06	3450	4898.9
3800	0.08	2.07	3650	5177.8
4000	0.1	2.58	3840	5451.8

Table 6: Primary side currents.

Output power[kW]	$I_{av,diode}$[A]	$I_{rms,diode}$[A]	$I_{av,igbt}$[A]	$I_{rms,igbt}$[A]
200	70	156.5	15.2	43.9
400	211	299.3	56.2	100
600	314	446.5	79.3	142.3
800	410	581.7	103.8	188.7
1000	515	731.7	130.5	236.3
1200	684	971.9	172.3	300.4
1400	892	1266.6	224.1	384.9
1600	1120	1596.6	282.3	479.6
1800	1390	1967.7	347.4	584
2000	1500	2126.2	375.5	633.1
2200	1710	2422.7	427.7	718.4
2400	2010	2853	503	836.8
2600	2320	3289	579.5	957.7
2800	2420	3437.6	605.9	1005.7
3000	2830	4012.2	706.8	1166.5
3200	3050	4328.5	762.2	1252.8
3400	3260	4623.6	814.2	1338.1
3600	3560	5059.5	890.8	1461.3
3800	3780	5360.2	943.8	1547.9
4000	3980	5651.1	995	1631.8

Table 7: Secondary side currents.

Output power[kW]	$R_{D,diode}$[mΩ]	$R_{on,igbt}$[mΩ]
200	0.833	1.18
400	0.833	1.011
600	0.833	1.09
800	0.833	0.92
1000	0.833	0.835
1200	0.833	0.749
1400	0.833	0.664
1600	0.833	0.579
1800	0.833	0.493
2000	0.833	0.408
2200	0.833	0.323
2400	0.833	0.313
2600	0.833	0.313
2800	0.833	0.313
3000	0.833	0.313
3200	0.833	0.313
3400	0.833	0.313
3600	0.833	0.313
3800	0.833	0.313
4000	0.833	0.313

Table 8: Primary side on-state resistances for the diodes and IGBTs.

Output power[kW]	$R_{D,diode}$[mΩ]	$R_{on,igbt}$[mΩ]
200	0.825	0.774
400	0.795	0.774
600	0.765	0.774
800	0.74	0.774
1000	0.632	0.774
1200	0.611	0.774
1400	0.589	0.774
1600	0.568	0.731
1800	0.547	0.689
2000	0.525	0.647
2200	0.504	0.605
2400	0.483	0.564
2600	0.461	0.564
2800	0.439	0.564
3000	0.439	0.564
3200	0.439	0.564
3400	0.439	0.564
3600	0.439	0.564
3800	0.439	0.564
4000	0.439	0.564

Table 9: Secondary side on-state resistances for the diodes and IGBTs.

Output power[kW]	$V_{D,diode}$[V]	$V_{ce,sat,igbt}$[V]
200	0.5	0.75
400	0.5	0.855
600	0.5	0.96
800	0.5	1.065
1000	0.5	1.17
1200	0.5	1.275
1400	0.5	1.38
1600	0.5	1.485
1800	0.5	1.59
2000	0.5	1.695
2200	0.5	1.8
2400	0.5	1.82
2600	0.5	1.85
2800	0.5	2
3000	0.5	2.1
3200	0.5	2.15
3400	0.5	2.2
3600	0.5	2.32
3800	0.5	2.4
4000	0.5	2.5

Table 10: Primary side on-state voltages for the diodes and IGBTs.

Output power[kW]	$V_{D,diode}$[V]	$V_{ce,sat,igbt}$[V]
200	0.55	0.5
400	0.6	0.542
600	0.65	0.583
800	0.675	0.625
1000	0.715	0.667
1200	0.756	0.708
1400	0.797	0.75
1600	0.837	0.79
1800	0.878	0.83
2000	0.918	0.87
2200	0.959	0.91
2400	1	0.95
2600	1.025	0.975
2800	1.05	1
3000	1.075	1.025
3200	1.08	1.05
3400	1.085	1.075
3600	1.1	1.1
3800	1.125	1.125
4000	1.15	1.13

Table 11: Secondary side on-state voltages for the diodes and IGBTs.